Universidad del País Vasco
Euskal Herriko Unibertsitatea
NAZIOARTEKO BIKAINTASUN CAMPUSA
CAMPUS DE EXCELENCIA INTERNACIONAL

PhD THESIS

APPROACHES FOR IMPROVEMENT OF EDM PERFORMANCE AND FOR THE UNDERSTANDING OF ELECTRODE WEAR PHENOMENA

Presented to obtain the degree of

Doctor in Industrial Engineering

Presented by:

Olatz Flaño Alaña

Thesis advisors:

Prof. Dr. Jose Antonio Sánchez

Asoc. Prof. Dr. Borja Izquierdo

February 2018, Bilbao

(c)2018 OLATZ FLAÑO ALAÑA

eman ta zabal zazu

Universidad del País Vasco Euskal Herriko Unibertsitatea

NAZIOARTEKO BIKAINTASUN CAMPUSA
CAMPUS DE EXCELENCIA INTERNACIONAL

PhD THESIS

APPROACHES FOR IMPROVEMENT OF EDM PERFORMANCE AND FOR THE UNDERSTANDING OF ELECTRODE WEAR PHENOMENA

Presented to obtain the degree of

Doctor in Industrial Engineering

Presented by:

Olatz Flaño Alaña

Thesis advisors:

Prof. Dr. Jose Antonio Sánchez

Asoc. Prof. Dr. Borja Izquierdo

February 2018, Bilbao

Made with passion and curiosity

ACKNOWLEDGEMENTS

The time for printing the work has reached, so now is the moment to express my gratitude to the ones that have contributed in the development of the present PhD Thesis.

To my advisors Jose Antonio and Borja. Because of your supervision, guidance, encouragement and critiques. Many thanks for giving me the chance to start my doctoral training and for all your effort. I will always be grateful.

To Izaro. You played different roles through these years: teacher, supervisor, workmate, cheerleader and above all, friend. Thank you for your constant dedication. No doubt, we make a good team.

To Professor Kunieda. For your passion, dedication, wisdom and willingness to share knowledge. Being part of your team was a turning point in my live. Thank you!

To Zhao. For your discipline and support. I learnt a lot working hand-to-hand with you. I wish you a successful career and the best in your new challenge.

A special thank you to my little sister Miren. I miss our chats in the canteen. You always know what I was doing even if you did not know what was about. You are the best! And to my parents. For your unconditional love and education. You have provided me through moral and emotional support. Thank you for being there!

A special gratitude goes out to my colleagues of Bilbao, IAC, Tokyo and ONA, and to my friends. In a direct or indirect way, you all are part of this work.

I also would like to acknowledge ONA for giving me the chance of continuing my career as a researcher in this interesting field.

Finally, I dedicate this work to all the researchers, those whose work I had the pleasure to enjoy, and those whose work I will read in the future. Thank you for your effort and for sharing your knowledge.

Olatz

SUMMARY

Improvements in computer science and measuring and analysing instruments, combined with constant research of the process, have made possible a better understanding of the material removal process. This has resulted in the enhancement of the machining process as well as in the widening of the application fields of electrical discharge machining. The present research work is focused on sinking electrical discharge machining process and has as objective to propose different techniques that can improve the machining efficiency of EDM jobs of current research.

The first challenge faced is the slicing of single-crystal silicon carbide material (SiC). Recent developments highlight the need to enhance the electrical and physical properties of power devices. Whilst SiC-based devices can realize great improvements, SiC fabrication technologies are still not sufficiently developed to the degree required for widespread technology. One reason is the high price of SiC wafer and its manufacturing cost. It is therefore, very important to reduce maximum material loss during the manufacturing process to decrease wafer costs. Thus, foil electrode serves as an alternative method for SiC slicing. However, due to the large side surface area of the foil electrode, there is a high occurrence probability of side surface discharges and high concentration of debris, which affects kerf width accuracy and machining stability. Hence, two different foil electrode designs have been studied to improve the machining performance.

Taking as background the conclusion obtained from that work, an electrode in which holes have been machined for the EDM’ing of high-aspect ratio slots has been proposed. Nowadays, EDM is a competitive solution in the machining of high-aspect ratio slots, mainly because during the material removal process there is not contact between electrode and workpiece. Nevertheless, due to debris accumulation in the narrow gap, the machining stability at high depths cannot be guaranteed, and the material removal rate decreases drastically with the machining depth. The work includes original findings about the influence of machning holes on the electrode in flushing efficiency.

Furthermore, the need to enhance aerodynamic performance with light weight design of aircraft engines has increase the demand of free form components, and multi-axis EDM has become a feasible solution. Considering that in EDM the final workpiece is principally affected by electrode wear and gap width, at present, before machining, highly cost consuming trial-and-error strategies are necessary. It is believed that further understanding of electrode wear and gap width distribution patterns could enhance the machining strategy. Hence, an easy-to-put in practice methodology for electrode wear and gap width analysis has been proposed. Moreover, based on conclusions obtained from experimental works, a thermal model for the prediction of temperature distribution in the electrode has been proposed.

CONTENT

I. INTRODUCTION 3

I.1. Industrial context 3

I.2. Objectives and contributions 4

I.3. Content layout 6

II. STATE OF THE ART 7

II.1. Latest developments in Electrical Discharge Machining 7

II.2. SEDM applications of current research 9

II.2.1. SiC slicing by foil electrode 10

II.2.2. High-aspect ratio slot machining 14

II.2.3. Free form complex geometries 17

II.3. Thermal problem in SEDM 19

II.3.1. Energy generation during SEDM process 19

II.3.2. Energy distribution 22

II.3.3. Definition of energy fraction to electrode by temperature measurements 23

II.4. Electrode wear in SEDM 27

II.4.1. Influence of process parameters on electrode wear 27

II.4.2. Influence of electrode geometry on electrode wear 29

II.4.3. Discharge location adaptive control based on discharge voltage 31

II.4.4. Carbon layer generation in electrode surface during machining 33

II.4.5. Electrode wear minimization techniques 35

II.5. Simulation of electrode wear during EDM process 38

II.5.1. Geometry considerations 39

II.5.2. Physical-thermal considerations 42

III. APPROACHES FOR IMPROVEMENT OF EDM CUTTING BY FOIL ELECTRODE 47

III.1. Introduction 47
III.2. SiC material. Main characteristics 48
III.3. Main equipment and machine tools used 48
III.4. Fixture for applying tension to electrode foil 50
III.5. Foil electrode: Copper 52
III.6. Proposal of new electrode 52
  III.6.1. Electrode with holes 53
  III.6.2. Coated electrode 54
III.7. Improvement of machining performance by the proposed electrodes 54
  III.7.1. Test definition and methodology 54
  III.7.2. Measuring outputs 57
  III.7.3. Effect of making holes on foil electrode. Experimental results and discussion 58
  III.7.4. Effect of side surface insulation. Experimental results and discussion 61
  III.7.5. Discussion: Influence of discharge delay time 64
  III.7.6. Strategy for optimal machining 70
III.8. Conclusions 70

IV. IMPROVEMENT OF EDM PERFORMANCE IN HIGH-ASPECT RATIO SLOT MACHINING 75

IV.1. Introduction 75
IV.2. Main equipment and machine tools used 76
IV.3. Improvement of EDM performance in high-aspect ratio slot machining using multi-holed electrodes 78

IV.3.1. Proposed multi-holed electrode 78

IV.3.2. Test definition and methodology 78

IV.3.3. Influence of hole diameter 79

IV.3.4. Influence of positioning of holes in the electrode 79

IV.3.5. Influence of hole geometry 80

IV.3.6. Process outputs 81

IV.3.7. Results and discussion 82

IV.3.8. Optimum electrode combination 86

IV.4. Analysis of discharges in the working gap 87

IV.5. Conclusions 91

V. DETERMINATION OF ELECTRODE WEAR AND GAP IN MULTI-STAGE EDM 95

V.1. Introduction 95

V.2. Main equipment and machine tools used 96

V.3. Proposed methodology for electrode wear and gap width definition 96

V.4. Case study: Shrouded blisk machining 99

V.4.1. Experimental set-up and procedure 99

V.4.2. Discussion of results 103

V.5. Case study: V-shape wedge 109

V.5.1. Experimental procedure 109

V.5.2. Discussion of results 112

V.6. Case study: Square cross section electrode 115

V.6.1. Experimental set-up and procedure. 116

V.6.2. Discussion of results 117

V.7. Conclusions 119

VI. A THERMAL MODEL FOR PREDICTION OF TEMPERATURE DISTRIBUTION IN THE ELECTRODE 123

VI.1. Introduction 123

VI.2. Principles of the thermal simulation model 124

VI.2.1. Main algorithm of the electrode thermal model 125

VI.2.2. Boundary conditions 126

VI.2.3. Method to consider the curvature effect 128

VI.2.4. Method to consider the discharge area effect 129

VI.2.5. Graphite properties 129

VI.3. Heat transfer definition during continuous EDM process 131

VI.3.1. Experimental set-up 132

VI.3.2. Temperature measurement results 136

VI.3.3. Discussion of results 138

VI.4. Preliminary proposal: Electrode material removal criteria 139

VI.4.1. Experimental set-up 140

VI.4.2. Experimental results. Results discussion 142

VI.4.3. Material removal criteria hypothesis 145

VI.5. Conclusions 145

VII. CONCLUSIONS AND FUTURE WORKS 149

VII.1. Conclusions 149

VII.2. Future works 151

REFERENCES 155

FIGURES

Figure 1: Scheme of the material removal mechanism. 7

Figure 2. Scheme of the assisting electrode method for the EDM'ing of insulating materials. 8

Figure 3: Relation between discharge current waveforms and output variables. 9

Figure 4: Multi-wire EDS prototype developed by Mitsubishi Electric Corporation [14]. 11

Figure 5: Scheme of principle of SiC slicing by foil electrode [18]. 12

Figure 6: Comparison of the cross-section area of wire and foil electrode. 12

Figure 7: Cross-section profiles of cut kerf in previous research works [18]. 13

Figure 8: Example of a high-aspect ratio slot machining on an NGV [5]. 14

Figure 9: 3D view of the design if the set-up [29]. 16

Figure 10: Example of a EDM'ed shrouded blisk [37]. 18

Figure 11: Example of voltage and intensity waveform of two consecutive discharges. 20

Figure 12: Example of the three types of discharges that may occur during EDM'ing. 21

Figure 13: Four different discharge current signal with the same discharge energy [50]. 22

Figure 14: Energy distribution scheme of a single discharge. 22

Figure 15: a) Temperature measurement experimental set-ups; b) Calculation models [56]. 24

Figure 16: Algorithm used for determining the energy distribution into electrode [56]. 25

Figure 17: Literature comparison of EDM power distribution ratios [60][61]. 26

Figure 18: Example of a severe electrode wear during machining. 27

Figure 19: a) Influence of discharge current and b) discharge duration on TWR [64]. 28

Figure 20: Electrode shape change during time [39]. 30

Figure 21: SEM imagines of electrode edges after EDM’ing. a) Round shape and b) diamond shape [65]. 31

Figure 22: Effect of discharge voltage value on discharge area and geometry [69]. 31

Figure 23: Definition of discharge location by discharge voltage [71]. 32

Figure 24: Discharge duration and discharge interval adaptation based on discharge voltage [72]. 32

Figure 25: Brief model to describe the carbon layer generation at micro scale [40]. 33

Figure 26: Example of unexpected material build-up during slot machining. 34

Figure 27: Influence of discharge duration on removal amount of electrode per pulse discharge [74]. 34

Figure 28: Experimental set-up for cryogenic cooling of tool electrode [51]. 37

Figure 29: General algorithm for EDM simulation method [84]. 38

Figure 30: Discharge location simulation algorithm for forward simulation [87]. 40

Figure 31: Scheme of the influence of curvature in material removal. 40

Figure 32: Method to compensate for error due to curvature [45]. 41

Figure 33: Long-term market forecast for SiC devices in various power applications [93]. 48

Figure 34: Illustration of the fixture for applying tension to the foil. 51

Figure 35: Analysis of electrode deformation due to discharge force [97]. 51

Figure 36: Set-up for copper foil preparation. 52

Figure 37: Scheme of electrical discharge slicing of SiC by foil electrode with holes. 52

Figure 38: Experimental set-up for machining the holes on the foil electrode. 53

Figure 39: Foil electrode ready for slicing. 54

Figure 40: EDM cutting of SiC by foil electrode. 55

Figure 41: Foil electrode proposed. 55

Figure 42: Effect of hole diameter on machining performance. 56

Figure 43: Parallelism error observation. 57

Figure 44: Cross section shape after slicing. 58

Figure 45: Foil tool wear in slicing of SiC with reciprocating motion. 58

Figure 46: Influence of holes on kerf loss. No coated electrode. 59

Figure 47: Influence of holes on cutting speed. No coated electrode. 60

Figure 48: Influence of holes on average tool wear ratio (%). No coated electrode. 60

Figure 49: Foil electrode with holes after slicing. 61

Figure 50: SiC workpiece cross section with different coating layer thickness. 61

Figure 51: Foil electrode with an insulation layer of 22 µm. 62

Figure 52: Influence of surface insulation on kerf width. Electrode without holes. 62

Figure 53: Influence of holes on cutting speed. Electrode without holes. 63

Figure 54: Influence of surface insulation on average tool wear ratio (%). Electrode without holes. 63

Figure 55: First attempt. Image in which the experimental set-up up is presented. 65

Figure 56: a) Parallelism error measurement. b) Correct positioning of the blocks in the machine tool. 66

Figure 57: Experimental set-up for the study of the discharge delay time. 66

Figure 58: Representation of the movement of the workpiece for obtaining two data. 67

Figure 59: Scheme of the copper block design studied. a) No coating, no holes; b) Coating, no holes; c) No coating, holes. 67

Figure 60: Copper block after the machining of the holes. 68

Figure 61: Discharge generation set-up for the analysis of the discharge delay time. 68

Figure 62: Example of a discharge waveforms for the case of no coating without holes. 68

Figure 63: Distribution of the discharge delay time. 69

Figure 64: Relation between proposed electrode designs and average discharge delay time. 69

Figure 65. Specially designed graphite electrode for slot machining. 78

Figure 66: Test definition for analysing the effect of holes. 79

Figure 67: Test definition for analysing the influence of positioning of the holes in the electrode. 80

Figure 68: Test definition for improving hole geometry. 80

Figure 69: Characterization of electrode wear. a) Edge radius; b) Length loss; c) Lateral wear. 81

Figure 70: Influence of flushing hole diameter in terms of: a) Machining time, b) Edge radius, c) Length loss. 82

Figure 71: Influence of position of flushing holes from discharge area in terms of: a) Machining time, b) Edge radius, c) Lost length. 83

Figure 72: Comparison of the displacement of feeding axis vs. machining time with the three different electrode designs. 84

Figure 73: Influence of flushing hole geometry in terms of: a) Machining time, b) Edge radius, c) Lost length. 85

Figure 74: Comparison of the displacement of feeding axis vs. machining time with three different electrode designs. 85

Figure 75: Example of electrode lateral wear for a machining depth of 6.5 mm. a) Electrode lateral wear for the different electrodes b) Microphotograph of worn electrode (Conventional, No holes). 86

Figure 76: Improvement in machining time at different depths using the electrode with flushing pockets. 87

Figure 77: Machining conditions in which machining parameters were recorded. 88

Figure 78: Effect of flushing holes on duty cycle (%) at different machining depths. 88

Figure 79: Effect of flushing holes on discharge frequency at different machining depths. 89

Figure 80: Discharge delay time at different machining depths for the different electrode geometries. a) Percentage of total discharges (up to 1000 ms); b) average values. 90

Figure 81: Average value of t_{off} at different machining depths. 91

Figure 82: Distribution of t_d by the representation of the Laue Plot. 91

Figure 83: Proposal of functions for representing the of electrode wear. 97

Figure 84: Proposal of functions for representing the gap width value. 98

Figure 85: Example of electrode and workpiece positioning technique. 98

Figure 86: Example of calculation G_w in symmetric geometries. The reference used is on Z axis. 99

Figure 87: Scheme of the workpiece, electrode and feeding path. 100

Figure 88: Electrode path of each step analysed. 101

Figure 89: Electrode design and nomenclature employed. 102

Figure 90: Example of a 0.5 mm thickness slice of the workpiece. Step 2. 102

Figure 91: Z axis defined by external references and X defined by Eq. 13 in the points highlight. 103

Figure 92: E_{wa} (mm^2) as a function of machining time and EDM regime. Above: Roughing regimens. Below: Finishing regimens. 104

Figure 93: E_{ll} (mm^2) as a function of machining time and EDM regime. Above: Roughing regimens. Below: Finishing regimens. 105

Figure 94: Results of E_{wd} (mm) for the studied regimens. 106

Figure 95: Observation of ‘Detail A’ of Figure 89 after EDM’ing. 107

Figure 96: Regions of material build-up when eroding with VDI 39. 108

Figure 97: Representation of the gap width value and deviation with respect to the theoretical value. 108

Figure 98: Results of G_w (mm) for the studied regimens. 109

Figure 99: Electrode geometry in which the measured electrode wear indicators have been illustrated. 110

Figure 100: Example of a wedge radius after erosion (machining depth=0.5 mm). 111

Figure 101: Example of the measurement of the electrode wear area, E_{wa}. 111

Figure 102: Example of the way to analyse gap width distribution, G_w. 112

Figure 103: Electrode wear process. Wedge radius. 112

Figure 104: Electrode wear process. Electrode lost length. 113

Figure 105: Electrode wear process. Electrode wear area.. 113

Figure 106: Superposition of electrode and workpiece profiles for gap width data acquisition. 114

Figure 107: Gap width results representation with the corresponding deviation lines. 115

Figure 108: Representation gap width results by average value. 115

Figure 109: Representation of the indicators for electrode wear analysis................................ 116

Figure 110: Representation of the outputs in terms of electrode wear. 117

Figure 111: Example of the superposition of both electrode and workpiece profiles. 117

Figure 112: Cross section electrode. Edge radius, E_r, results... 118

Figure 113: Cross section electrode. Electrode lost length, E_{ll}, results. 118

Figure 114: Cross section electrode. Electrode gap width profile representation at different machining stages. 119

Figure 115: Flowchart to predict electrode geometry after EDM process. 125

Figure 116: Scheme that represents the boundary conditions. 126

Figure 117: Scheme for illustrating the energy simulation method. 127

Figure 118: Example of the value of edge radius on the coefficient that consider the curvature effect.. 128

Figure 119: Definition of the areas considered in the model for the application of the heat input. 129

Figure 120: Thermal conductivity vs. temperature. a) Theoretical values [106]. b) Output for the model. 130

Figure 121: Heat capacity VS temperature. a. Theoretical values [106]. b. Output for the model. 130

Figure 122: Flowchart for F_E value determination. 131

Figure 123: Set-up during the electrode temperature recording. 133

Figure 124: Scheme of thermocouple displacement. 134

Figure 125: Example that shows the contact between electrode and workpiece. 134

Figure 126: Experimental set-up for dielectric temperature measurement. 135

Figure 127: Experimental set-up for dielectric temperature measurement in the discharge gap. 135

Figure 128: Temperature in the electrode at 2 mm form the discharge gap. 136

Figure 129: Temperature in the dielectric that is surrounding the electrode. 137

Figure 130: Temperature measurement for obtaining the temperature of the dielectric of the discharge gap. 137

Figure 131: Temperature in the contact between electrode holder and electrode. 138

Figure 132: Temperature results. Experimental measurement vs. simulation result. 138

Figure 133: Temperature of the electrode after the machining was stopped. Experimental measurement vs. simulation result. 139

Figure 134: Electrode geometry and representation of electrode wear indicators. 140

Figure 135: Feeding axis vs. machining time. 142

Figure 136: E_{ll} progress during the machining of a slot of 6.5 mm. 143

Figure 137: Current waveform. a) Stable machining, b) Unstable machining. 143

Figure 138: Electrode temperature field. a) Stable machining, b) Unstable machining. 144

Figure 139: E_r progress during the machining of a slot of 6.5 mm. 144

Figure 140: Electrode temperature field at early stage of machining. 145

TABLES

Table 1: Comparison of material properties between SiC and steel [94]. 48

Table 2: Sodick C32 machine main specifications [6]. 49

Table 3: Keyence LK-G10 CCD laser displacement [95]. 49

Table 4: Example of the machining tool equipment used [96]. 50

Table 5: Machining and experimental conditions. 56

Table 6: Parameter settings for jump motion and reciprocating motion. 57

Table 7: Machining conditions for analysing distribution of discharge delay time. 65

Table 8: ONA CS300 SEDM machine main specifications. 76

Table 9: ONA PRIMA E250. WEDM machine main specifications. 76

Table 10: Mitutoyo PJ-3000F profile projector [104]. 77

Table 11: Leica DCM 3D optical surface metrology system [105]. 77

Table 12: Machining and experimental conditions. 79

Table 13: ZEISS MC 850 Coordinate Measuring Machine. 96

Table 14: Graphite properties. POCO EDM-200® [108]. 100

Table 15: Parameter settings of the test. 101

Table 16: Parameter settings for an VDI 38. 110

Table 17: Parameter settings for an VDI 39. 116

Table 18: Machining and experimental conditions. 132

Table 19: Main specification of the thermocouple used [115]. 133

Table 20: Main specifications of POCO EDM-3® [108]. 140

NOMENCLATURE

CFAA	Center for Advanced Aeronautic Manufacturing
CNTs	Carbon Nanotubes
DoE	Design of Experiment method
EDM	Electrical Discharge Machining
EDS	Electrical Discharge Slicing
EDX	Energy Dispersive X-ray spectroscopy
EPMA	Electron Probe micro-analyser
FEM	Finite Element Model
GaAS	Gallium Arsenide
MRR	Material Removal Rate
NGV	Nozzle Guide Vanes
PMEDM	Powde Mixed EDM
SEDM	Sinking Electrical Discharge Machining
SEM	Scanning Electron Microscopy
SiC	Silicon Carbide

SKD 11	Tool steel
TWE	Tool Wear Rate
WEDM	Wire Electrical Discharge Machining
WZL	laboratory for Machine Tools and Production Engineering
Δt	Simulation time interval (s)
β_i	Coefficient to consider the curvature effect of the electrode (-)
σ	Ultimate tensile stress (MPa)
δ_0	Electrode deformation (µm)
λ	Thermal conductivity (W/(m.K))
ρ	Density **(**kg/m^3)
area	Discharge area (mm^2)
conc	Concentration of debris particles (-)
C_p	Heat specific capacity (J)
E	Energy generation in a single discharge (J)
E_{cond}	Energy conducted through the electrode (J)
E_{conv}	Energy transferred by convection from the electrode to the oil (J)

$E_{conv+rad}$	Energy loss by radiation and convection from the discharge area (J)
E_d	Energy absorbed by dielectric (J)
E_{deb}	Energy carried away by debris removed from the electrode (J)
E_E	Energy distributed into the electrode (J)
E_{Ei}	Energy value assigned to the section i of the electrode (J)
E_{ll}	Electrode lost length (mm)
E_r	Electrode wear edge radius (mm)
E_{others}	Energy lost due to radiation, ionization, light, sound, etc. (J)
E_w	Energy distributed into the workpiece (J)
E_{wa}	Electrode wear area (mm^2)
E_{wd}	Electrode wear distribution (mm)
$E_{working}$	Energy generated during $t_{working}$ (J)
f	Discharge frequency (Hz)
F_0	The force resulting from discharges (N)
F_E	Fraction of energy absorbed by the electrode (-)
G_w	Gap width distribution (mm)

G_{wmax}	Maximum gap along the profile (mm)
G_{wmin}	Minimum gap along the profile (mm)
I	Discharge current (A)
N	Number of measurements carried out for drawing the Laue Plot (-)
q	Specific heat source (J)
r	Debris particle diameter (μm)
R_a	Surface roughness (μm)
R_t	Maximum height of the profile (μm)
S	Cross-section area of the electrode (mm^2)
SV	Servo reference voltage (V)
T	Maximum applicable tension force (N)
$t_{backward}$	Backward time (s)
t_d	Ignition delay time (μs)
$t_{d,ave}$	Average of the measured t_d (μs)
$T_{eq.attachment}$	Equivalent temperature for material attachment (K)
$T_{eq.removal}$	Equivalent temperature for material removal (K)

$T_{experimental}\ (t,Z)$	Experimentally measured temperatures of the electrode (K)
$T_{model}\ (t, Z)$	Temperatures of the electrode calculated by the simulation model (K)
$T_{model}\ (t, Z)$	Simulated electrode temperature (K)
t_{off}	Discharge interval (µs)
t_{on}	Discharge duration (µs)
$t_{working}$	Working time (s)
U_0	Open circuit voltage (V)
U_e	Discharge voltage (V)
W_{cond}	Energy conducted through the workpiece (J)
W_{conv}	Energy transferred by convection from the workpiece to the oil (J)
W_{deb}	Energy carried away by debris removed from the workpiece (J)

Chapter I: Introduction

I. INTRODUCTION

Electrical discharge machining (EDM) is a thermo-electrical process in which the material is removed by a serial of rapidly occurring electrical discharges generated between the electrode and workpiece, which are immersed in a dielectric medium. The number of discharges and the power of each discharge is controlled by the main EDM parameters. By modifying them, the material removal rate, electrode wear rate, attained surface finishing and the resulting accuracy can be controlled.

While EDM is commonly thought as a slow manufacturing process, improvements in computer science and measuring and analysing instruments, combined with constant research of the process, have made possible a better understanding of the material removal process. This has resulted in the enhancement of the machining process, improving machining times, surface quality and widening the application fields. This way, in recent years, EDM has become a competitive solution in a wide range of part jobs.

I.1. Industrial context

The high complexity of the machining process, makes necessary continuous research in the field of EDM, in both academic and industrial terms. On the one hand, fundamental studies make possible a better understanding of the material removal process, which can result in findings applicable in industrial jobs. On the other hand, the industry is constantly facing new challenges driven by the market demands, such as the machining of more complex parts or the machining of new materials. This way, both scientific and industrial work, make possible the constant research of EDM technology. In this sense, the research work carried out in the present PhD dissertation combines both fundamentals studies with industrially practical studies.

The research work is focused on Sinking Electrical discharge machining (SEDM) technology and has as background three different applications: the slicing of single-crystal silicon carbide (SiC) material, the machining of high-aspect ratio slots and the machining of complex free form components.

Slicing of SiC material. SiC, due to its outstanding properties, can realize improvement of efficiency in several applications fields, such as electric power distribution and aerospace applications. However, the brittleness and hardness of the material makes the manufacturing of SiC wafer difficult. This fact, combined with the high cost of the material, makes necessary doing research to improve the manufacturing process, and thus, make possible the widespread of SiC-based devices.

Machining of high-aspect ratio slots. Machining of high-aspect ratio slots is a common operation in industry, particularly in mold and die and aerospace sectors. Considering that in EDM material hardness is not a limitation and that there is not contact between tool electrode and workpiece, EDM is a competitive solution in the machining of high-aspect ratio slots. Nevertheless, the EDM'ing of narrow slots is not a simple job, because debris accumulation makes the process unstable and the machining efficiency decreases. Thus, with the main objective of making the process more efficient, the machining of high-aspect ratio slots is a constant topic of research.

Machining of complex free form components. The need to enhance aerodynamic performance with light weight design of aircraft engines has increased the demand of free form components, such as bladed integrated disks (blisk) or impellers. The geometrical requirements combined with the materials of those components, has become multi-axis EDM a feasible solution in the manufacturing of those components, especially for the manufacturing of aerospace and energy turbine components. However, each part should be analysis in detail, due to its complexity. Because of that, also encouraged by the growing demand of those parts, it is necessary to develop more competitive machining strategies and reduce the required large practical expertise, and in many cases, trial-and-error strategies.

I.2. Objectives and contributions

The present Section summarizes the main objectives of the PhD Thesis and the contributions arisen form them.

To improve EDM cutting performance of SiC with specially designed foil electrode.

The main objective is to reduce the side surface area of the foil electrode, in order to reduce the high occurrence probability of side surface discharges and the high concentration of debris, which affects kerf width accuracy and machining stability.

In the aim to overcome both problems, two electrode designs were proposed: a foil electrode in which holes are machined and the insulation of the side surface areas by a resin layer.

To improve EDM performance in high-aspect ratio slot machining using multi-holed electrodes.

Due to debris accumulation in the narrow gap, the machining depth for stable machining is limited. The present study, proposed a multi-holed electrodes that guaranties the machining stability when machining high-aspect ratio slots, by the improvement of the flushing conditions. The geometry and the position of the holes machined on the electrode lateral faces were studied.

To develop a methodology for the determination of electrode wear and gap in multi-stage EDM.

With the main objective of studying electrode wear phenomena, a methodology for studying electrode wear pattern and gap width in multi-stage EDM of complex geometries, in which the average definition of wear is not enough, has been proposed. The methodology established different indicators for defining the electrode worn geometry and gap width distribution.

To study electrode wear phenomena ang gap width distribution.

The methodology proposed has been used for the study of different EDM jobs and to gather information in terms of both electrode wear and gap width patterns.

To propose a thermal model for prediction of temperature distribution in the electrode.

The main feature is that instead of simulating the temperature after the generation of each discharge, the model considers the energy generated during continuous EDM process and this energy is distributed over the electrode discharge area. This sets great value to the applicability of the model in industrial EDM jobs.

To propose a thermal simulation model for the definition of the heat transfer during continuous EDM process.

Based on the principles of the proposed thermal simulation model, an inverse simulation model is proposed to define the heat transferred to the electrode during continuous EDM. The methodology is based on the comparison of temperature results obtained experimentally with simulated temperatures.

I.3. Content layout

The work starts with a brief review of the State of the Art of the EDM process, **Chapter II**. Three are the main topics described: the thermal problem, the electrode wear phenomena and simulation works.

Chapter III describes a serial of cutting experiments and a study of the distribution of the discharge delay time carried out, for testing the effectiveness of the two foil electrodes proposed for SiC slicing by foil electrode.

Chapter IV, presents the findings of machining holes on flushing efficiency in high-aspect ratio slot machining. The usefulness of the proposed electrode has been validated by a serial of experiments as well as an analysis of discharges in the working gap.

After that, in **Chapter V**, a methodology proposed for electrode wear and gap width analysis is described in detail. Moreover, the methodology has been applied to three different EDM job, with which information in terms of electrode wear and gap width patterns has been gathered.

From the experimental studies, the importance of developing an electrode simulation model was highlighted. Consequently, **Chapter VI** proposes a thermal model for prediction of temperature distribution in the electrode.

Finally, **Chapter VII** enumerates the main conclusions drawn from the PhD Thesis and the future research interest generated during the doctoral training.

Chapter II: State of the art

II. STATE OF THE ART

Electro Discharge Machining (EDM) has become an indispensable technology in a wide range of manufacturing applications. Moreover, the continuous technological and scientific advantages, have resulted in a better understanding of the material removal process, which has not only enhanced the efficiency of EDM process, but also has enlarged the application fields of EDM.

The present Chapter has the aim of describing a series of industrial applications in which EDM is an indispensable technology and of describing the latest research works in terms of EDM technology. Firstly, three Sinking EDM (SEDM) applications of current research are described. Then, the thermal problem in SEDM is presented. After that, the electrode wear phenomena is described, and for finishing, the latest approaches for electrode wear simulation during EDM process are discussed.

II.1. Latest developments in Electrical Discharge Machining

EDM is a thermo-electrical process in which the material is removed by a serial of rapidly occurring electrical discharges generated between the tool electrode and workpiece, which are immersed in a dielectric medium.

The material removal mechanism is a very complex phenomenon which involves many physical processes. Figure 1 shows a scheme of the removal mechanism. A detailed explanation of EDM process is described in the PhD Thesis of Dr. Izquierdo [1].

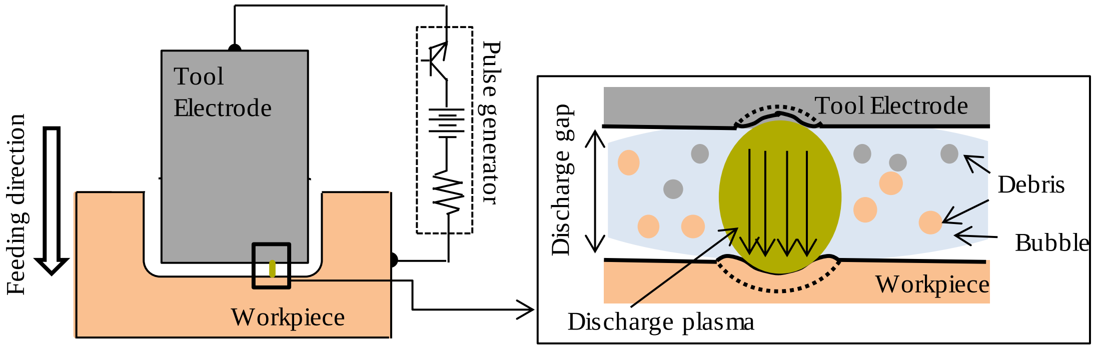

Figure 1: Scheme of the material removal mechanism.

EDM process has become an indispensable technology in a wide range of manufacturing applications, such as die mould making, aerospace and energy industry and micro-machining. One of the great advantages over conventional manufacturing processes is that material hardness is not a limitation, which enables the processing of complex geometries in difficult to machine materials [2]. Moreover, in EDM there is not contact between electrode and workpiece, which avoids mechanical stresses, chatter and vibration problems during machining.

EDM technology has developed rapidly in recent years. Improvements in computer science and measuring and analysing instruments have made possible a better understanding of the process, enhancing the removal mechanism and widening the application fields. One example is the possibility of processing insulating materials such as, ceramics by using the assisting electrode method by Sinking EDM (SEDM) or by Wire EDM (WEDM) in working oil [3]. A scheme is shown in Figure 2. In this machining method, a conductive carbonized layer is continuously generated on the workpiece surface, resulting in a stable machining. Therefore, EDM has become a potential technology for the machining of a wide range of ceramics in various industries [4].

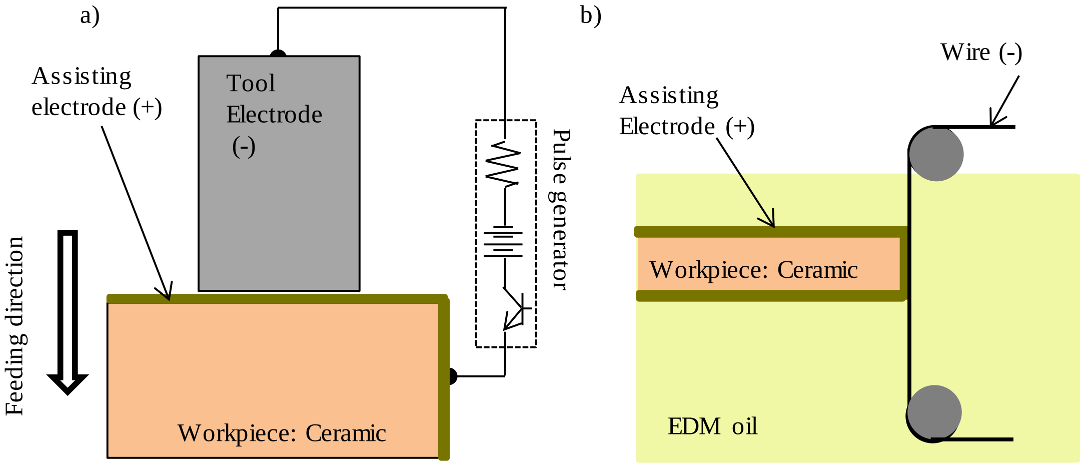

Figure 2. Scheme of the assisting electrode method for the EDM'ing of insulating materials.

Another technology that will bring great improvement in SEDM is the 'ultra low wear technology' developed by commercial EDM machine tool manufactures. Two examples are the QX Project technology of ONA Electroerosion S.A. [5] and AD35L and ADL55L EDM machines of Sodick Co., Ltd. [6]. Nevertheless, electrode wear phenomenon is not yet fully understood, and it is expected that its understanding will bring improvements in the capability and productivity of the machining process. Hence, the understanding of electrode wear process is an active topic of research.

Furthermore, different EDM machine manufactures, such as Sodick Co., Ltd. and Makino, INC. , have implemented a linear motor technology over the basic ball screws system for axis movement. They confirmed that this technology offers improvement in accuracy, repeatability, speed and acceleration, as well as maintenance cost reduction. The use of high-speed jump motion of tool electrode enhances the flushing conditions, resulting in great benefits in the manufacturing of high-aspect ratio slots or deep holes in which the concentration of debris results in a decrease of the material removal rate [7].

In addition, Makino, INC., for instance, developed an ‘ArcFree’ system, which sets safety settings to prevent damaging discharges [8]. This technology, coupled with fast servo control response time, enables safe, unattended burning, even when the current applied to an electrode exceeds its maximum current density, which frequently occurs when machining complex geometries.

Moreover, mechanical and technological advanced have made possible the implementation of two machining heads, which can reduce the total machining time up to 50%. For instance, ONA Electroerosion S.A. offers different machine sizes with two heads [5]. Each machine head is controlled by an independent machine control, which allows two shapes to be machining simultaneously and independently.

On the whole, there is no doubt that the active research of EDM process not only brings scientific knowledge, but also advances in machine tools, improving productivity and capability of EDM process.

II.2. SEDM applications of current research

When analyzing the feasibility and efficiency of the process, three are the main outputs that are considered: tool wear ratio (TWR), material removal rate (MRR) and surface roughness (R_a). Those output parameters are the results of the combination of different factors, such as machining parameter setting, the flushing efficiency in the narrow gap and the electrode geometry.

In the clear majority of applications, the ideal scenario will be to work with the machining conditions that result in the lowest TWR and maximum MRR at the required R_a. However, as a wide range of factors are implied in the material removal mechanism, it is not possible to work in those conditions. Hence, the optimum EDM parameters are conditioned by the requirements of the EDM job. For example, in some cases, TWR will be a priority and in others the surface roughness. For instance, Figure 3 shows a simple scheme of three different discharge current waveforms [7]. It shows the importance of choosing the right machining parameters for a given application.

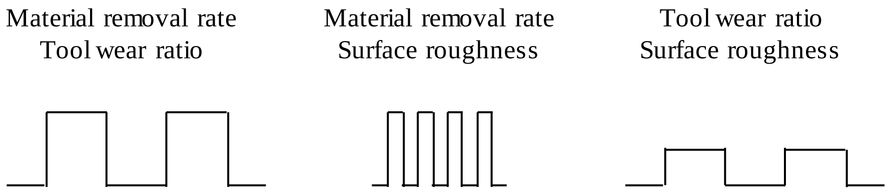

Figure 3: Relation between discharge current waveforms and output variables.

Therefore, in the industry the workpiece requirements are essential for defining the machining strategy. To understand this, three different industrial applications of SEDM of current research are described, which are:

- Silicon Carbide (SiC) slicing by foil electrode.

  SiC is a semi-conductive material, and due to the high price of SiC wafer and its manufacturing cost, a narrow kerf loss is necessary. Hence, the kerf loss minimization is a topic of research (see Section II.2.1).
- High-aspect ratio slot machining.

  High-aspect ratio machining operation is used in a wide range of components. Due to debris accumulation in the narrow gap, MRR decreases with the machining depth and thus, machining time increases. Considering the high competitiveness of the market, a reduction of machining time is a key factor. Thus, effort should be paid in the enhancement of the flushing conditions (see Section II.2.2).
- Free form complex geometries.

  This type of components have a high added-value, because of the part materials, the tight tolerance and the complexity of the manufacturing process. In this type of operations, for obtaining the final workpiece shape, a large number of electrodes are necessary. Furthermore, the electrodes are difficult to machine and thus, their cost is considerable. Consequently, an electrode design and machining path that minimizes the number of electrodes per operation will carry huge economic advantages. Thus, contributions of electrode wear phenomena when working with free form complex geometries are necessary for both industrial and academic terms.

  The objective is to obtain a precise geometry; thus, the control of the electrode wear is of high interest (see Section II.2.3).

In the following sub-sections, each technology is described.

II.2.1. SiC slicing by foil electrode

Recent developments highlight the need to enhance the electrical and physical properties of power devices. Conventional semiconductors such as Silicon and Gallium arsenide (GaAs), are reaching their limits in terms of maximum operating temperature, power handling and conversion efficiency in power modules. Therefore, single crystal SiC is becoming a promising material.

SiC has superior properties over Si in terms of wider bandgap energy, higher electron saturation drift velocity, and higher thermal conductivity etc. Hence, SiC-based electronic devices can work under extreme environments such as high temperature, high voltage, and high frequency, in which conventional semiconductors cannot function [9]. For this reason, SiC has become one of the most suitable materials for next generation power electronic devices [10]. It can realize improvement of efficiency in several application fields, such as electric power distribution and aerospace applications [11]. A further description of SiC material, applications and material processing was described in the PhD Thesis of Dr. Zhao [12].

Whilst SiC-based devices can realize great improvements, SiC device fabrication technologies are still not sufficiently developed to the degree required for widespread technologies. One of the main obstacles is the high price of SiC wafer and its manufacturing cost. It is therefore very important to reduce maximum material loss during the manufacturing process in order to decrease wafer costs. Moreover, SiC is considered an extremely difficult-to-machine material, due to its high hardness and brittleness, which causes great problems in machining. Hence, challenges are faced in terms of SiC slicing due to the need to reduce kerf loss and slicing time [13].

One available alternative method for SiC wafer slicing is wire electrical discharge slicing (EDS). Figure 4 shows a prototype multi-wire electrical discharge processing technology developed by Mitsubishi Electric Corporation [14]. However, there is a high risk of wire breakage due to discharge concentration. This drawback sets limits to the improvement of machining performance and it limits the minimum wire diameter, which results is a widen kerf loss. Furthermore, the tension force that can be applied to the wire is limited and wire vibration occurs, significantly affecting machining accuracy [15][16].

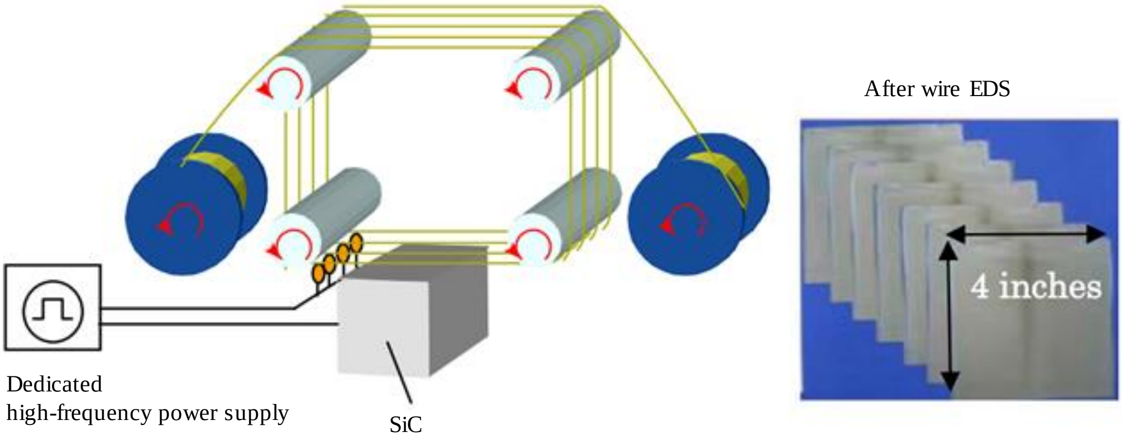

Figure 4: Multi-wire EDS prototype developed by Mitsubishi Electric Corporation [14].

In order to reduce wire vibration by applying a larger tension to the wire, Okamoto *et al.* [17] proposed a track-shaped section electrode. They proposed a brass coated steel wire with a track-shape section of aspect ratio 1:2:0. By this method, they improved the kerf shape. Nevertheless, the wire vibration problem cannot be eliminated.

As a consequence, in order to improve the machining performance and decrease the kerf loss, Zhao *et al.* [18][19][20] developed an EDS with a thin foil electrode. With this technique, a thin rectangular foil is used instead of wire. Figure 5 shows a scheme of the technique. Moreover, with the aim of avoiding foil electrode vibration during machining, and thus improve kerf accuracy, the foil electrode is tensioned with a specially designed tensioner and is placed in the main axis of the sinking EDM machine. Machining is conducted by servo feeding the foil electrode to the workpiece with the way of sinking EDM. The process is explained in detail in the PhD Thesis of Dr. Zhao [12].

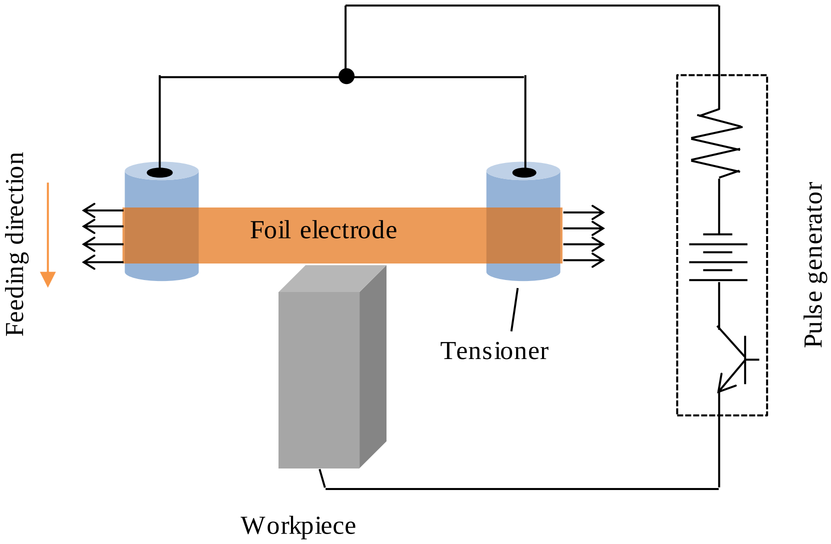

Figure 5: Scheme of principle of SiC slicing by foil electrode [18].

One of the advantages over wire EDM is that the thickness of the foil can be made smaller than the wire diameter under the same tension force, which results in a smaller kerf loss. Figure 6 compares the cross section of both wire electrode and blade electrode. Furthermore, as high tension can be applied to the foil electrode, tool vibrations can be avoided. These two factors have a high impact in the value of kerf loss. Moreover, this technique has a lower risk of tool breakage problems, which is an advantage in the optimization and monitoring of the machining process.

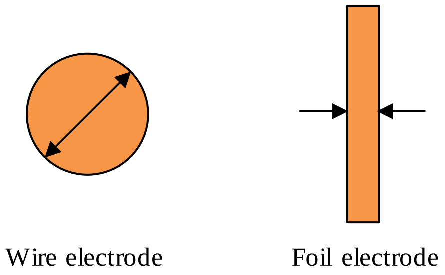

Figure 6: Comparison of the cross-section area of wire and foil electrode.

In terms of machining parameters optimization, Zhao *et al.*[18] concluded that negative polarity of tool electrode and short discharge duration are more suitable for EDS by foil electrode in terms of electrode wear, kerf loss and machining time. Furthermore, a comparative study between the use of EDM oil and deionised water when EDS SiC indicated that EDM oil is more appropriate in terms of kerf width, workpiece surface damage and tool electrode wear ratio [19].

Moreover, in order to reduce electrode tool wear and to improve the flushing conditions,the an experimental set-up for EDM reciprocating was developed [20]. This set-up is thought for the slicing of SiC ingot during continuous machining.

In comparison with WEDM, Zhao *et al.* [18] demonstrated that by using a thin foil electrode, the kerf width value can be reduced from 200 µm, which is a typical value for WEDM, to 100 µm. Moreover, analysis of the cross-section profiles of cut kerf indicates that the inlet kerf width value is larger than that of the outlet and that a larger cutting depth results in a widened kerf loss. Figure 7 shows an example of the cross-section of a cut kerf obtained using a foil electrode of 15 mm in width with a pre-set cut depth of 19 mm. The widening of the kerf can be attributed to the increase of the occurrence probability of side surface discharges due to the large surface area of the foil electrode and the concentration of debris particles in the narrow side gap.

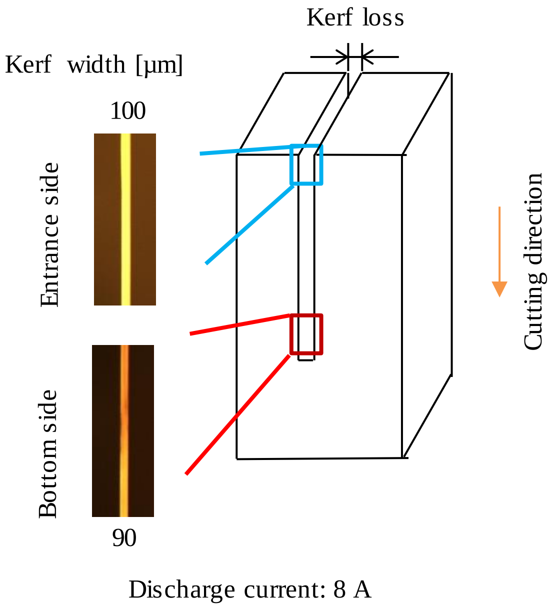

Figure 7: Cross-section profiles of cut kerf in previous research works [18].

Thus, it is clear that one of the main drawbacks of this technology is the large surface area of the foil electrode, which has a high impact on the machining performance and kerf loss.

With the goal of reducing the kef loss and improve the machining performance, in Chapter III two electrode designs are proposed: a coated foil electrode and an electrode with holes. The feasibility has been tested with three different slicing strategies: no strategy, applying jump motion of the tool electrode, and applying reciprocating motion. The output parameters discussed are: electrode wear, cutting speed and kerf loss. Moreover, a fundamental study of the influence of electrode design on the probability of occurrence of side surface discharge has been carried out.

II.2.2. High-aspect ratio slot machining

In EDM the material hardness is not a limitation, which has implied benefits in comparison with the conventional machining method, particularly in the machining of high-aspect ratio slots in difficult-to-machine materials, in which EDM has become an indispensable technology.

Manufacturing of deep slots is a common operation in industry, with special focus on two sectors: mold and die industry and aerospace industry. In the former, for instance, narrow slots are machined in the mold in order to provide thin strengthening ribs. In the latter, due to the working requirements of turbine engines, high temperature resistant materials are used, such as Titanium-base or Nickel-base alloys.

One example is the machining of the slots used to join the NGVs (Nozzle Guided Vanes). Currently, in this application, EDM is regarded as the most competitive solution [21]. Figure 8 illustrated a slot machining by EDM. For further information of this part and other parts of aerospace engines, look up the PhD Thesis of Dr. Ayesta [22].

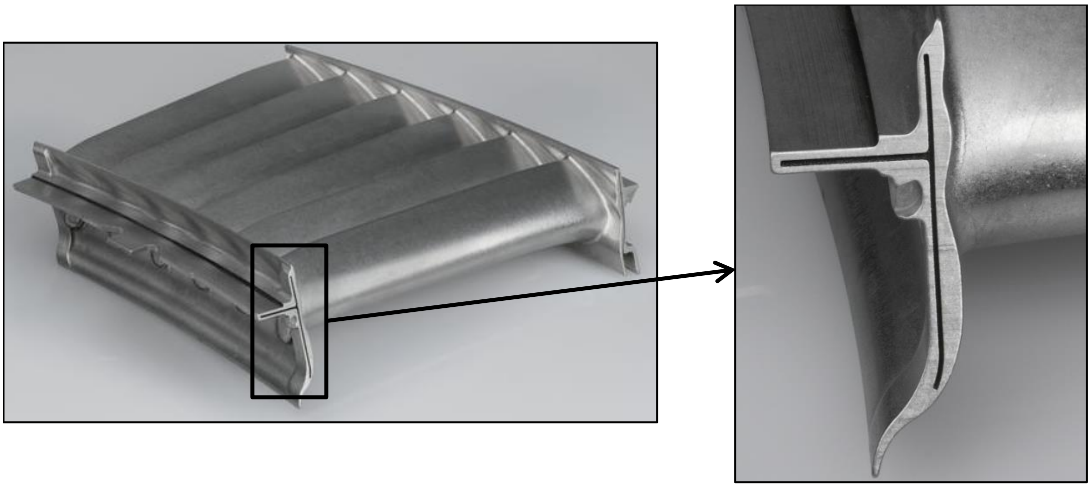

Figure 8: Example of a high-aspect ratio slot machining on an NGV [5].

However, the machining of high-depth slots is not an easy task. The main drawback is that there is a high concentration of discharges in the bottom section of the electrode, and that as the depth increases debris evacuation becomes difficult or even impossible. As a consequence, the stability of the process get affected and the material removal rate decreases [23].

Recent studies can be found in the scientific literature concerning the optimization of the EDM process of high-aspect ratio slots. Much of those works are focused on aerospace applications, mainly due to the high competitiveness of the market. In those applications, the key objective is to reduce the machining time or the total production time.

A number of researchers have explored the effectiveness of choosing different EDM process parameters and electrode materials. Uhlmann and Domingos [24] optimized the machining parameters for the EDM'ing of high-aspect ratio slot machining in MAR-M247 material with graphite electrodes. Firstly, they estimated the maximum discharge current that can be used in order to fulfil the workpiece surface quality requirements. Then, they carried out a serial of experiments planned by Design of Experiments Methods (DoE). By adjusting the process parameters, they reduced the machining time of 11 mm depth slots with an electrode discharge area of 89.50 mm^2, from 48 min to 21.9 min adjusting the process parameters.

Ayesta *et al.* [25], by a DoE too, analysed the influence of process parameters. They used 0.8 mm graphite sheets for electrode and C1023 for workpiece. The discharge area was of 40 mm^2 and pre-set machining depth was of 6.5 mm. They conducted a serial of experiments to understand the effect of discharge current, discharge duration and servo voltage on electrode wear and machining time. They concluded that lower machining times were obtained by a combination of high discharge current, high pulse time, and low servo voltage.

In terms of electrode material, Aas [26] compared the machining outputs of two types of graphite qualities, Poco EDM-3® and Poco EDM-AF5®, in an IN 100 mod Ni-base alloy workpiece material. They studied the influence on MRR and electrode wear when EDM'ing slots of 4.4 mm depth with an approximate discharge area of 125 mm^2. From those experiments, it was concluded that if productivity is a priority, the use of graphite of large grain size is more appropriate.

However, as reported by Klocke *et al.* [27], because of debris particle concentration in the narrow gap, gap temperature and the ionization conditions of the dielectric fluid, the stability of the process cannot be guaranteed. During the early stage of machining, debris evacuation is relatively effortless and as a consequence machining is stable. Nevertheless, when the depth increases, debris particles become stuck in the narrow gap and the process becomes unstable, resulting in a dramatic decrease in the rate at which material can be removed.

This phenomenon was also reported by Obaciu *et al.* [28] when comparing the machining performance of two different workpiece materials. They observed that as the erosion depth increases, MRR decreases and the number or short circuits increases. Thus, the increase of process time can be explained with the difficulty of removing debris particles as the machining depth increases. As a consequence, it is expected that an enhancement of flushing conditions will contribute to the optimization of the process.

Following that hypothesis, various strategies have been developed in order to improve debris removal from the working gap. Uhlmann and Domingos [29] [30] developed a vibration-assisted EDM-machining technology, Figure 9 shows the 3D view of the developed piezo-unit, and they observed improvements in material removal as well as in electrode wear. This technology was validated by machining a 11 mm depth slot with an aspect ratio of 12 in MAR-M247 material workpiece. With the optimization of frequency and amplitude, an increase of 11% of the MRR and the reduction of 21% of tool electrode wear was achieved [29]. The improvement was attributed to the enhancement of machining stability, due to the importance of the flushing conditions in the narrow gap. Furthermore, in a further study they analysed the influence of the vibration assisted EDM process applying a high-frequency oscilloscope. At the beginning of the machining, no difference was observed, however as machining depth increases the difference became clear. The quality of discharges was better when vibration was applied. However, they observed that once the erosion depth exceeded 8 mm the machining performance decreased [30].

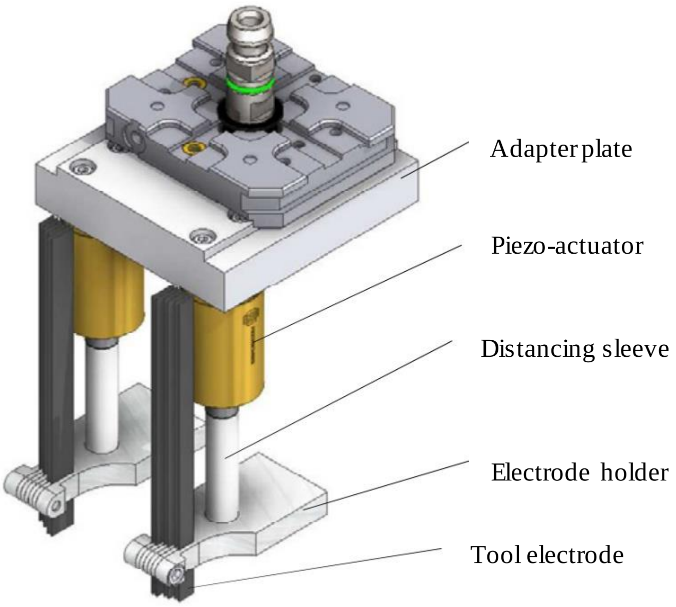

Figure 9: 3D view of the design if the set-up [29].

A further technology that brings improvement in terms of flushing conditions is the use of jump motion by linear motor equipped machines. Cetin *et al.* [31] studied the effect of jump motion when using a 10 mm diameter cylindrical electrode. They observed that the electrode jump height is the most relevant factor in machining speed. However, as reported by Liao *et al.* [32], the work presented in [31] does not take into account the fact that the effectiveness of debris evacuations is related with electrode geometry. Hence, Liao *et al.* [32], observed the gap conditions in two different electrode geometries: square electrode and thin-wall electrode. Debris evacuation becomes more difficult when working with thin electrodes than with square section electrodes.

In practice, both vibration-assisted EDM-machining and the use of high-acceleration linear motors require the use of extra equipment, which is not available to many users. Hence, Chapter IV introduces a new electrode design that improves the flushing conditions and thus, the EDM process is enhanced. Results have been discussed in terms of electrode wear, machining time and by a fundamental study of discharge parameters.

II.2.3. Free form complex geometries

The need to enhance aerodynamic performance with light weight design of aircraft engines has increased the use of complex free form components, such as bladed integrated disks (blisks), impellers and NGVs among others. Those turbomachinery parts do not only require complex design, but also materials must have high resistance to temperature, creep, corrosion and fatigue [33]. Therefore, multi-axis EDM has become a feasible solution in the manufacturing of aerospace and energy turbine components. For further information of turbomachinery parts look up the PhD Thesis of Dr. Ayesta [22].

In EDM, the accuracy of the cavity is largely affected by electrode wear and gap value. Moreover, the material removal mechanism is a very complex phenomenon which involves many physical processes [7]. Thus, nowadays, when machining complex geometries, for instance shrouded blisk, the process requires large practical expertise, and in many cases, trial-and-error strategies, involving costly manufacture of electrodes [34].

In the machining of shrouded blisks or other geometries that require multi-axis operations, electrode feeding path and electrode designs are the two main challenges to achieve the required accuracy. Considering the growing demand of this type of free form geometries, in the last years different researchers have developed different electrode path and electrode design searching algorithms.

Wu *et al.* [35] used Lagrange equations to solve the electrode feeding path searching algorithm. However, the solving method is very complicated and not useful for standards applications. Li *et al.* [36] proposed an electrode searching path method in which the main electrode feeding freedom degree is chosen and the others are classified as auxiliary. Firstly, the main degree is move backwards along the actual feeding direction and then, the others are moved to avoid the contact between the electrode and the workpiece. If the electrode is not able to leave the workpiece, the electrode size is reduced until a solution is achieved.

Ayesta *et al.* [37] also proposed a similar method which is described in detail in her PhD Thesis [22]. Ayesta *et al.* proposed an objective function which calculates the erosion paths in multi-axis

EDM. The path generation algorithm was verified by the manufacturing of the shrouded blisk presented in Figure 10.

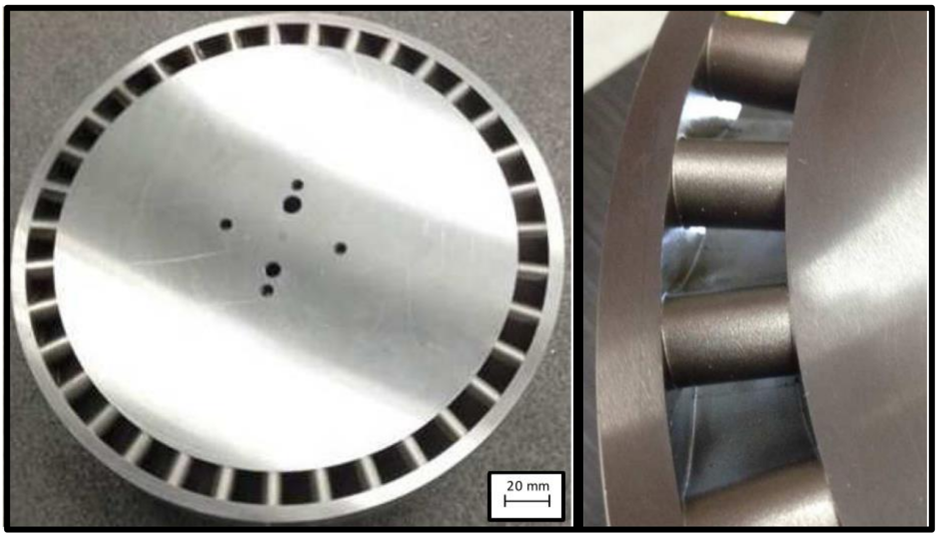

Figure 10: Example of a EDM'ed shrouded blisk [37].

Nevertheless, as well as in the other models, electrode wear is not considered when obtained both the electrode feeding path and the initial electrode design. This indicates, that even if advances have been done, the optimum algorithms should consider electrode wear and adjust the electrode geometry based on it. This is the main reason that justified the huge effort that should be paid in terms of electrode wear phenomena analysis when working with free form complex geometries. In the following paragraphs, the most relevant research works concerning electrode wear are described.

In terms of machining parameters, discharge duration, discharge interval and rising current slope are recognized by Maradia *et al.* [38] as the primary parameters affecting electrode wear. Moreover, it has been reported [39][40] that large pulse duration leads to a smaller electrode wear. As a wide range of studies have concluded, the increase of discharge current results in the increase of electrode wear. This is because with large discharge current the overheats of the electrode increases [25][41][42]. Mohri *et al.* [39] and Maradia *et al.* [40] reported that large discharge duration leads to a smaller electrode wear. This phenomenon is caused by the formation of a carbonaceous protective layer on the electrode surface, in such a way that electrode wear is prevented.

Furthermore, if machining parameters are not suitable, as Itoh and Meadows [43] and Klocke *et al.* [44] described, this layer, also known as material build-up, is likely to appear on the edges and the corners of graphite electrodes. A more detailed description of electrode wear phenomena has been presented in Section II.4.

Another source of inaccuracy is the lack of knowledge of gap dimensions, especially when machining complex geometries. Gap width is not only conditioned by machining parameters, but also by discharge area and gap conditions [45][23].

Former works and industrial practice show the influence of process parameters, electrode geometry and time dependence on electrode wear, however, the influence of machining path has not been studied yet. This last, is a critical factor in high-added value sectors such as aerospace and energy turbine manufacturing. In those cases, the average definition of wear commonly found on EDM technology is not enough. Hence, Chapter V proposes an easy to put in practice methodology that defines a serial of wear and gap width indicators for the analysis of both electrode wear and gap width in complex geometries. Moreover, those indicators have been used in different EDM machining cases for collecting information of electrode wear patterns.

II.3. Thermal problem in SEDM

The main mechanism of material removal in EDM is the thermal heating of both electrode and workpiece due to the heat generated by the plasma channel in the gap between electrode and workpiece. When the surface temperature reaches the melting or vaporization point a crater is generated and material is removed. Therefore, the understanding of the thermal problem plays a vital role in EDM process.

Considering the complexity of the material removal process, even if research works have been carried out during the last decades, nowadays there is not a full understanding of the process. Two are the main reasons. One reason is that, in the discharge gap several factors take place at the same time, which leads to difficulties in terms of process analysed. The other reason is that, even if in EDM process the material removal is the result of an accumulative discharges, actual EDM cannot be analysis as a linear superposition of the result of single discharges. This is because the gap conditions change during machining, such as the temperature of the dielectric in the gap, the debris particles movement and quantity and bubble generation. In this section the most relevant factors that researches have studied to understand the material removal in EDM are described in detail.

II.3.1. Energy generation during SEDM process

The discharge generation can be divided in three main phases: preparation phase for ignition, phase of discharge and interval phase between discharges. Figure 11 represents a real current and voltage signal in which the three phases are clearly presented.

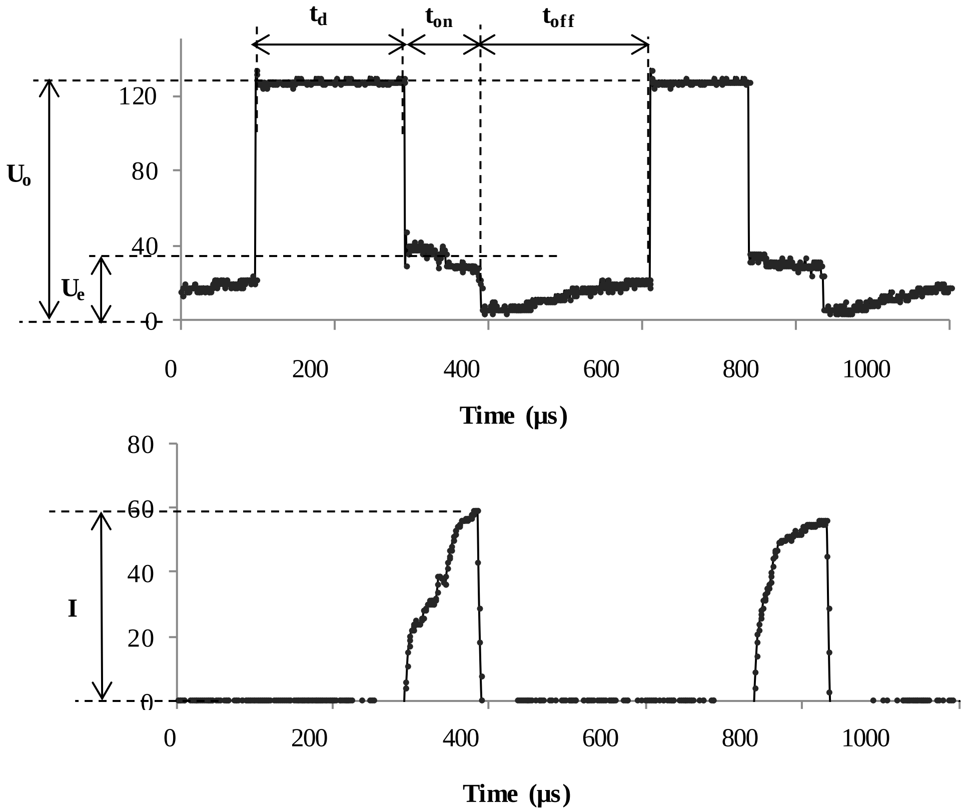

Figure 11: Example of voltage and intensity waveform of two consecutive discharges.

Where U_o refers to open circuit voltage, U_e to discharge voltage, I to discharge current, t_{on} to discharge duration, t_{off} to discharge interval and t_d to ignition delay time.

The preparation phase for ignition takes places during t_d. The purpose of the phase is to break down the dielectric strength to generate the plasma channel. Then, the discharge phase takes place during t_{on}, in which the energy for material removal is generated. As reported by Natsu *et al.* [46] the plasma channel is expanded rapidly after the dielectric breakdown, and then, it remains constant until the extinction. The intense heat generated in the plasma channel is the main cause of material removal. Finally, during the interval phase the discharge ends and the plasma channel is de-ionized. For a stable machining, discharge interval time, t_{off}, should be sufficiently long for the plasma extension and the recovery of the dielectric breakdown strength.

The amount of energy generated in a single discharge (E) is defined by three parameters: t_{on}, I and U_e and it is calculated by the following equation:

$$E = \int_0^{t_{on}} U_e \cdot I \, dt \qquad \text{Eq.1}$$

From Eq.1, it may seem that the calculus of the total energy generated during machining is a simple calculation. However, as illustrated by Figure 12, in actual machining different types of discharges occur: normal discharges, arc discharges and short-circuits.

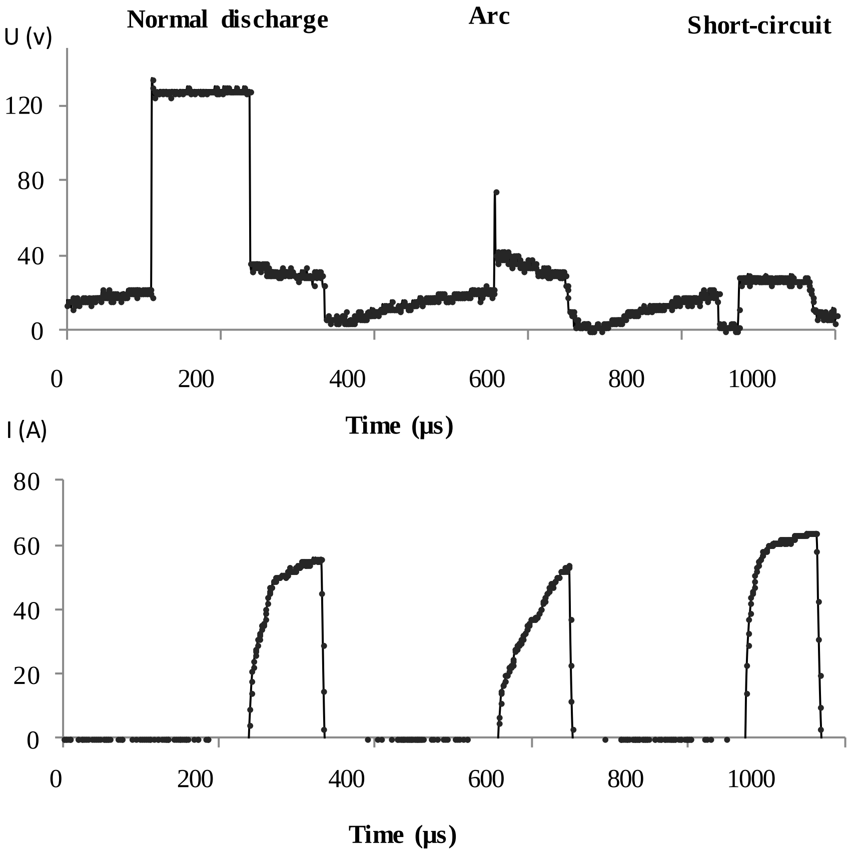

Figure 12: Example of the three types of discharges that may occur during EDM'ing.

The optimum discharge, and the one that is desirable during the actual machining, is the normal discharge. However, due to debris generation, electrode geometry, incorrect machining parameters etc. the machining conditions are affected, and the other two types of discharges are also generated.

Arc type discharges are a consequence of early ionization. In this case, the discharge is generated before reaching the open voltage. The most damaging discharges are the short-circuits. They are a result of contact between the electrode and the workpiece [47]. Consequently, as during actual machining the three types of discharges are generated, numerous researchers have reported that the uncertainty nature of multi-discharges is the main obstacle in the analysis of EDM process [48].

At this point it should be mentioned, that modern advanced machine generators automatically detect unstable machining conditions by the analysis of the discharges in order to avoid machine inaccuracies. When unstable conditions are detected, the first step of the adaptive power control is to extend t_{off} value [49].

Furthermore, not only the energy per discharge will condition the material removal, but also the discharge current and voltage signal shape. In the patent developed by Boccaoro and Bonini [50], the effect of *I* shape is described. Figure 13 represents four different current waveforms with the same discharge energy (which can be calculated by Eq.1). They observed that even if *E* is the same in the fourth cases, the results of MRR and electrode wear differ. For instance, a) discharge will produce higher MRR and higher electrode wear than b) discharge.

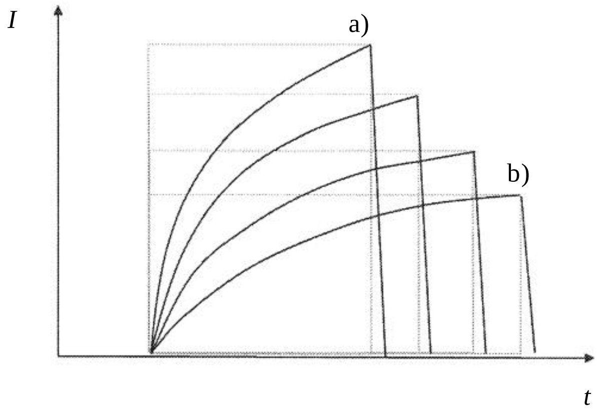

Figure 13: Four different discharge current signal with the same discharge energy [50].

II.3.2. Energy distribution

Another factor to consider when studying the material removal mechanism is the distribution of the energy generated. Figure 14 shows a simple scheme of the energy distribution of a single discharge.

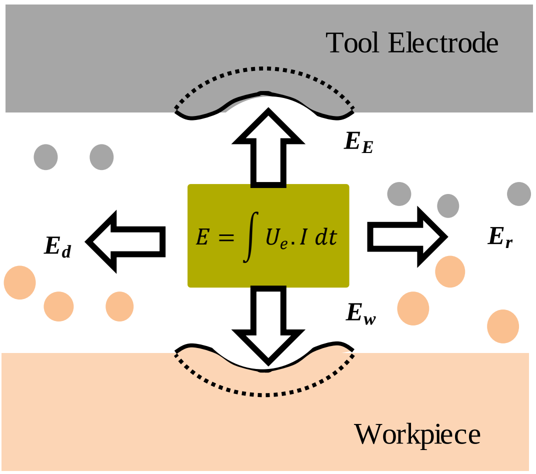

E	Energy generated during the discharge
E_e	Energy distributed into the electrode
E_{cond}	Energy conducted through the electrode
E_w	Energy distributed into the work piece
E_d	Energy absorbed by dielectric
E_r	Energy lost due to radiation, ionization, light, sound etc.

Figure 14: Energy distribution scheme of a single discharge.

The total discharge energy, E, supplied into the discharge gap is distributed among four main parts: Energy into workpiece E_w, energy into electrode E_e, energy into dielectric E_d and energy loss by radiation, ionization, light, sound etc. E_{others}.

$$E = E_E + E_W + E_d + E_{othres} \quad \text{Eq.2}$$

In terms of process efficiency two are the main energy fractions that must be studied E_e and E_w. E_e can be defined by three ratios: energy evacuated from the electrode by conduction E_{cond}, energy carried away by debris E_{deb}, and energy loss by radiation and convection from the discharge area $E_{conv+rad}$.

$$E_E = E_{cond} + E_{conv+rad} + E_{deb} \quad \text{Eq.3}$$

The same explanation can be given for the energy distributed to workpiece Eq.4.

$$E_W = W_{cond} + W_{conv+rad} + W_{deb} \quad \text{Eq.4}$$

Both energy indicators can be used as indicators of the efficiency of the process. For instance, higher MRR and lower electrode wear will be obtained if higher energy is distributed to workpiece and less to electrode.

Furthermore, researchers such as Vinoth Kumar and Pradeep Kumar [51] have described the effect of the amount of energy dissipated to dielectric. They compared the MRR and TWR between conventional EDM and cryogenic cooling of the electrode. Results showed that lower MRR and lower TWR is expected by cryogenic cooling. They concluded that MRR reduction is due to the increase of the energy absorbed by the dielectric and TWR due to the decrease of electrode temperature.

II.3.3. Definition of energy fraction to electrode by temperature measurements

The energy generated can be defined by U_e, I and t_{on}, see Eq.1. The energy is distributed in the discharge gap and only part of the energy is transferred to the electrode. One of the contribution of the present PhD Thesis is to develop a novel method that predicts the temperature of the electrode during continuous machining. The first step, is to develop a method for the definition of the energy absorbed by the electrode, F_E.

The fraction of energy absorbed by the electrode, F_E, can be defined by Eq.5. The present section reviews the main publications that have contributed to the definition of F_E.

$$E_E = F_E \cdot U_e \cdot I \cdot t_{on} \quad \text{Eq.5}$$

Many works examined the energy distribution of a single discharge in order to determine the energy absorbed by electrode and/or workpiece. For instance, Xia *et al.* [52][53], by considering copper as electrode and workpiece, concluded that the influence of t_{on} is small and that the material removal difference between both electrodes is attributed to carbon adhesion in the cathode and not due to energy distribution [52]. Furthermore, by measuring the temperature of dielectric fluid during continuous machining, they observed that the energy absorbed by the dielectric is small in comparison with the energies absorbed by the workpiece and the electrode [53]. Additionally, by comparing the temperature rise on electrode by a finite-difference method, they determined that 34% is the percentage of the total energy absorbed by the electrode [54].

Okada *et al.* [55], by measuring the temperature of both electrode and workpiece and by applying the heat transfer equations, concluded that F_E is in the range between 24% and 29% depending on the discharge parameters used. Electrode temperature was measured at three different heights from the discharge area: 10 mm, 20 mm and 25 mm. Moreover, to avoid the effect of conduction between electrode and EDM oil, they used a methacrylate box. Nevertheless, in actual machining the effect of conduction should be considered. In terms of machining parameters, as previously reported by Xia *et al.* [52][53] too, they confirmed that discharge duration does not have significant influence on the energy distribution ratio and they also observed that larger I results in the decrease of the fraction of F_E.

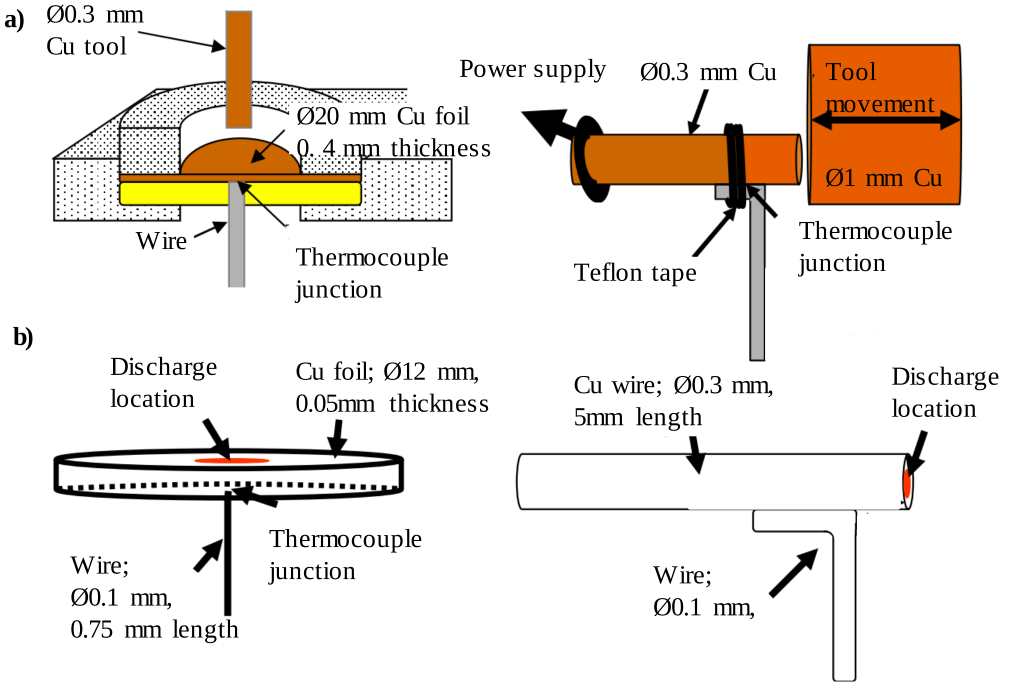
a)
Ø0.3 mm Cu tool
Ø20 mm Cu foil 0. 4 mm thickness
Wire
Thermocouple junction
Power supply
Ø0.3 mm Cu
Tool movement
Ø1 mm Cu
Teflon tape
Thermocouple junction
b)
Discharge location
Cu foil; Ø12 mm, 0.05mm thickness
Thermocouple junction
Wire; Ø0.1 mm, 0.75 mm length
Cu wire; Ø0.3 mm, 5mm length
Discharge location
Wire; Ø0.1 mm,

Figure 15: a) Temperature measurement experimental set-ups; b) Calculation models [56].

Zahiruddin and Kunieda [56][57] concluded that in micro-EDM energy distribution ratio is between 10% and 15%. They used copper for both electrode and workpiece. They highlighted that contrary to conventional EDM process, in micro EDM the ratio of energy carried away by debris should be considered. Therefore, they summated the fraction of energy loss due to convection with the fraction of energy carried away by electrode debris. They compared the temperatures on electrode with a 3D model for the calculus of energy distribution. Figure 16 shows the algorithm used. Furthermore, they considered that material removal should be divided in terms of material removal by melting and material removal by vaporization.

In their work they used two different experimental set-ups: set-up for copper foil and set-up for wire. Figure 15.a shows the experimental set-ups and Figure 15.b shows the calculation model developed. Moreover, the efficiency of the model was validated at two positions, at 1.59 mm and at 0.88 mm from discharge area.

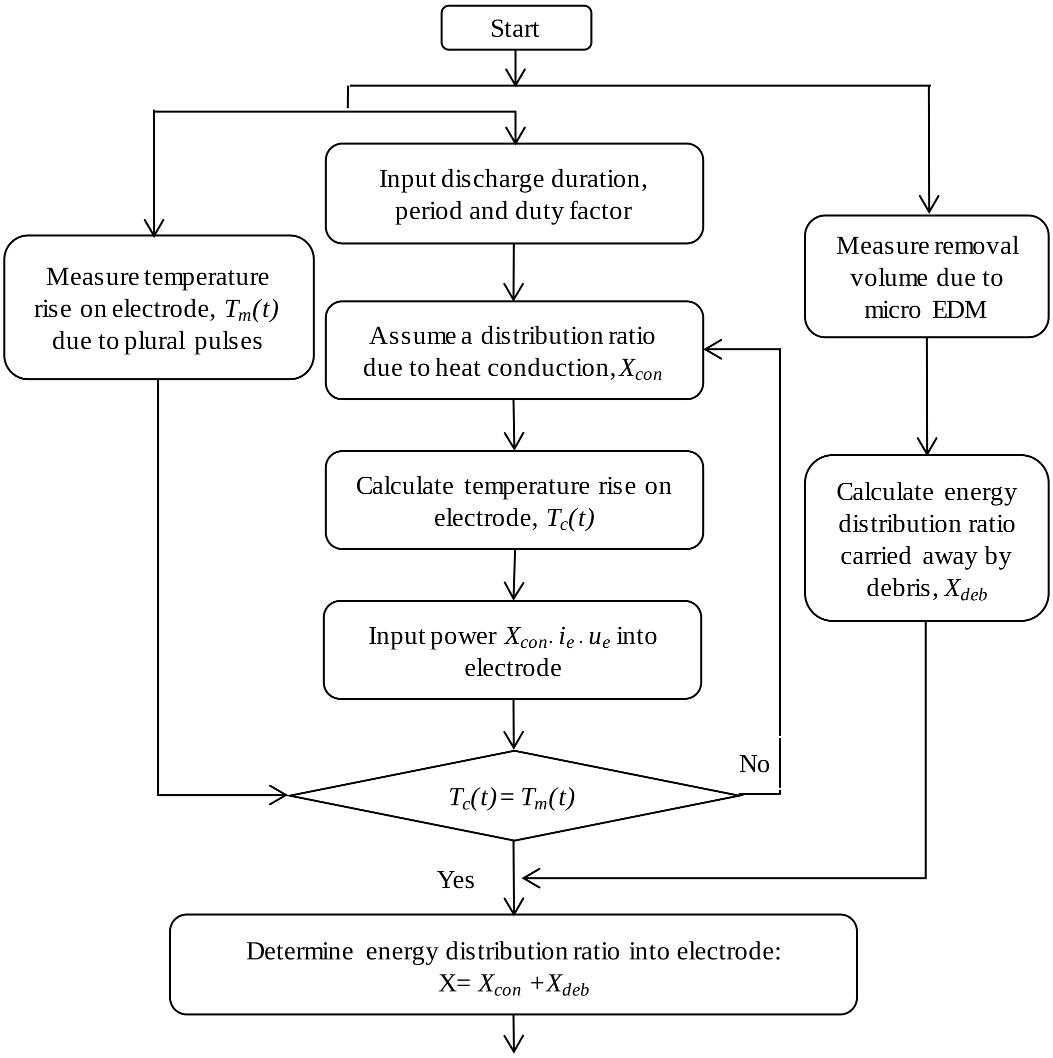
Start
Input discharge duration, period and duty factor
Measure temperature rise on electrode, $T_m(t)$ due to plural pulses
Assume a distribution ratio due to heat conduction, X_{con}
Calculate temperature rise on electrode, $T_c(t)$
Input power $X_{con} \cdot i_e \cdot u_e$ into electrode
Measure removal volume due to micro EDM
Calculate energy distribution ratio carried away by debris, X_{deb}
$T_c(t) = T_m(t)$
No
Yes
Determine energy distribution ratio into electrode: X= $X_{con} + X_{deb}$

Figure 16: Algorithm used for determining the energy distribution into electrode [56].

Revaz *et al.* [58] with the objective of studying the properties of the plasma channel calculated that F_E was close to 10% when using steel as cathode. They measured the temperature variation caused by a single discharge generated in a controlled gap of 10 μm by micro-thermocouples inserted at various locations.

Another technique for F_E calculations is the one used by Di Bitonto [59]. They assumed that F_E value was 0.183 by studying the experimental data provided by the technology table of AGIE Corporation machine tool manufacturer.

Furthermore, other researches have also made attempts for the definition of F_E. Figure 17 shows a literature comparison of EDM power distribution carries out by Klocke *et al.* [60][61].

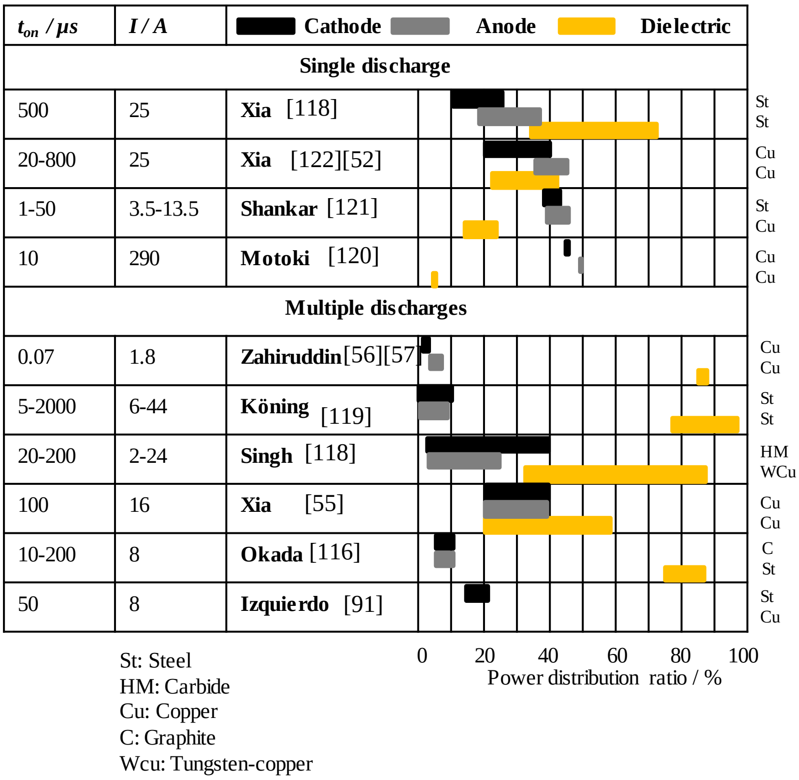

Figure 17: Literature comparison of EDM power distribution ratios [60][61].

Analysing Figure 17, there is no doubt that there is high uncertainty for F_E definition. Moreover, no comprehensive simulation model was found in the literature. One of the reason for the dispersion of results in the definition of F_E is that energy distribution is strongly dependent not only on the machining parameters but also on electrode materials, machining area, electrode geometry etc. [62]. In addition, different types of discharge occur during machining, as explained in Section II.3.1 by Figure 12, and with different efficiency even under stable machining conditions [63]. Hence, is expected that F_E value during continuous EDM machining is much lower than during a single discharge process.

At this point, it should be highlighted two contributions carried out by Klocke *et al.* in the Laboratory for Machine Tools and Production Engineering (WZL) of RWTH Aachen University recently [61][60]. They proposed an inverse simulation method for defining the energy fraction absorbed by the electrode [61] and then, they studied how different EDM parameters affect the energy distribution during continuous EDM process [60]. Those works prove that the simulation of continues EDM process is a present topic of research.

Hence, in Chapter VI, a simulation model for the definition of F_E has been developed. The model is based on the comparison between the temperatures reached in the model and the experimentally measured temperatures.

II.4. Electrode wear in SEDM

One of the main advantages of EDM over conventional machining is that high accurate workpieces can be achieved even when machining complex geometries, no matter the material hardness. However, as mentioned before, electrode wear during machining makes necessary the use of more than one electrode per operation, which is time and cost consuming. Figure 18 shows an example of electrode wear. Considering that high knowledge of electrode wear phenomena can enhance the electrode and the feeding path design, a wide range of researchers have studied electrode wear phenomena during EDM process. This section summarizes the most relevant works in this matter.

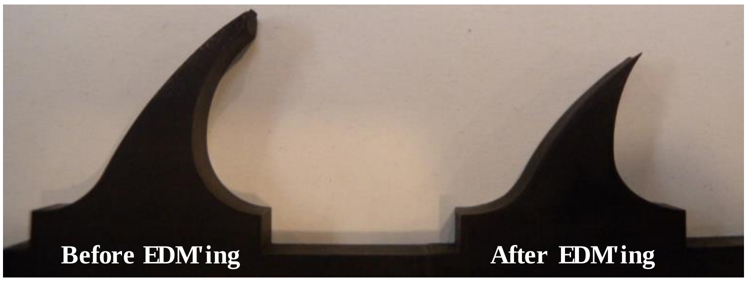

Figure 18: Example of a severe electrode wear during machining.

Firstly, the influence of process parameters on electrode wear are described. Then, the influence of electrode geometry on electrode wear is summarized. After that, the recently developed discharge location adaptive control based on discharge voltage is explained. Then, phenomena of material attachment on the electrode is described. Finally, the most relevant electrode wear minimization techniques are discussed.

II.4.1. Influence of process parameters on electrode wear

As explained previously, during the machining process, the amount of energy generated in the discharge gap is determined by I, t_{on} and U_e, and it can be calculated by Eq.1.

An increase in discharge current increases the pulse energy which leads to an increase in discharge energy rate. Moreover, from Eq.6 and Eq.7 is concluded that the average servo voltage not only conditions MRR, but also TWR. For example, a low value will imply a high concentration of discharges, resulting in the increase of electrode temperature in the discharge area and an increase of electrode wear.

$$SV = \frac{t_d \,.\, U_o + t_{on} \,.\, U_e + t_{off} \,.\, 0}{t_d + t_{on} + t_{off}} \qquad \text{Eq.6}$$

$$f = \frac{t_{on}}{t_d + t_{on} + t_{off}} \qquad \text{Eq.7}$$

Where *SV* refers to the servo reference voltage and *f* to the discharge frequency.

A wide range of experimental studies have confirmed that *I* and t_{on} are the EDM parameters that most affect electrode wear. When *I* increases, electrode wear increases, as high current density rapidly overheats the electrode, which is accompanied by an increase in TWR. When high *I* is combined with long t_{on}, machining time is reduced, which means that the electrode will suffer during less time, decreasing thus electrode wear [64][65]. In fact, t_{on}, t_{off} and rising current slopes are recognized by Maradia *et al.* [38] as the primary parameters affecting electrode wear.

A research work that supports the above paragraph is the study carried out by Ayesta *et al.*[25] and Uhlmann and Domingos [24]. Those authors, as explained in Section II.2.2, analysed the effect of erosion parameters on machining time and on electrode wear in the EDM'ing of narrow slots. They confirmed that *I* and t_{on} have the largest influence on electrode wear.

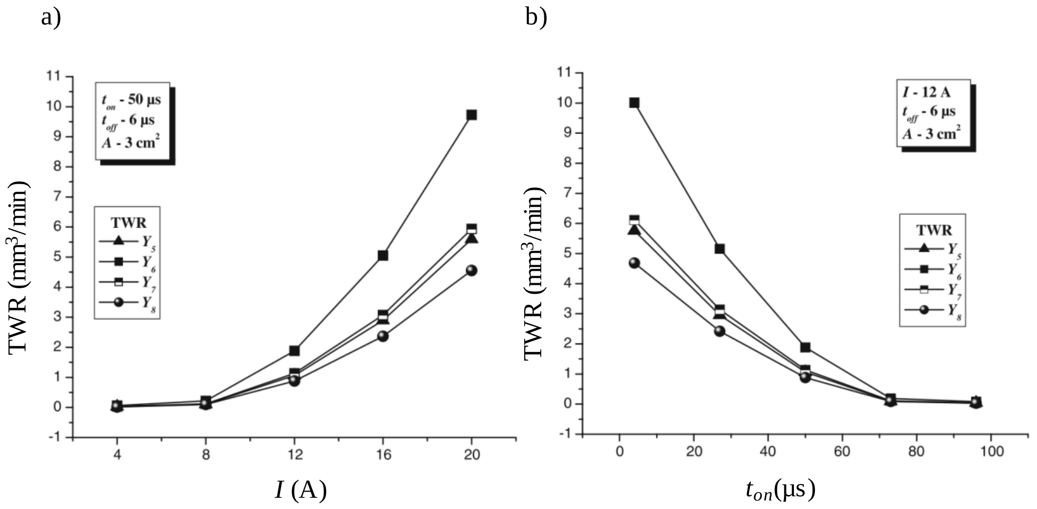

Figure 19: a) Influence of discharge current and b) discharge duration on TWR [64].

Besides, Gostimirovic *et al.* [42] studied the effect of discharge current, discharge duration and current density on MRR, TWR, gap width and surface roughness. Results also showed that I and t_{on} are the most relevant machining parameters in the definition of the outputs. For instance, a larger discharge current will result in a larger gap due to the increase of the plasma channel.

Furthermore, by studying the influence of electrode shape on machining outputs, Sohani *et al.* [64] and Khan *et al.* [65] also observed the dependency of TWR on I and t_{on} no matter the electrode shape. Figure 19.a shows the influence of discharge current on TWR and Figure 19.b. shows the influence of discharge duration on TWR. TWR increases nonlinearly with discharge current, which results in an increase in heat energy rate and thus, more electrode surface is affected. Long discharge duration leads to a smaller TWR and then it becomes constant. The main explanation is related to the fact that with long discharge duration a carbon layer that prevents tool wear is generated on the electrode surface. A detailed explanation of carbon layer generation on electrode surface phenomena is given in Section II.4.4.

II.4.2. Influence of electrode geometry on electrode wear

The electrode geometry and the feeding path determine the discharge area. Its value will affect the energy density, and hence, the amount of energy absorbed by the electrode. Its shape will condition the regions of electrode with higher concentration of discharges and thus, higher heat concentration. Both factors will determine the overheating of some parts of the electrode and it will result in a non-uniform electrode wear along the electrode.

One of the first research work studying the influence of electrode geometry on electrode wear lies in the 70s. Crookall and Fereday [66][67] carried out a serial of experiments with V-shape electrodes in order to understand the influence of electrode geometry on electrode wear pattern. They carried out experiments with V-shape electrodes of 60°, 90° and 120° and they studied the electrode wedge radius change during machining. The main conclusion was that the radius of the wedge increases at the beginning of machining but then as the process progresses it slows down. Furthermore, they concluded that the change of the radius during machining is more prominent with smaller wedge angles. This last effect can be explained by the heat concentration at sharp edges.

Time dependence on electrode wear was also observed by Mohri *et al.* [39], in this case using a cylindrical electrode. Experiments were conducted using a 10 mm diameter copper electrode and carbon steel as workpiece. Electrode profile was measured at different machining times in the range of 8 min to 106 min. They found that at the beginning of machining edge radius was several hundred times the worn length and in the stationary state 10 times the worn length. Results were attributed to the concentration of discharges and to the fact that a carbon layer that protects the electrode during machining cannot be attached at surface with large curvature. Material attachment phenomena will be explained in detail in Section II.4.4.

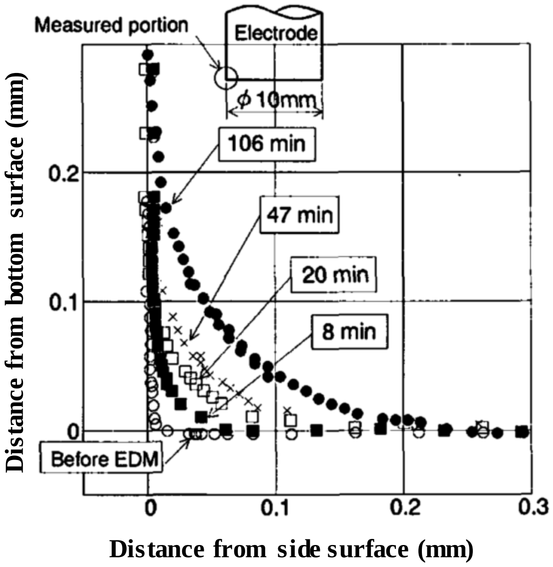

Figure 20: Electrode shape change during time [39].

Sohani *et al.* [64] and Khan *et al.* [65] carried out a serial of experimental tests for analysing the effect of electrode shape on electrode wear, as well as the influence of machining parameters (explained in Section II.4.1). In both studies, the material used were copper for electrode and steel for workpiece.

Sohani *et al.* [64] considered four different electrode shapes: triangular, square, rectangular and circular shape. Their work revealed that electrode shape conditions TWR. The lower TWR values were obtained with a circular electrode, followed by triangular, rectangular and square cross section electrode. Moreover, the effect of area was studied. They observed that lower electrode wear occurs with larger discharge areas. The main reason is that in larger areas the electrode sufferers less, because the energy density is lower.

Khan *et al.* [65] considered the following electrode shapes: circular, square, triangular and diamond cross-section. By maintain the same discharge area value, they demonstrated that under the same machining conditions, higher TWR is observed in electrodes with longer peripheral length. Furthermore, higher rounded edges were observed in sharper corners, see Figure 21, which represents an example of two electrode edges observed by a SEM under the same EDM’ing conditions. Figure 21a. represents the edge of a rounded shape electrode after machining and Figure 21b. shows the edge of a diamond shape electrode after machining. In both studies [64] [65], the electrode shape was not analysed in a quantitative way.

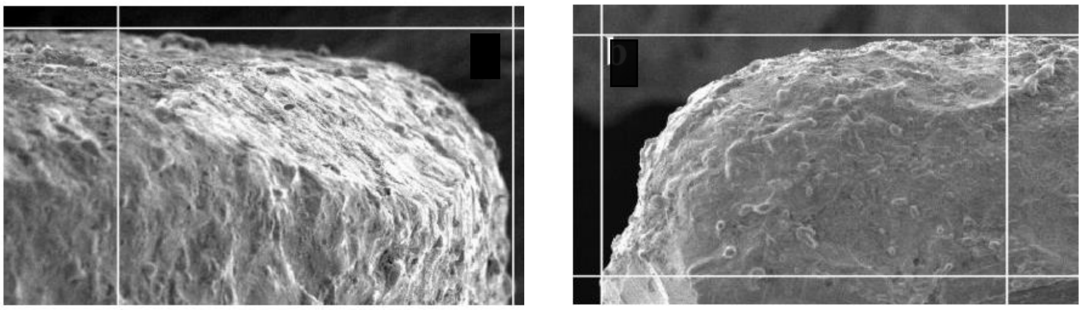

a. Round shape electrode

b. Diamond shape electrode

Figure 21: SEM imagines of electrode edges after EDM'ing. a) Round shape and b) diamond shape [65].

II.4.3. Discharge location adaptive control based on discharge voltage

As discussed, especially in Section II.4.2, some parts of electrode (sharp edges or small protrusion for instance) suffer more deterioration during EDM'ing. This means, that the number of electrodes to use will be conditioned mainly by those features and not by the wear that suffer flat areas. Considering this fact, it is believed that applying suitable machining parameters depending on discharge location will result in more uniform electrode wear. In the literature review some theoretical studies have been found.

Valentinčič *et al.* [68][69][70] by a series of experiments, observed that discharge voltage value depends on the size and geometry of the machining area. Figure 22 shows part of the results that they obtained when machining with constant machining parameters in flat surface and in a conical surface. The main conclusion was that at constant machining conditions, if the discharge area is large, the value of U_e was also higher. As a consequence, they proposed an algorithm that determinates machining parameters based on discharge area. Nevertheless, the proposed model is unable to react in a scale of microsecond, which is necessary for practical application.

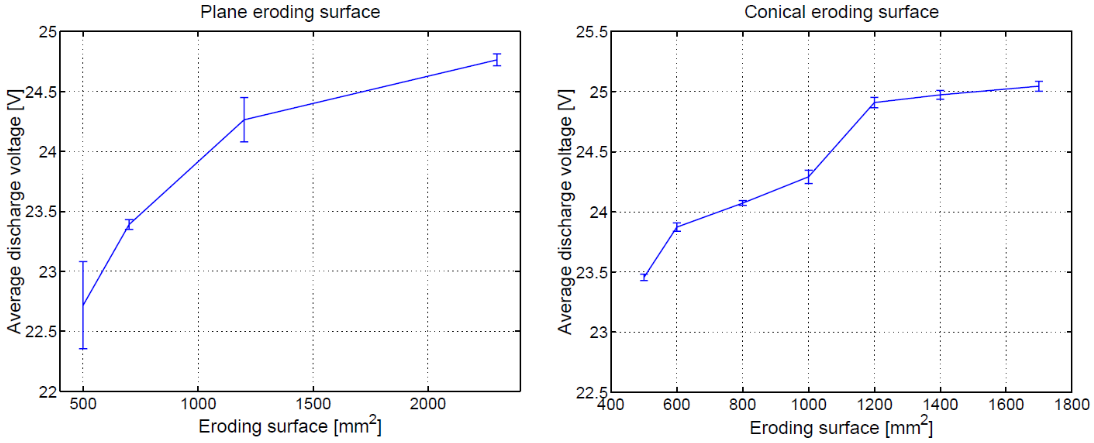

Figure 22: Effect of discharge voltage value on discharge area and geometry [69].

Maradia *et al.* [71] also demonstrated the dependence of U_e value with the discharge position (side surface discharge, normal discharge and discharge at micro-regions such as edges or corners) by a series of experiments, see Figure 23. They concluded that discharges occurring on side surfaces have higher U_e than normal discharges, and those occurring at micro-regions have lower values.

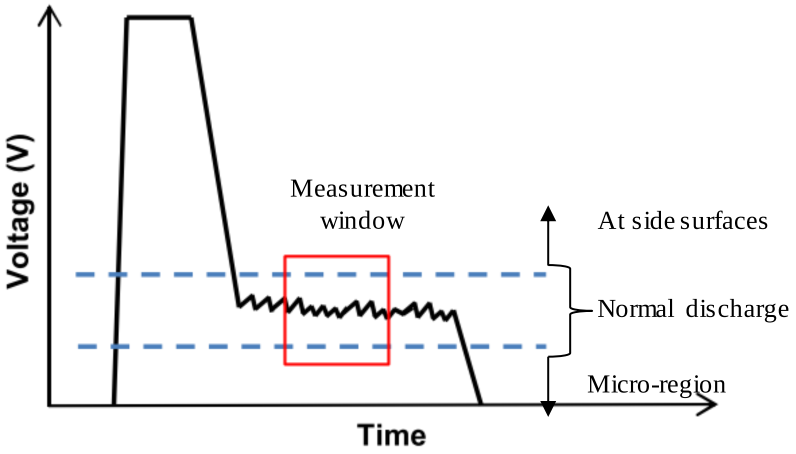
Voltage (V)
Measurement window
At side surfaces
Normal discharge
Micro-region
Time

Figure 23: Definition of discharge location by discharge voltage [71]**.**

Based on this work, Maradia [72] proposed a real-time monitoring system that adapts the discharge duration based on the measured discharge voltage, as shown in Figure 24. The control can enhance the machining accuracy by adapting the machining parameters to the discharge spot and in that way, reduce the problem of pronounced electrode wear in corners and sharp edges of electrode.

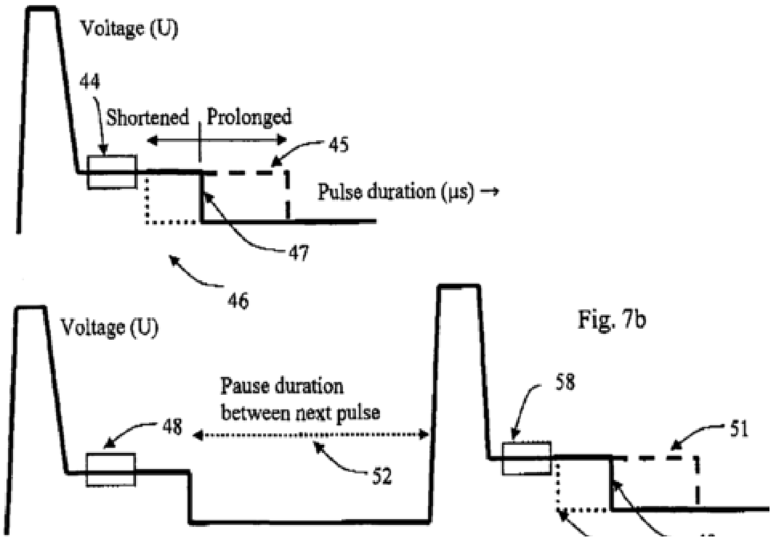
Voltage (U)
44
Shortened
Prolonged
45
Pulse duration (µs) →
47
46
Voltage (U)
Fig. 7b
Pause duration between next pulse
48
52
58
51

Figure 24: Discharge duration and discharge interval adaptation based on discharge voltage [72].

II.4.4. Carbon layer generation in electrode surface during machining

For a full explanation of electrode wear phenomena during EDM process, the possible carbon layer generation in electrode surface during machining, also known as material build-up phenomena, should be described.

The use of long t_{on} when EDM'ing in EDM oil, can create a protective layer on electrode surface. Maradia *et al.* [40] described the mechanism in detail. It is assumed that the carbonaceous layer is deposited to the electrode when the temperature in the discharge area is above the dielectric vaporisation temperature and below the electrode material melting point or the graphite sublimation temperature when EDM oil is used as dielectric medium. Figure 25 shows a brief scheme of gap region during a single discharge in order to understand the carbonaceous layer formation. Figure 25.a shows the gap region after the dielectric breakdown, Figure 25.b illustrates the plasma channel expansion, Figure 25.c shows the carbon layer deposition over the electrode surface, Figure 25.d represents the end of the discharge, Figure 25.e shows the bubble implosion and removal of the molten material and Figure 25.f illustrates the gap region during the discharge interval [40].

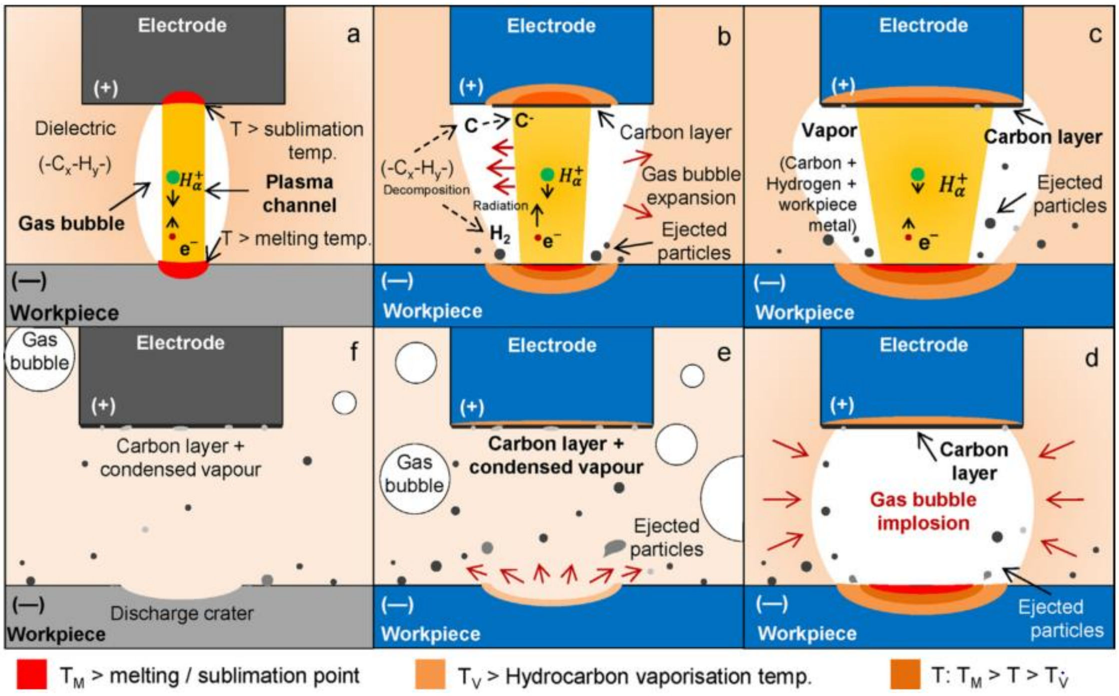
Electrode
a
(+)
Dielectric
(-C$_x$-H$_y$-)
T > sublimation temp.
H_α^+
Plasma channel
Gas bubble
e$^-$
T > melting temp.
(—)
Workpiece
Electrode
b
(+)
C -> C·
Carbon layer
(-C$_x$-H$_y$-)
Decomposition
Gas bubble expansion
H_α^+
Radiation
H$_2$
e$^-$
Ejected particles
(—)
Workpiece
Electrode
c
(+)
Vapor
(Carbon + Hydrogen + workpiece metal)
Carbon layer
H_α^+
Ejected particles
e$^-$
(—)
Workpiece
Gas bubble
Electrode
f
(+)
Carbon layer + condensed vapour
(—)
Workpiece
Discharge crater
Electrode
e
(+)
Gas bubble
Carbon layer + condensed vapour
Ejected particles
(—)
Workpiece
Electrode
d
(+)
Carbon layer
Gas bubble implosion
(—)
Workpiece
Ejected particles
T$_M$ > melting / sublimation point
T$_V$ > Hydrocarbon vaporisation temp.
T: T$_M$ > T > T$_V$

Figure 25: Brief model to describe the carbon layer generation at micro scale [40].

However, especial attention should be paid, because a non-controlled material build-up can lead to process instabilities, increasing machining time and defects in the final workpiece [73]. Figure 26 shows an example of material build-up that resulted in defects in the workpiece. This fact highlights the importance of understanding the carbon layer generation in the electrode surface during machining in order to control it and enhance the machining performance.

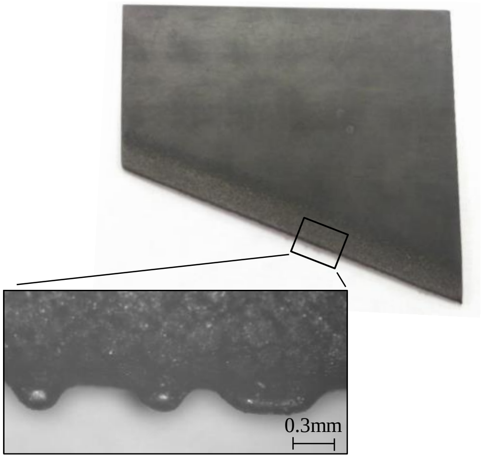

Figure 26: Example of unexpected material build-up during slot machining.

With regard to machining parameters, Mohri *et al.* [39] confirmed the influence of discharge duration on the amount of carbon attached to the electrode. They measured the carbon generation of a single discharge under a wide range of different t_{on}..

This effect was also observed by Klocke *et al.* [44] when machining with graphite electrodes. They studied the influence of five different graphite grades when machining high-aspect ratio slots on MRR and on electrode wear. Using Energy Dispersive X-ray spectroscopy (EDX) analysis they also observed the dependency on electrode geometry. They observed that material deposition was more likely to be found in sharp edges, which correspond to the points with the highest discharge concentration.

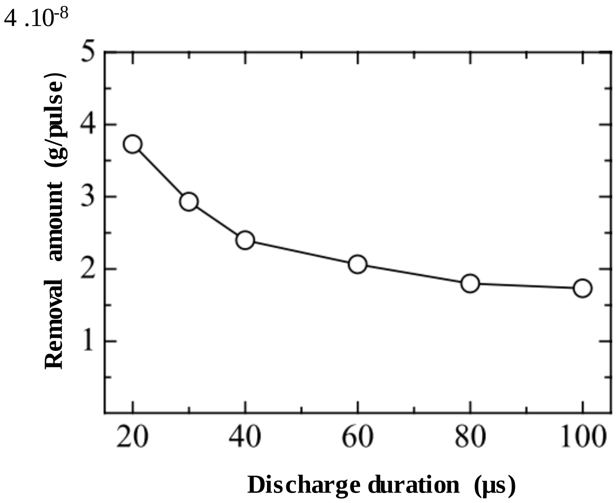

Figure 27: Influence of discharge duration on removal amount of electrode per pulse discharge [74].

Kunieda and Kobayashi [74] set a fundamental study with the aim of understanding the effect of carbon layer deposition on TWR. They measured the vapor density of copper vapor in EDM arc plasma by a spectroscopic measurement of a single discharge. They also confirmed the influence of t_{on} on electrode material removal. Figure 27 shows the relationship between t_{on} and electrode material removal per pulse discharge. Results show that electrode material removal can be reduced by the use of long t_{on} values.

Furthermore, the workpiece material is also a factor to consider: material attachment can easily be generated when EDM'ing carbon steel, but it is not possible when machining aluminum or Titanium alloy, TiAl6V4 for instance [40]. Moreover, as reported by Mohri *et al.* [39], the larger the amount of the equivalent total carbon in workpiece, the smaller the electrode wear become.

Marafona and Wykes [75] proposed a two stage machining in order to take advantage of the material build-up mechanism. Firstly, low I and long t_{on} are programmed in order to generate the black layer, and then, normally given parameters are used. Its feasibility was tested by a rectangular cross section electrode of 225 mm^2 discharge area. Furthermore, the influence of current shape was considered by Maradia *et al.* [38] in order to develop a low wear strategy for micro-scale machining by graphite electrode. They confirmed that there are two ways for generating a carbonaceous layer on the electrode: the use of rising current slopes and the use of long discharge duration.

Moreover, Marafona [76] analyzed the black layer by the use of scanning electron microscopy (SEM), electron probe micro-analyzer (EPMA) and quantitative energy dispersive spectroscopy (EDS) and he provided a relation between the percentage of equivalent carbon and relative electrode wear. Maradia *et al.*[40] also tried to characterize the black layer by Raman spectroscope. They observed that the layer has lower conductivity and higher hardness than electrode base material. This last feature may withstand the abrasion generated by debris particles in the narrow gap, and hence reduce electrode wear.

Those works are focused on the effect of machining parameters and they are not focused on the influence of electrode geometry and electrode feeding path. Thus, considering the high added value of complex geometries and the benefits that a controlled carbonaceous layer generation can implies, this phenomenon is still a topic of research.

II.4.5. Electrode wear minimization techniques

Although a wide range of works have been published in terms of electrode wear, as explained in the present section, electrode wear is still the main cause of inaccuracies on the workpiece.

In the literature different techniques have been proposed for the minimization electrode wear: the use of special electrode materials that minimize electrode wear [77][78], the use of low-frequency vibration of workpiece [79], electrode wear compensation techniques [80][81], the use of cryogenic electrode cooling [51], or the use of powder mixed dielectric (investigation of carbon nanotube added dielectric) [82]. Those techniques are described in the following paragraphs.

One technique is the use of special electrode materials that minimize electrode wear [77][78]. A research work worth mentioning is the one carried out by Uhlmann and Roehner [77]. They investigate electrode wear and process performance on PCD and B-CVD diamond electrode material for micro SEDM operations.

Prihandana *et al.* [79] proposed the application of low-frequency vibration on the workpiece. They did not only increase the material removal due to the improvement of flushing conditions, but they also observed a reduction of TWR.

Another technique used is the electrode compensation during machining [80][81], which is common for EDM milling operations or in the machining of deep cavities. The goal is to compensate the length reduction of electrode during machining by adjusting the downward movement of tool electrode. However, this technique is limited to simple machining paths and it cannot be implemented in free-form EDM operations.

Furthermore, as previously explained in Section II.3, a reduction of electrode temperature results in lower electrode wear. Kumar [51] proposed the use of cryogenic electrode cooling by the experimental set-up presented in Figure 28. Results show that with this technique electrode wear can be reduced in a range between 8 and 20.9%. However, MRR is affected because of the decrease of temperature in the gap.

Moreover, the used of powder mixed dielectric was proposed by Shabgard and Khosrozadeh [83] among others. The technique is known as powder mixed electrical discharge machining (PMEDM). The goal of the powders is to change the thermal and electrical properties of the dielectric increasing the thermal and electrical conductivity coefficients and thus, enhance EDM performance owing to different discharge attributes [82]. In their work, they studied the effect of Carbon nanotubes (CNTs) mixed dielectric on MRR, TWR and surface quality when working with Ti-6Al-4V alloy workpiece and copper electrode. In terms of TWR they observed that by powder mixed dielectric TWR decreases, especially when machining with short discharge durations and high discharge current.

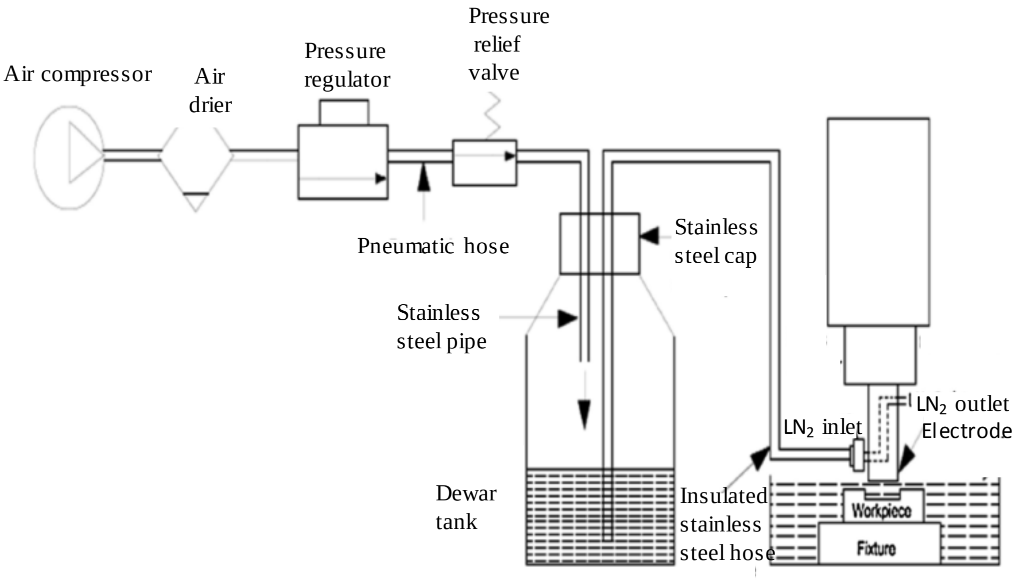
Air compressor
Air drier
Pressure regulator
Pressure relief valve
Pneumatic hose
Stainless steel cap
Stainless steel pipe
Dewar tank
Insulated stainless steel hose
LN₂ inlet
LN₂ outlet
Electrode
Workpiece
Fixture

Figure 28: Experimental set-up for cryogenic cooling of tool electrode [51].

However, those techniques described above are not always possible to put in practice because of the equipment needed and the cost they involved. Thus, in the industry the main technique is the multi-electrode strategy, in which a serial of electrodes is used until the final workpiece is achieved. This method is effective as the final workpiece can be achieved if a large number of electrodes are used. Nevertheless, the final machining cost increases due to the electrode machining cost, time and energy consumption. Actually, the machining of electrode can exceeded to a 70% of the total machining cost [64].

At this point, it should be mentioned, as also stated in Section II.1, that EDM machining tool manufacturers have implemented a low electrode wear technology in their cutting-edge generators. This leads to a significant reduction of the number of electrodes per workpiece, however, the need of roughing and finishing strategies and the use of a serial of electrodes is still necessary.

Therefore, even though advances have been made towards electrode wear reduction, electrode wear is still a topic of research. Hence, in order to gain knowledge about electrode wear phenomena, Chapter V proposes a method for defining electrode wear and gap width along electrode when working with complex geometries. The methodology has been used in several experimental studies to understand electrode wear mechanism when working with different electrode geometries and electrode feeding paths.

II.5. Simulation of electrode wear during EDM process

As highlighted in previous sections, the geometrical accuracy of the workpiece is largely affected by two main phenomena: electrode wear and uneven gap width value. Because of that, when EDM'ing complex geometries, the process requires large practical exercise, and in many cases, trial-and-error strategies involving a costly manufacture of electrode. For this reason, a simulation model of EDM applications can contribute to the enhancement and competitiveness of the machining process.

The main difficulty for EDM process simulation can be attributed to the complex removal phenomena and the uneven electrode wear distribution. Moreover, the removal mechanism involves several effects: thermal, mechanical, chemical and electric effects, which difficulties the modelling of the process. A generalized algorithm for EDM process modelling is shown in Figure 29.

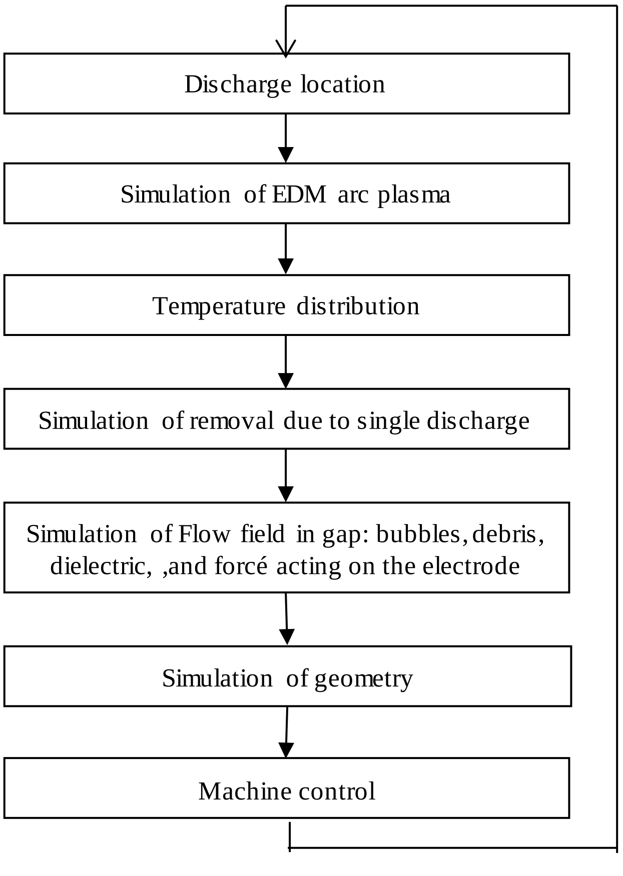
Discharge location
Simulation of EDM arc plasma
Temperature distribution
Simulation of removal due to single discharge
Simulation of Flow field in gap: bubbles, debris, dielectric, ,and forcé acting on the electrode
Simulation of geometry
Machine control

Figure 29: General algorithm for EDM simulation method [84].

During the last decade a number on papers concerning simulations have been published. The simulation models can be divided in two main groups: based on electrode geometry and based on physical-thermal aspects. Moreover, simulation works have been carried out to simulate the carbon layer generation over electrode surface. The present section describes the most relevant publications in this fields.

II.5.1. Geometry considerations

Even if the simulation of electrode geometry during erosion can contribute to the efficiency of the machining process, due to its complexity, few are the researchers that have tried to develop electrode simulation models. The most relevant are reviewed in the present section.

The simulation models can be divided in two main groups: forward simulations, in which the electrode is fed towards the workpiece, and reverse simulations, which used the same algorithm, but the workpiece is fed toward the electrode. Contrary to the forward simulation, by the reverse simulation methods the initial tool electrode shape is obtained, which is more practical in terms of electrode design and electrode feeding path generation.

Tricarico *et al.* [85] developed a forwards simulation method based on an iterative algorithm that considers the material removal of electrode and the workpiece for small feed step until the final depth is reached. The main weakness of the model is that the method can only be applied for shapes which can be generated by 2D geometrical functions.

Jian *et al.* [86] also attempted to simulate electrode geometry transformation after machining. One of the hypothesis of the model was that the gap width and the electrode material removal do not vary during the process and along the profile. Thus, the effect of discharge area and electrode geometry was not considered. Apart from that, the effect of debris accumulation, which will affect the process stability and the carbon deposition, were also ignored.

The most advanced and relevant works concerning EDM simulation have been published by Kunieda during the last decades. They are described in the following paragraphs.

Kunieda *et al.* developed a reverse simulation method, where the principle is that the workpiece is fed toward the electrode. In 1999 Kunieda *et al.* developed a simulation method that considered electrode wear, gap width distribution and debris particles concentration [87]. Figure 30 shows the basic discharge location searching algorithm.

In 2009, considering that in actual machining the occurrence probability of a discharge increases with discharge area, they introduced the effect of the area on the simulation model [88]. The simulation algorithm was based on the hypothesis that the discharge occurs on the voxel with the minimum t_d time, defined as $t_{d,ave}$. The discharge delay time was calculated by Eq. 8.

$$t_{d,ave} = 8.2\ x\ 10^{12} \left(\frac{gap^{8.8} r^{2.9}}{area^{1.2} conc^{1.6}} \right) \qquad \text{Eq. 8}$$

Here *conc* indicates the concentration of debris particles, *gap* the gap width value, *area* the machining discharge area and *r* the debris particle diameter.

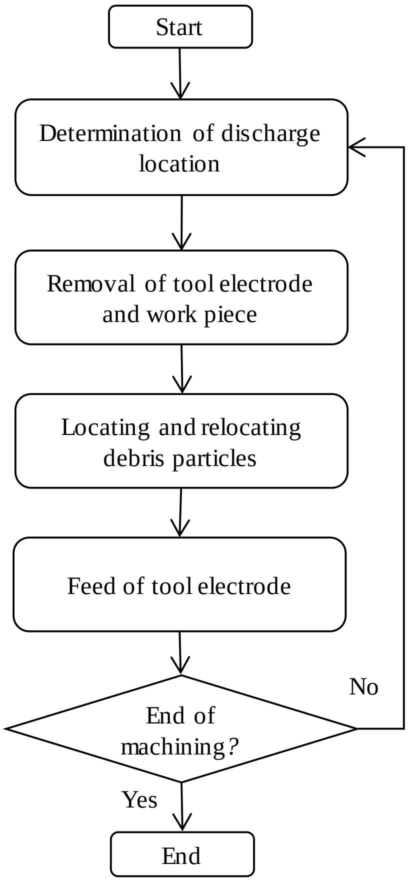
Start
Determination of discharge location
Removal of tool electrode and work piece
Locating and relocating debris particles
Feed of tool electrode
End of machining?
No
Yes
End

Figure 30: Discharge location simulation algorithm for forward simulation [87].

However, the definition of the variables during machining is a difficult task, which limits the feasibility of the model. In addition, as previously stated, electrode wear is dependent on electrode geometry. Higher electrode wear is expected in the edges than on flat areas due to discharge area concentration [39]. Because of that, Kunieda *et al.* [45] proposed a method that compensate the error due to curvature of the electrode facing the workpiece. Figure 31 shows a scheme to describe the need to consider this effect.

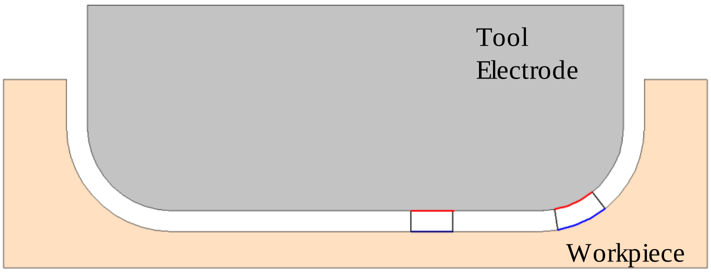
Tool Electrode
Workpiece

Figure 31: Scheme of the influence of curvature in material removal.

They modified the removal per discharge obtained from experiments based on the theory that in a flat area the material of electrode per area unit that faces the workpiece is smaller than in a curved area. Figure 32 shows the scheme and equations for applying the proposed method. They demonstrated that the workpiece geometry was closer to the theoretical workpiece shape than if the ordinary method of off-setting the electrode was used. Considering the high value of this information, the error of curvature will be implemented in the simulation model developed in Charter VI.

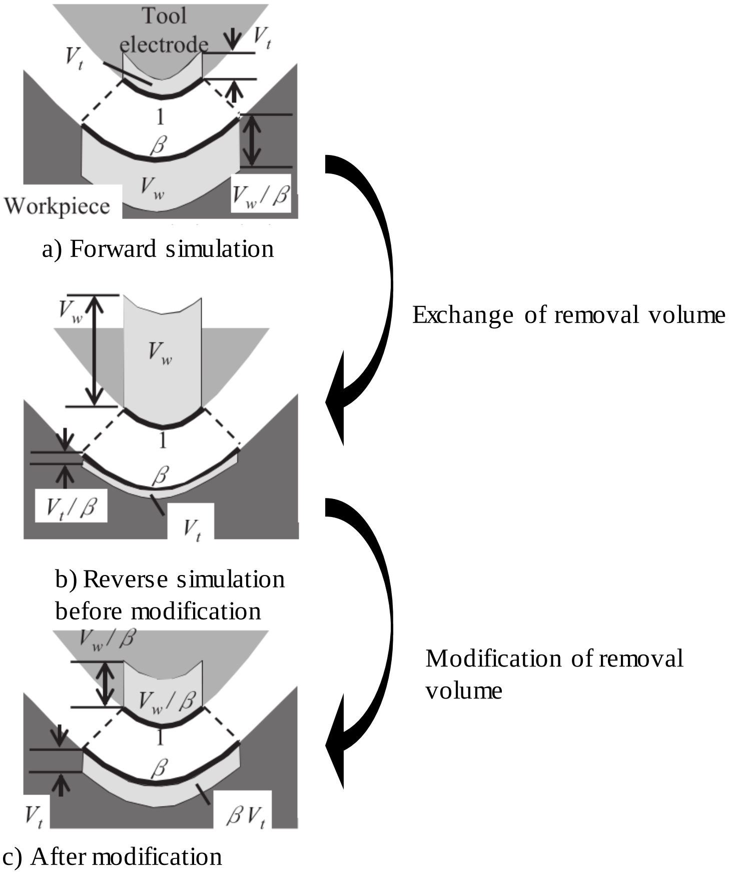
Tool electrode
V_t
V_t
1
β
V_w
V_w/β
Workpiece
Exchange of removal volume
V_w
V_w
1
β
V_t/β
V_t
Modification of removal volume
V_w/β
V_w/β
1
β
V_t
βV_t

a) Forward simulation

b) Reverse simulation before modification

c) After modification

Figure 32: Method to compensate for error due to curvature [45].

In the studies mentioned above the algorithms are run after the generation a single discharge and it is repeated for a given time. This limits its applicability in large discharge areas and long machining operations, due to the high computational cost of the simulation.

In order to solve this problem, and to be able to simulate under industrial conditions, the model developed in Chapter VI, considers the energy generated during continuous EDM process and this energy is distributed over the electrode discharge area.

II.5.2. Physical-thermal considerations

Considering that in EDM, for the commonly machining materials, the main material removal mechanism is melting and/or evaporation, it is believed that the process can be analysed by a thermal model. The objective of thermal models is to define material removal by the temperatures reached in the electrodes.

Following this approach, a number of publications have been found in the literature review. Most of them are focused on workpiece material removal based on single discharge models. A rigorous review of the State of the art can be found in the PhD dissertation of Dr. Izquierdo [1].

Even if as described in Section II.3 a wide range of factors affect the thermal conditions of the electrode, when it comes to simulate a single discharge two are most critical boundary conditions: the energy distribution ratio and diameters of the plasma channel [84]. Furthermore, the outputs will vary according to the hypothesis put forward in the model [89]. Hence, in this section, even if it will be focused on workpiece and not on the electrode, the most relevant works will be described as an insight for the model of electrode presented on the present PhD dissertation.

The model of DiBitonto *et al.* [59] was the first work that consideres power rather than temperature as the boundary condition at the plasma-workpiece interface. From it, they defined a constant energy fraction of the total energy generated that is transferred.

Based on this work, Marafona and Chousal [90] introduced the Joule heating factor in the simulation model of a single discharge, which until then it was considered negligible [59]. By a single discharge Finite Element Model (FEM), they estimated the surface roughness, the removal material and the maximum temperature in the discharge channel. They considered that the discharge channel has a cylindrical shape and the heat dissipation was a function of I and t_{on}.

The literature survey reveals that the vast majority of works are focused on single-discharge analysis, nevertheless attempts have been also made to simulate the discharge superposition. The main objective was to understand the effect of continuous discharges on the temperature distribution [91][92].

A work to highlight is the contribution of Izquierdo *et al.* [91]. They presented a model capable of simulating discharge superposition for obtaining the resulted surface roughness. On the other hand, Xie *et al.* [92] by ANSYS software established the temperature distribution of workpiece after two consecutive discharges.

However, the machining conditions of a single discharge or some hundreds of discharges differ from the actual EDM machining process. Furthermore, if a real application wants to be modelized a single-discharge model is not a feasible solution, due to the high computational cost.

Chapter III: Approaches for improvement of EDM cutting by foil electrode

III. APPROACHES FOR IMPROVEMENT OF EDM CUTTING BY FOIL ELECTRODE

Electrical discharge machining by foil electrode serves as an alternative method for SiC slicing. This technology uses a highly tensioned thin foil as tool electrode. The main advantages over wire EDM are that the foil thickness can be made smaller than the wire diameter, vibrations can be avoided by applying high tension, and higher current can be supplied since there is less risk of tool breakage. However, due to the large side surface area of the foil electrode, there is a high occurrence probability of side surface discharges and high concentration of debris, which affects kerf width accuracy and machining stability. Aiming to improve the machining rate and kerf width accuracy the present research work has been carried out.

III.1. Introduction

The present work was developed in the facilities of the department of Precision Engineering of the University of Tokyo in the Faculty of Engineering in KUNIEDA-MIMURA Research group.

As described in the revision of the State of the art, Section II.2.1, single crystal SiC is becoming a promising material due to its outstanding electrical and physical properties. Those properties can be summarized as follows: wide band gap, high electron saturation drift velocity and high thermal conductivity. These properties bring high benefits to SiC-based electronic devices, as they enable to work at extreme environments of elevated temperature and with high efficiency. Figure 33 represents that a high growth of SiC devices is expected in the following years. However, nowadays SiC device fabrication technology is still not sufficiently developed to the degree required for widespread technology, mainly because of its manufacturing challenges.

One of the developed and widely studied alternative for SiC slicing is WEDM. Nevertheless, it has two main drawbacks: the risk of wire breakage and the wire vibration with enlarge the kerf loss. Hence, Zhao *et al.*[18][20] developed Electrical Discharge Slicing (EDS) by foil electrode, which correspond with the technology studied in the present experimental work.

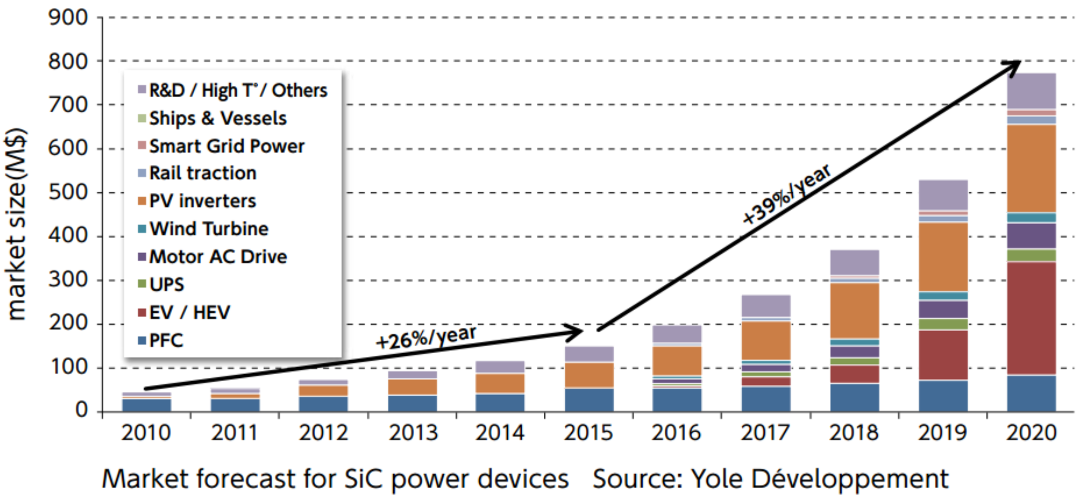

Market forecast for SiC power devices Source: Yole Développement

Figure 33: Long-term market forecast for SiC devices in various power applications [93].

III.2. SiC material. Main characteristics

The workpiece material used is SiC, which is considered as an extremely hard and inert semiconductor material with a hexagonal close packed crystal structure. SiC material was supplied by Hamada Heavy Industries Ltd. company thanks to Mr. Abe.

Table 1: Comparison of material properties between SiC and steel [94].

	SiC	**SKD steel**
Knoop hardness (kgf/mm^2)	2400-3000	-
Electrical resistivity (Ωcm)	2 x 10-2	1.5 x 10-5
Melting point (^{0} C)	-	1540
Sublimation point (^{0} C)	2000-2200	-
Thermal conductivity (W/(m.K))	490	40

In Table 1 the main properties of SiC have been compared with the properties of SKD steel, which is widely used material in the mold and die industry. The material removal mechanism of both materials is compared in the research work carried out by Zhao *et al.* [94].

III.3. Main equipment and machine tools used

In this section, a description of the main equipment and machine tools used are mentioned.

- The EDM cuttings were carried out on a Sodick C32 conventional SEDM machine. Table 2 shows its main specifications.
- The foil electrodes were prepared on a Sodick AP200L machine.

- The electrode blocks, in order to guarantee the required flatness, were ground on a conventional grinding machine.

Table 2: Sodick C32 machine main specifications [6].

Sodick C32 Specifications		
Height (mm)	1815	
Weight (kg)	1600	
X-axis travel (mm)	300	
Y-axis travel (mm)	200	
Z-axis travel (mm)	150	
Max. suspension weight (kg)	20	
Table size (mm)	450x300	
Max. workpiece weight (kg)	50	
Machine tank dimensions (mm)	600x454x260	
Height (mm)	1815	

- The kerf loss was measured by a microscope.
- The parallelism error between electrode foil surface and the feeding trajectory was verified by a CCD laser displacement sensor (Keyence, LK-G10) shown in Table 3.

Table 3: Keyence LK-G10 CCD laser displacement [95].

Keyence LK-G10 CCD laser displacement		
Measuring range		±1 mm
Light source	Type	Red semiconductor laser
	Wavelength	655 nm
	Control output	0.3 mW
Spot diameter		Approx. Ø20 µm
Repeatability		0.02 µm

- The observation of the discharge current and voltage waveforms was carried out by a high-frequency oscilloscope (DPO 4104 Digital Phosphor Oscilloscope).
- Furthermore, different chuck and holders of System 3R company were used in the experimental set-up. Table 4 shows two examples of the equipment used.

Table 4: Example of the machining tool equipment used [96].

Reference	Application	Image and dimensions
MiniBlock 3R-321.46	Manual hydraulic chuck for vertical and horizontal mounting on the machine table.	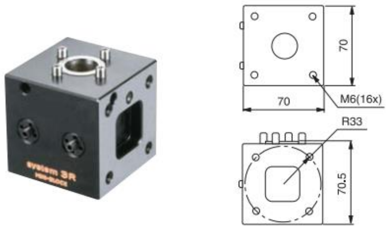 70 70 M6(16x) R33 70.5 System 3R MiniBlock
Three-jaw chuck 3R-311.4	Chuck Ø20mm for Ø0.1-3mm electrodes.	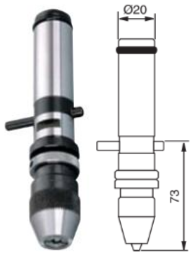

III.4. Fixture for applying tension to electrode foil

As discussed, wire electrode has limited further development of WEDM slicing of SiC. Mainly because the wire diameter conditions the tension that can be applied, and thus, a large tension cannot be applied, and wire vibration problems can easy occur, which results in a large kerf width.

To overcome the vibration problem and improve the kerf loss, Zhao *et al.* [18] proposed a substitution of the wire electrode for a thin rectangular foil electrode aiming to further improve the kerf loss accuracy in terms of dimension and uniformity. Figure 34 illustrates the scheme of the fixture for controlling the tension force applied to the foil electrode. In the experiments, sufficient tension force was applied to the foil electrode by the compression spring to make the parallelism error within the requirement limits.

Since high tension can be applied to the foil electrode, tool vibrations can be reduced. The maximum applicable tension force to the tool electrode can be calculated by the following equation:

$$T = \sigma \cdot S \qquad \text{Eq. 9}$$

Where T indicates the maximum applicable tension force, σ the ultimate tensile stress of the electrode material and S the cross-section area of the electrode.

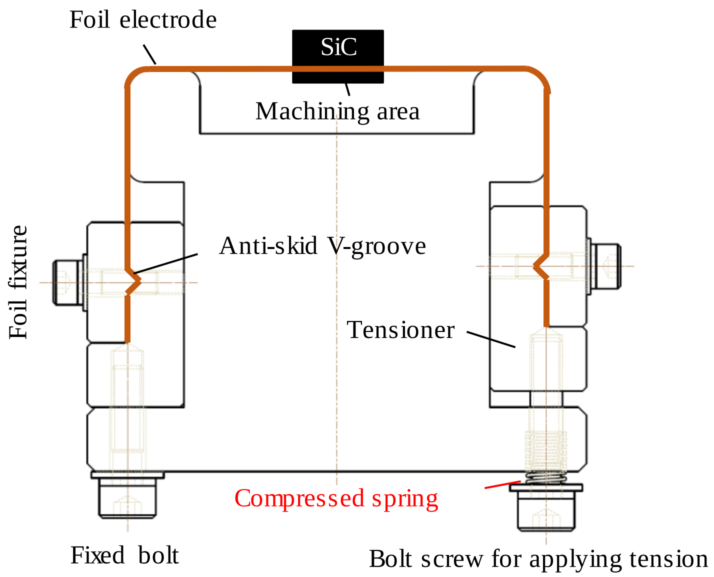
Foil electrode
SiC
Machining area
Foil fixture
Anti-skid V-groove
Tensioner
Compressed spring
Fixed bolt
Bolt screw for applying tension

Figure 34: Illustration of the fixture for applying tension to the foil.

Figure 35 shows a simplified analysis model of the vibration of the tool electrode (wire or foil). Assuming that the force resulted from discharges, F_0, is applied to the tool, when the tool electrode tension is as large as the maximum applicable tension force of the tool, the electrode deformation δ_0 due to the discharge force F_0 can be calculated by the following equation [97]:

$$\delta_0 = \frac{1}{2} \cdot F_0 \cdot \frac{1}{\sigma \cdot S} \qquad \text{Eq. 10}$$

As it can be seen, the electrode vibration during machining is decided by the cross-section area S of the electrode.

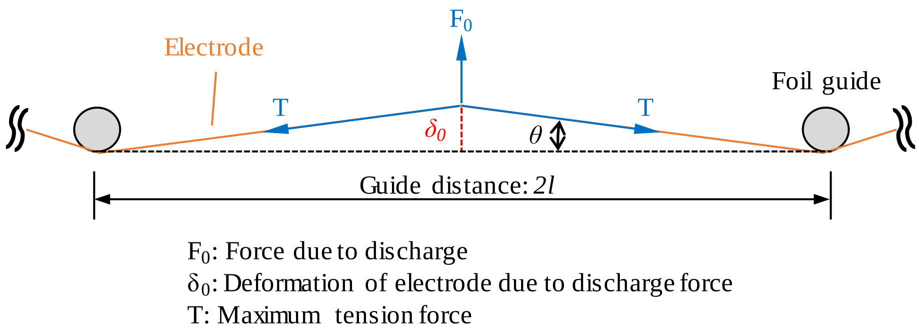
F_0
Electrode
Foil guide
T
T
δ_0
θ
Guide distance: $2l$
F_0: Force due to discharge
δ_0: Deformation of electrode due to discharge force
T: Maximum tension force

Figure 35: Analysis of electrode deformation due to discharge force [97].

III.5. Foil electrode: Copper

In the present work copper was used as foil electrode material, with a thickness of 0.05 mm. The dimensions of the foil were: 5 mm in width and 150 mm in length.

Copper was supplied in large sheets with a thickness of 0.05 mm. Thus, the preparation of the foil electrode was necessary. For ensuring the machining accuracy, the foil needed to avoid burrs and crumples. Hence, the foil electrode was cut by WEDM by the set-up described in Figure 36. Firstly, the copper sheet was inserted between two aluminum plates, Figure 36.a, and then the assembly was cut by WEDM, Figure 36.b.

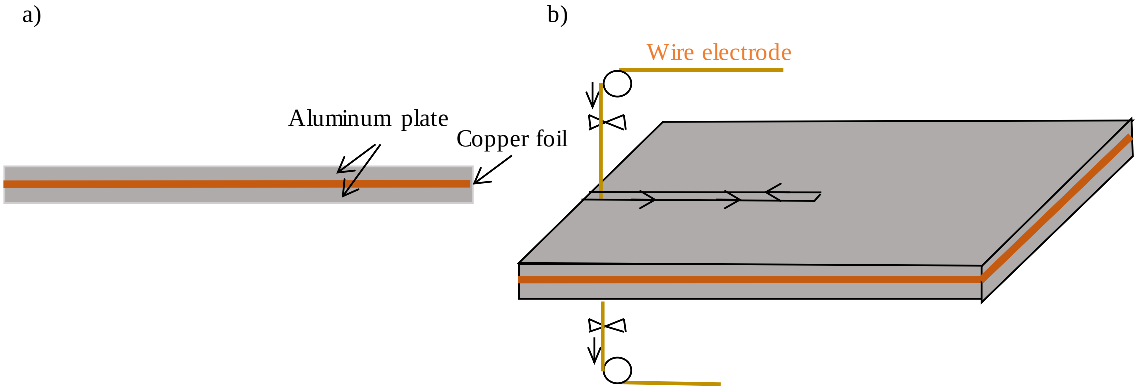
a)
b)
Aluminum plate
Copper foil
Wire electrode

Figure 36: Set-up for copper foil preparation.

III.6. Proposal of new electrode

The main objective of the work is to improve kerf width accuracy and machining performance of SiC slicing by foil electrode. With this aim, two foil electrode designs have been proposed.

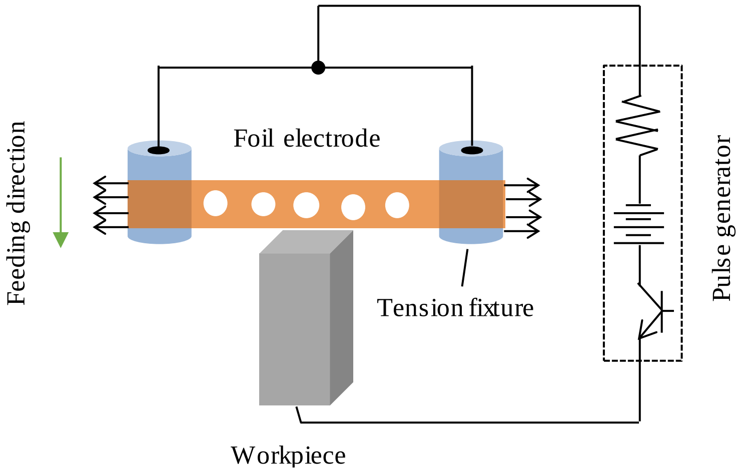
Foil electrode
Feeding direction
Tension fixture
Pulse generator
Workpiece

Figure 37: Scheme of electrical discharge slicing of SiC by foil electrode with holes.

The first alternative considers the reduction of the tool electrode side surface area by machining holes in the electrode foil, as illustrated in Figure 37. This method has two objectives, reduction of the side surface area and the improvement of flushing conditions in the side gap due to the chip pocketing effect of the holes. Both effects contribute to the reduction of side surface discharges, resulting in the decrease of kerf loss. In Section III.6.1 the procedure followed for machining the holes in the foil is described.

The second alternative method uses a foil electrode in which the electrode side surface has been insulated by a resin coating layer. The objective is to avoid the side surface discharges and thus, reduce the kerf loss. This theory is based on the work presented by Okada *et al.*[98]. They reduced the kerf width by decreasing the side surface discharges by forming a high-resistance layer on the wire surface. Section III.6.2 describes the type and method used for coating the thin foil electrode.

The effectiveness of both foil electrodes: electrode with holes and electrode with an insulation layer, was verified through a series of machining experiments as well as with a fundamental study of the distribution of the discharge delay time.

III.6.1. Electrode with holes

The holes were machined by sinking EDM using a copper electrode as shown in Figure 38. Firstly, the foil was tensioned, and the parallelism error was check. Then, the tensioned foil was placed in the worktable of the machine tool and holes were machined one by one. Considering the tool wear length at the bottom region of the foil tool electrode during the slicing, the holes were machined in the upper part of the foil electrode. After machining the holes, again the parallelism error was checked, in order to ensure that the heat generated during the machining of the holes did not deform the foil electrode. In case that the parallelism was lost, the foil was again tensioned. Figure 39 shows the foil electrode ready for slicing.

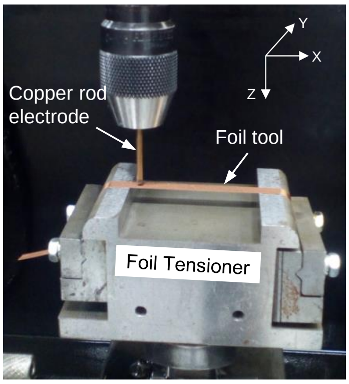

Figure 38: Experimental set-up for machining the holes on the foil electrode.

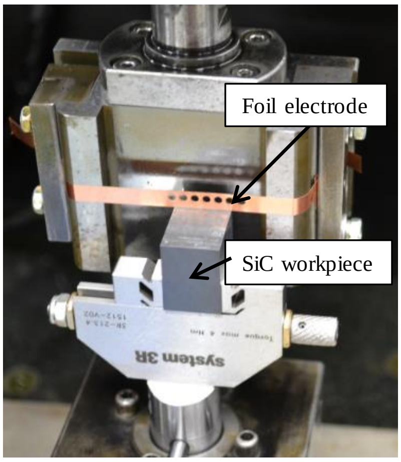

Figure 39: Foil electrode ready for slicing.

III.6.2. Coated electrode

The influence of insulating the side surface of the foil electrode was studied by three different film layer thickness, 5 µm, 10 µm and 22 µm.

The material of the insulation film was silicone modified epoxy resin (HIRESIN 018, Takamatsu oil & Fat Co.,Ltd.) and the resin was pasted on the foil electrode by a wire bar coater. To solidify the resin film, firstly the film was applied on one side of the electrode and heated for 1 minute at 100°C by an oven (DF410, Yamato Scientific Co., Ltd.) and then the film was applied to the other side and heated for 5 minutes at 100°C, followed by room temperature cooling. The coated foil electrode was prepared by Mr. Kunio Tawara of Takamatsu oil & Fat CO., Ltd.

III.7. Improvement of machining performance by the proposed electrodes

In this Section the effectiveness of both foil electrodes: electrode with holes and electrode with an insulation layer, has been verified through a series of machining experiments as well as with a fundamental study of the distribution of the discharge delay time, t_d.

III.7.1. Test definition and methodology

Experiments were carried out on a Sodick C32 sinking EDM machine. Figure 40 shows the image of the experimental set-up. The slicing was conducted by feeding the foil electrode downward to the SiC workpiece in Z direction. In the experiments, sufficient tension force was applied to the foil electrode by the compression spring to make the parallelism error within 10 µm.

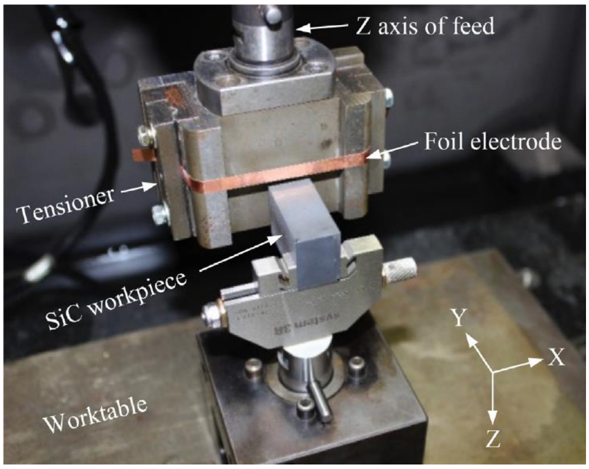

Figure 40: EDM cutting of SiC by foil electrode.

As discussed above, two electrode designs were proposed: electrode with holes and coated electrode. Figure 41 illustrates different types of foil tool electrodes used in the experiments.

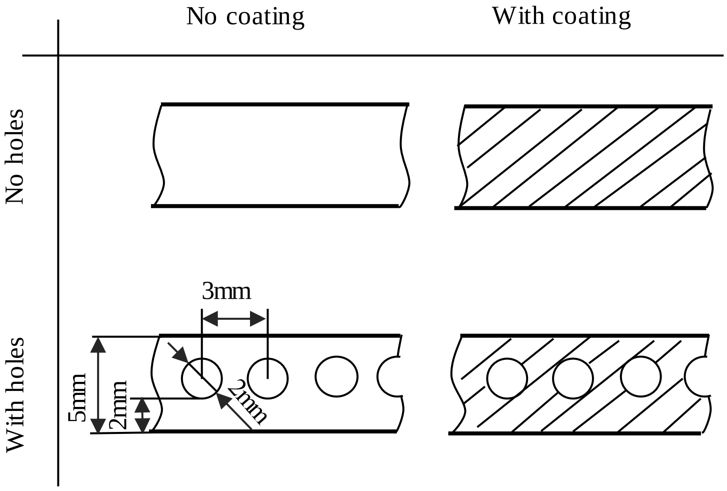

Figure 41: Foil electrode proposed.

In order to avoid the foil breakage from the edge of the holes, the hole pitch was set as 3 mm. In addition, test machining experiments were carried out comparing the effect of the holes of 1 mm and 2 mm in diameter, in both cases the same area reduction was considered. Results show that 2 mm was better in terms of machining rate. Therefore, holes of 2 mm in diameter were used in this study. Figure 42 shows the results of the feeding displacement axis over the machining time for the case of holes of 2 mm and 1 mm in diameter.

With machining holes on the foil tool electrode, the maximum applicable tension force is reduced to some extent due to the reduced cross section area. Nevertheless, the cross-section area of the foil electrode is still larger than that of Ø50 μm wire electrode even if the holes are made on the foil. Therefore, compared to wire electrode, larger tension force can be applied, and foil vibration can be reduced.

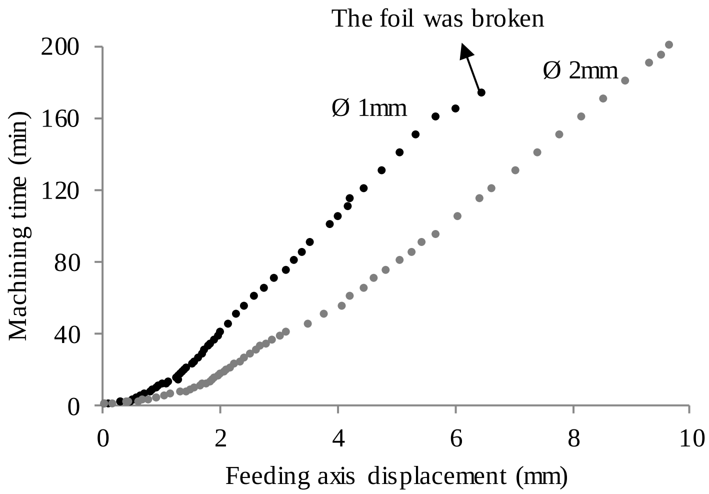

Figure 42: Effect of hole diameter on machining performance.

The machining conditions were determined based on previous research works [18][20]. Table 5 shows the machining and experimental conditions.

Table 5: Machining and experimental conditions.

Working fluid	EDM oil
Foil electrode	Copper, thickness of 50 µm
Workpiece	SiC, thickness of 15 mm
Polarity (workpiece)	+
U_e (V)	120
I (Measured) (A)	8
t_{on} (µs)	1
t_{off} (µs)	30
SV (V)	70

Moreover, the influences of both foil electrode designs were tested with three different slicing strategies: no strategy, applying jump motion to the tool electrode, and application of reciprocating motion to the tool along *X* direction. The machining conditions of jump and reciprocating strategy are shown in Table 6.

As explained, the foil electrode was loaded with tension to avoid the foil electrode vibration. After tensioning the foil electrode, parallelism error between the foil surface and the feeding trajectory was measured using a CCD laser displacement sensor. When reciprocating motion strategy was used, the parallelism error between the foil surface and the trajectory of the feeding axis was smaller than 15 µm. For the other two slicing strategies, the parallelism error between the foil plane and the trajectory of the feeding axis in the cutting direction was smaller than 7 µm. Figure 43 shows the experimental procedure for parallelism error observation.

Table 6: Parameter settings for jump motion and reciprocating motion.

Jump motion	Jump up time (s)	0.08
	Jump speed (mm/s)	3
	Jump interval time (s)	0.2
Reciprocating motion	Reciprocating speed (mm/min)	30
	Reciprocating amplitude (mm)	20

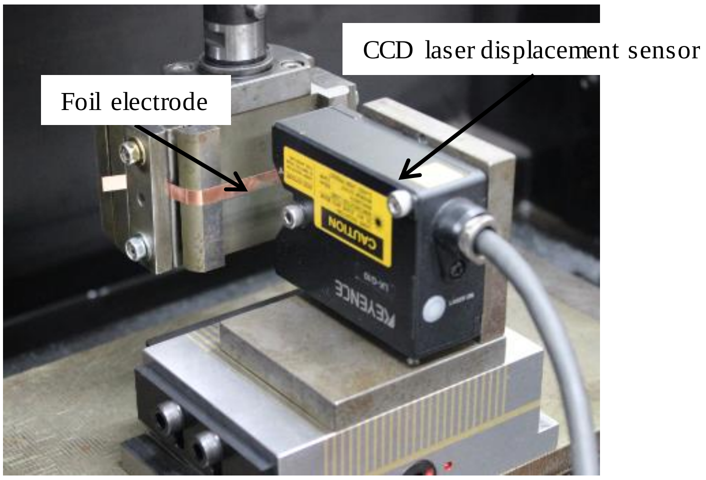

Figure 43: Parallelism error observation.

III.7.2. Measuring outputs

To investigate the effects of the holes and side surface insulation, three factors were studied: kerf loss, cutting speed and foil electrode wear ratio.

With regard to the kerf loss, the kerf width at the inlet was larger than that at the bottom of the cut kerf and the difference between those values varied from 3 µm to 11 µm in the experiments. Figure 44 shows an example of a cross section shape after slicing. However, from the point of view of the final slicing results, the kerf loss at the inlet is the most important parameter to evaluate the machining performance. Therefore, in the present work the kerf loss represents the inlet kerf width and it was measured by an optical microscope.

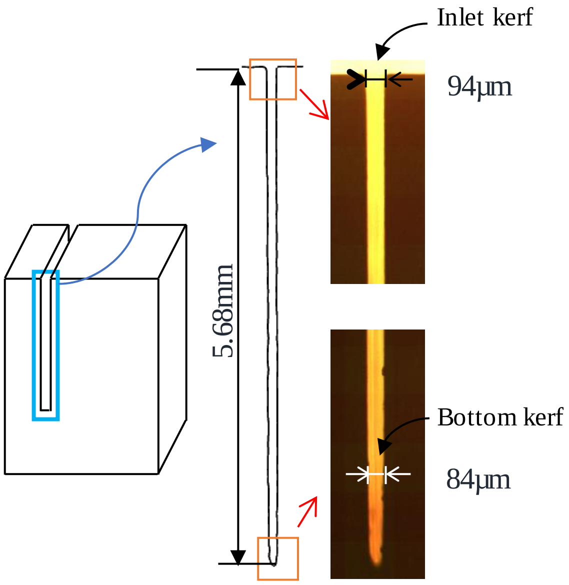

Figure 44: Cross section shape after slicing.

The cutting speed refers to the cut surface area of the workpiece per unit time. The electrode wear ratio refers to the ratio of the lost tool area to the cut depth area of the workpiece, which indicates that for the case of jump and no strategy, the values are comparable to the ratio of the lost tool length to the depth of cut. Figure 45 shows an example of one of the experiments in which the electrode wear is observed.

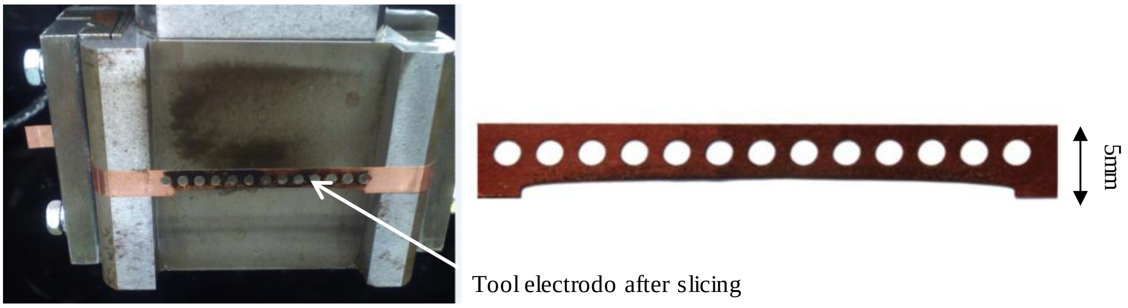

Figure 45: Foil tool wear in slicing of SiC with reciprocating motion.

III.7.3. Effect of making holes on foil electrode. Experimental results and discussion

This section presents a comparative analysis of kerf loss, cutting speed, and tool wear results between foil electrodes with and without holes. For the study, no coated electrode has been used.

III.7.3.1. Kerf loss

Figure 46 shows the kerf loss obtained under different conditions. It was found that using electrodes with holes, in the case of reciprocating motion, the kerf loss was reduced. However, in the cases of jump and no strategy motion, the kerf loss did not vary significantly. The lowest values of kerf loss were achieved when jump motion was applied, suggesting that improving flushing conditions in the gap, and hence decreasing debris concentration, has a significant impact on decreasing the occurrence probability of side surface discharges [99].

A further study concerning the influence of holes has been carried out as described in Section III.7.5. The effects of holes on the discharge delay time were analyzed for a better understanding of the possibility of reducing side surface discharges.

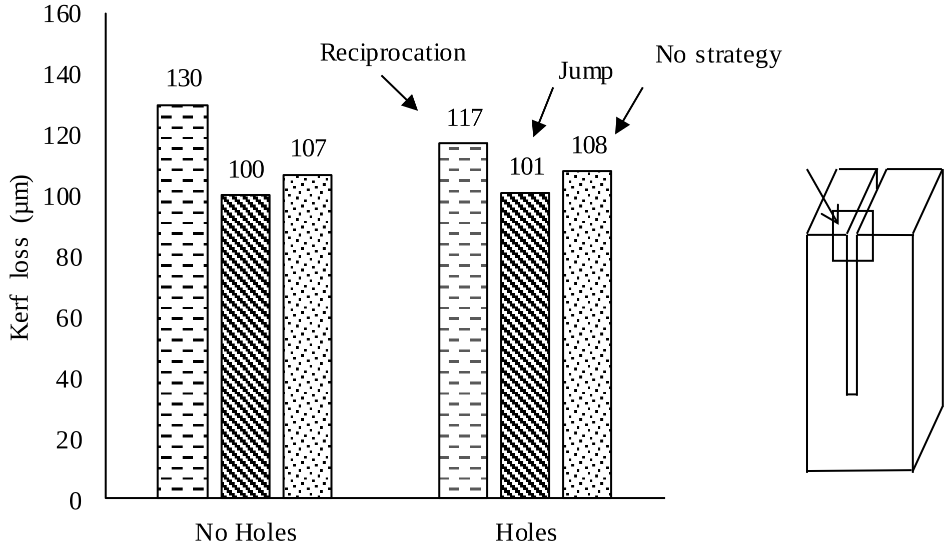

Figure 46: Influence of holes on kerf loss. No coated electrode.

III.7.3.2. Cutting speed

Figure 47 shows that cutting speed was improved with a foil electrode with holes when no strategy or reciprocating motion was used. The increase of the cutting speed is related with the improvement of machining stability, due to the chip pocketing effect of holes in the improvement of debris removal. Comparing the results between with and without holes, significant improvement of 47% by reciprocating motion was found. This may be because the debris stuck and accumulated in the holes is easier to remove when the foil is moving in the *X* axis direction. In the case of no strategy, the increase was 23%. On the other hand, the jump motion shows the highest cutting speed with or without holes. However, the cutting speed did not improve with the holes when the jump motion was used.

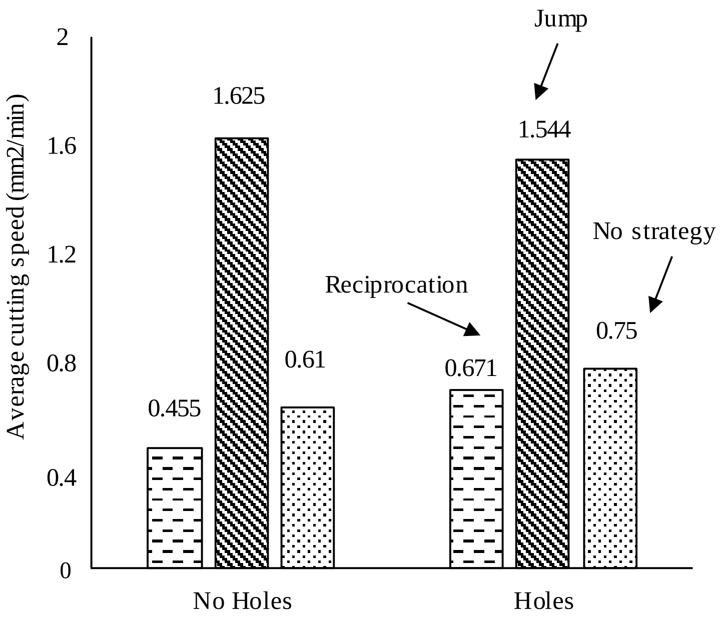

Figure 47: Influence of holes on cutting speed. No coated electrode.

III.7.3.3. Tool wear ratio

As shown in Figure 48, holes were effective in terms of the electrode tool wear ratio. This effect was attributed to the higher cooling efficiency resulting from the higher convection heat transfer on the foil electrode surface due to the enhanced circulation of the dielectric liquid, which resulted in a lower thermal load on the edge of the thin foil electrode [7].

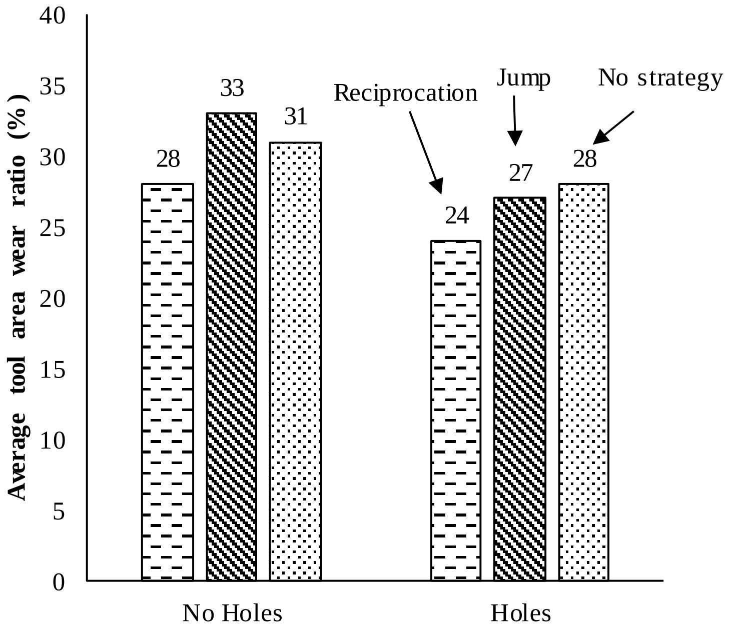

Figure 48: Influence of holes on average tool wear ratio (%). No coated electrode.

Figure 49 shows an image of the foil tool with holes after machining. They show different electrode wear patterns.

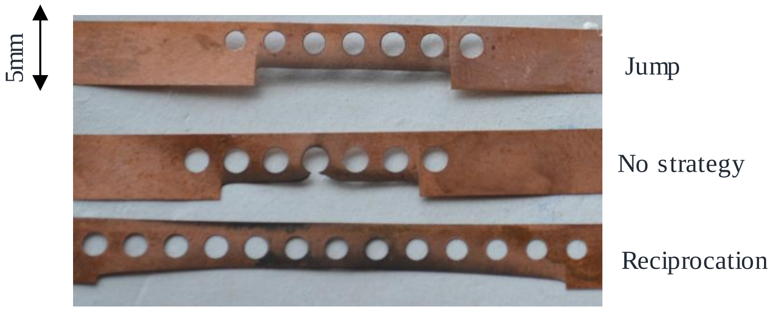
5mm
Jump
No strategy
Reciprocation

Figure 49: Foil electrode with holes after slicing.

III.7.4. Effect of side surface insulation. Experimental results and discussion

This section presents a comparative analysis of kerf loss, cutting speed, and tool wear results between a foil electrode without insulation layer, defined as no coating, and a foil electrode with side surface insulation, defined as coated.

III.7.4.1. Preliminary test for analysis the thickness of the coated layer

As a preliminary step, foil electrodes without holes coated with a resin coating layer of 5 µm, 10 µm and 22 µm in thickness were studied using the reciprocating motion.

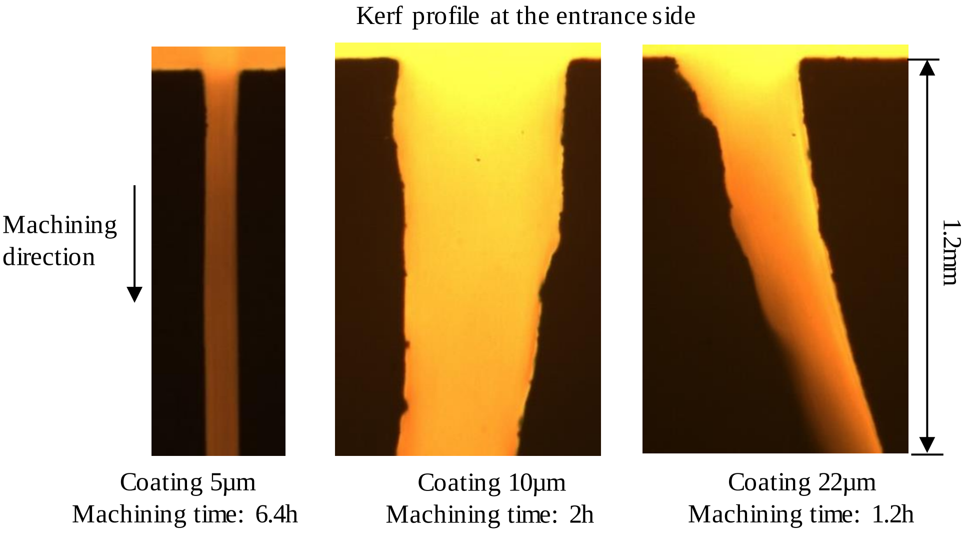
Kerf profile at the entrance side
Machining direction
1.2mm
Coating 5µm
Machining time: 6.4h
Coating 10µm
Machining time: 2h
Coating 22µm
Machining time: 1.2h

Figure 50: SiC workpiece cross section with different coating layer thickness.

Figure 50 shows that for the case of 10 µm and 22 µm, the machined kerfs were curved and Figure 51 an electrode foil with 22 µm of resin layer after machining, indicating that the foil electrode was deformed during machining due to collision between the tool and workpiece. The reason is considered as the following. When the side-surface of the foil tool electrode is completely insulated, debris particles accumulated in the side gap cannot be removed because discharge does not occur in the side gap, while with using no-coated tools, debris particles in the side gap can be flushed away by the explosive force due to discharge ignited in the side gap.

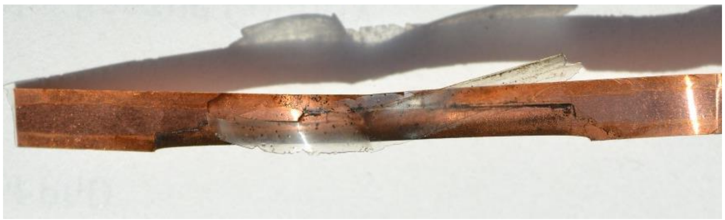

Figure 51: Foil electrode with an insulation layer of 22 µm.

These results demonstrate that the resin insulation layer thickness must not exceed the discharge gap width value to realize stable machining. Furthermore, the thickness should be thin enough to maintain a certain level of electric conductivity through the resin coating layer. Consequently, an electrode foil with an insulation layer of 5 µm was used in the experiments described below. Here, it should be noted that the surface was not insulated completely with the coated thickness of 5 µm, which was verified using a circuit tester, suggesting that discharge can occur even on the side surface through the resin coating layer.

III.7.4.2. Kerf loss

As results of Figure 52 show, it is found that the kerf loss decreases when coated foil electrode is used, demonstrating that the occurrence probability of discharges can be reduced by coating the side surface with a resin of 5 µm in thickness. The effect is more significant in the case of reciprocating motion. A further study was carried out as described in Section III.7.5, in which the effect of coating was analyzed by the distribution of the discharge delay time, which is a measure to quantify the dielectric breakdown strength of the gap.

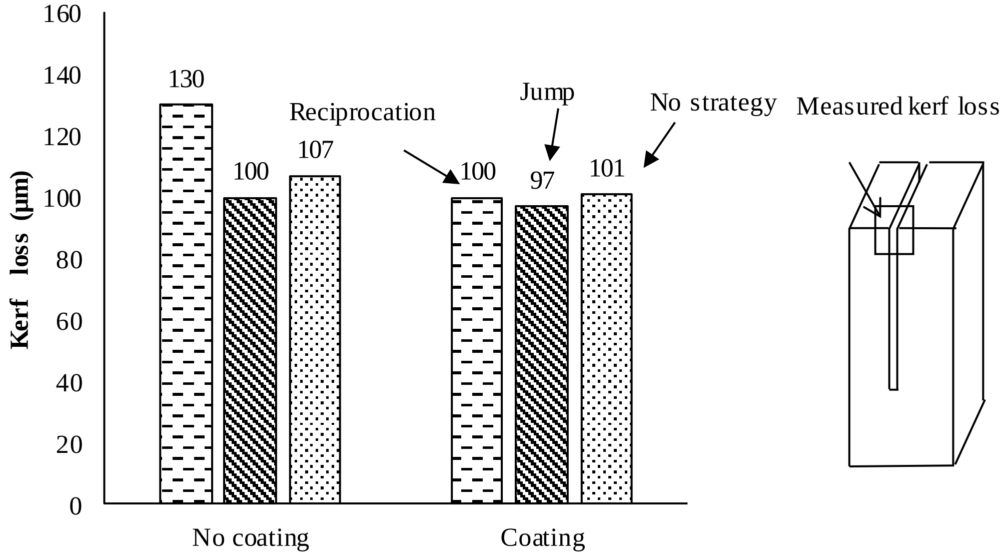

Figure 52: Influence of surface insulation on kerf width. Electrode without holes.

III.7.4.3. Cutting speed

With regard to cutting speed, Figure 53 shows that the cutting speed decreased when the coated electrode was used. This indicates that machining stability was affected by the insulation layer. A possible explanation is that the reduced gap width resulted in the elevation of temperature due to restricted fluid flow and accumulation of debris particles, leading to unstable discharges [84].

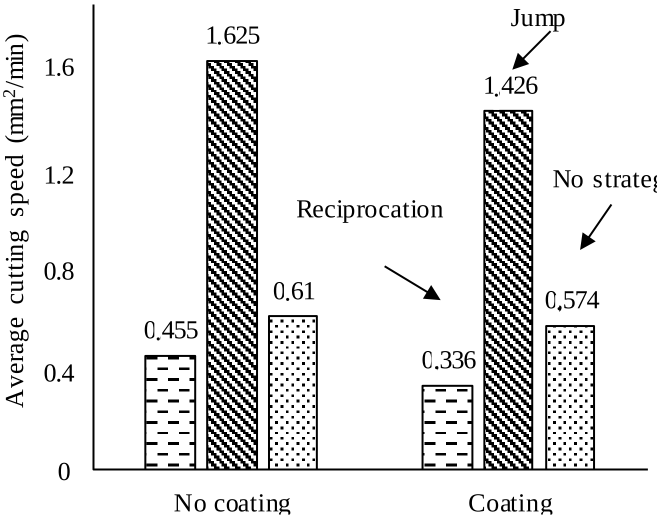

Figure 53: Influence of holes on cutting speed. Electrode without holes.

III.7.4.4. Tool wear ratio

Figure 54 shows the results of tool wear ratio. When reciprocating motion of the tool electrode was applied, electrode wear ratio decreased in the case of the coated foil electrode. However, in the case of no strategy and jump motion, electrode wear slightly increased probably because the tool temperature increased.

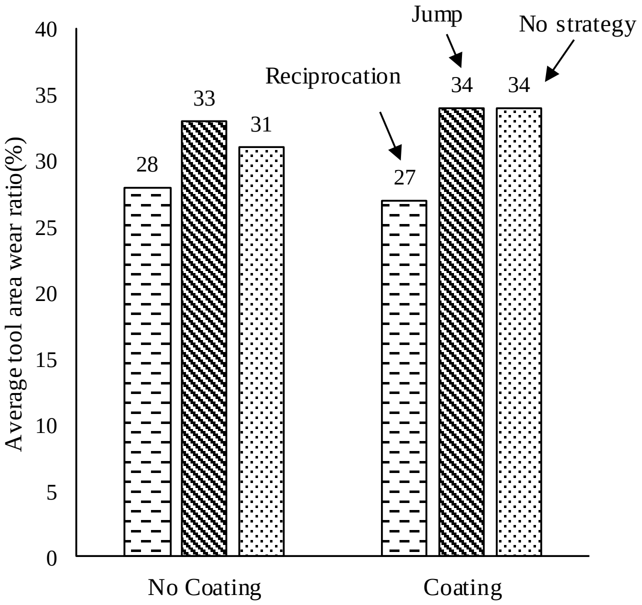

Figure 54: Influence of surface insulation on average tool wear ratio (%). Electrode without holes.

III.7.5. Discussion: Influence of discharge delay time

From the machining experiments described in Section III.7.3 and in Section III.7.4, it was concluded that holes and surface insulation are useful for reducing kerf loss. The results are explained by the decrease of the occurrence probability of side surface discharges. In order to prove the hypothesis, the influence of the foil electrode design on the occurrence probability of the discharge was investigated by the analysis of the distribution of discharge delay time.

The discharge delay time, t_d, is defined as the interval between the application of the voltage pulse and dielectric breakdown, and it reflects the dielectric breakdown strength of the gap. Its value is difficult to establish, since the discharge delay time is determined by various factors, such as debris concentration, discharge area, surface profile and gap width. The discharge delay time cannot be defined in a deterministic way, but in a probabilistic way. Bommeli *et al.*[100] verified that due to the great dispersion of results, an exponential distribution model can be used for the analysis. For this reason, different authors have made use of the Laue Plot as a comparison tool for studying different factors related to the discharge delay time. Araie *et al.* [101] investigated the effect of the surface roughness of a wire electrode on the discharge delay time by Laue plot. Morimoto *et al.*[99] found that the discharge delay time was longer with a wider gap width, less debris concentration and smaller machining area.

The Laue plot shows the percentage, n/N, of electric insulation that does not break down until time t after the supply of pulse voltage. It is expressed by Eq.11 [99]:

$$\frac{\mathrm{n}}{\mathrm{N}} = \exp\left(-\frac{\mathrm{t}}{\mathrm{t}_{\mathrm{d,ave}}}\right) \quad \text{Eq.11}$$

Here, N represents the number of measurements carried out for drawing the Laue plot and $t_{d,ave}$ is the average of the measured t_d, calculated by Eq.12:

$$\mathrm{t}_{\mathrm{d,ave}} = \frac{\sum \mathrm{t}_{\mathrm{d}}}{\mathrm{N}} \quad \text{Eq.12}$$

III.7.5.1. Test definition and methodology

The distribution of the discharge delay time was obtained using the Laue plot. The experiments were carried out and analyzed according to the procedure used by Morimoto and Kunieda [99].

The material used in the experiments were a copper electrode and a cold tool steel (SKD 11) workpiece. The preparation of the materials will be described in Section III.7.5.2. The reason why SiC was not used in the experiments is because of its difficulty in grinding and the material cost.

However, since the purpose of this study is to conduct a relative investigation on the influence of the electrode design on the discharge delay time in EDM, it does not matter what workpiece material is used. The trend will be the same no matter the workpiece material.

Table 7: Machining conditions for analysing distribution of discharge delay time.

Tool electrode (-)	Cu
Workpiece (+)	SKD11
Open circuit voltage (V)	120
Dielectric fluid	EDM oil
Gap width (µm)	10
Discharge area (mm^2)	64

As it will be described, a single discharge was generated between the Cu and SKD11 by a bipolar power source and a function generator, and the value of the discharge delay time was measured by a high-frequency oscilloscope. For drawing the Laue Plot, 20 data were obtained per electrode type, which were: No coating without holes, no coating with holes and coating without holes. The machining conditions are presented in Table 7.

III.7.5.2. Preparation of the electrodes

For the generation of the single discharge, the gap width considered was of 10 µm. This indicates that the gap width during experiments should be controlled, as a slight deviation will disturb the results.

As first attempt, a block of SKD 11 and a foil electrode of 0.05 mm were used. The experimental set-up for generating the singles discharge is presented by Figure 55.

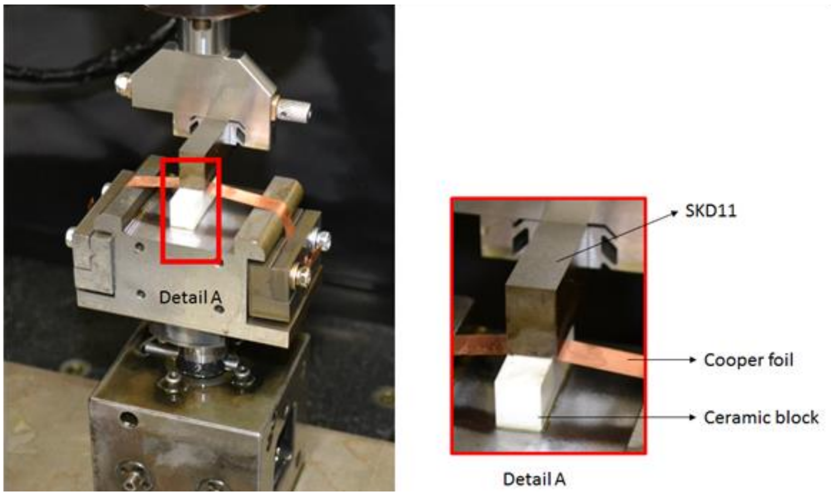

Figure 55: First attempt. Image in which the experimental set-up up is presented.

In this case, as shown in Figure 55, a ceramic gauge block was used for ensuring the parallelism of the foil as well as avoiding the retraction of the foil to the workpiece. With this set-up, the parallelism error measured along the discharge area was of 5 µm. Thus, the set-up was dismissed.

The second alternative, which was the one used for data acquisition, consists in using two blocks, one of SKD 11 and other of copper. The parallelism was ensuring by grounding the block fixed in their precision fixture. Then, the parallelism error was checked by the CCD laser displacement sensor and the position was checked by an indicator. Figure 56 presents a couple of photographs taken during the checking.

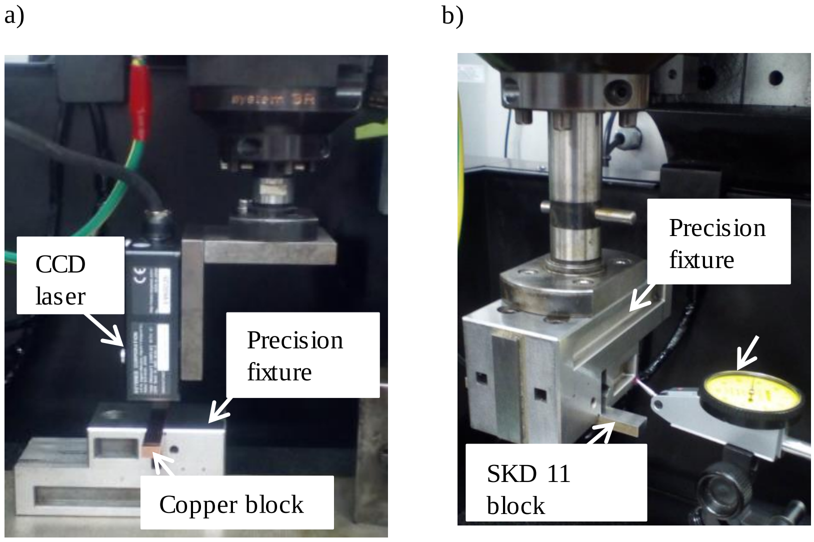
a)
b)
CCD laser
Precision fixture
Copper block
Precision fixture
SKD 11 block

Figure 56: a) Parallelism error measurement. b) Correct positioning of the blocks in the machine tool.

Figure 57 shows the experimental set-up instants before the discharge generation.

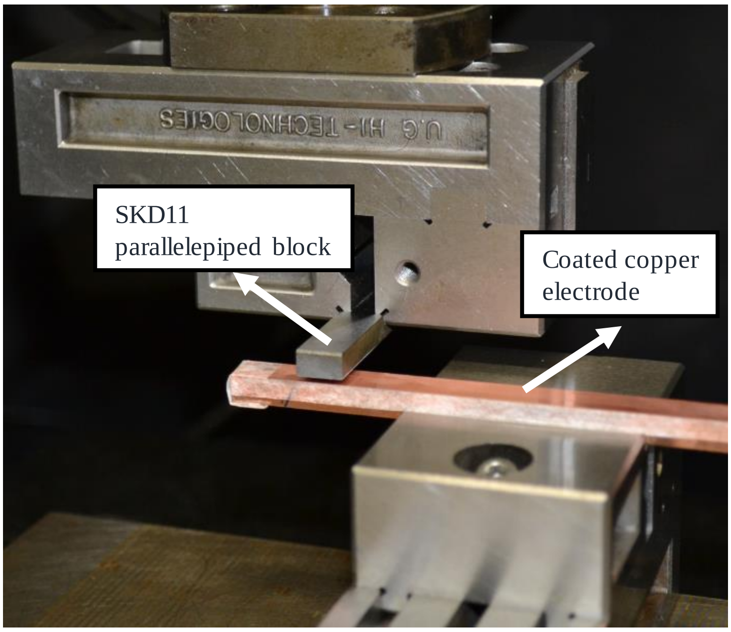
U.G HI-TECHNOLOGIES
SKD11 parallelepiped block
Coated copper electrode

Figure 57: Experimental set-up for the study of the discharge delay time.

For a reliable discharge delay time measurement, each discharge must be generated in a clean and smooth surface in which no previous discharges were generated. Because of that, after a discharge was generated, the SKD 11 block was moved to another position. The block movement is shown by Figure 58.

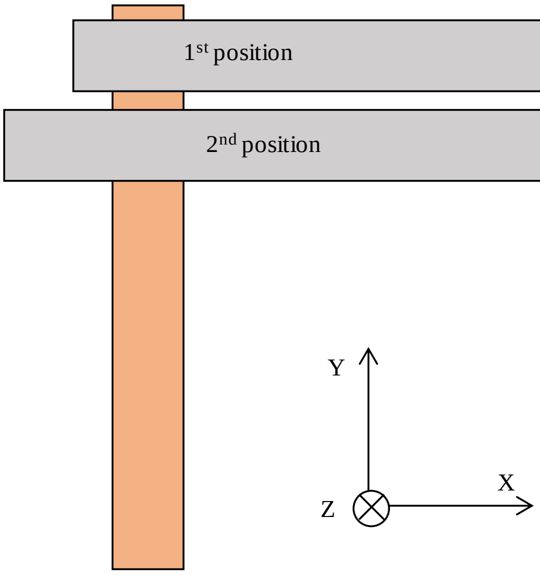

Figure 58: Representation of the movement of the workpiece for obtaining two data.

Figure 59 illustrates the electrode blocks compared in the present study.

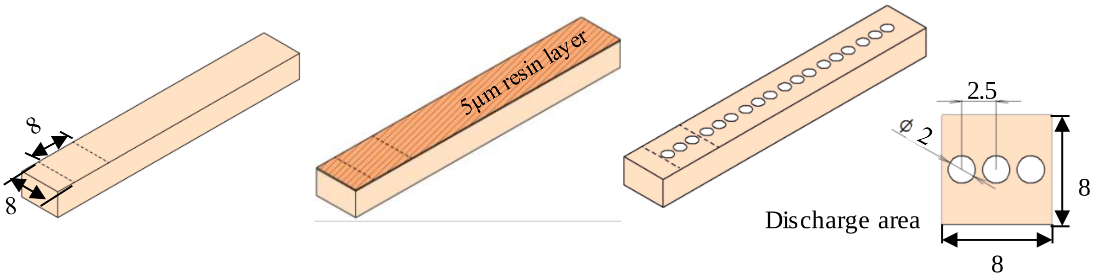

Figure 59: Scheme of the copper block design studied. a) No coating, no holes; b) Coating, no holes; c) No coating, holes.

In the case of c), holes are machined on the copper block by sinking EDM using rod electrodes. Figure 60 shows the copper block after hole machining, then it was grounded. For the three cases studied, the gap width of 10 µm represents the distance between SKD11 surface and copper top surface under the coating film.

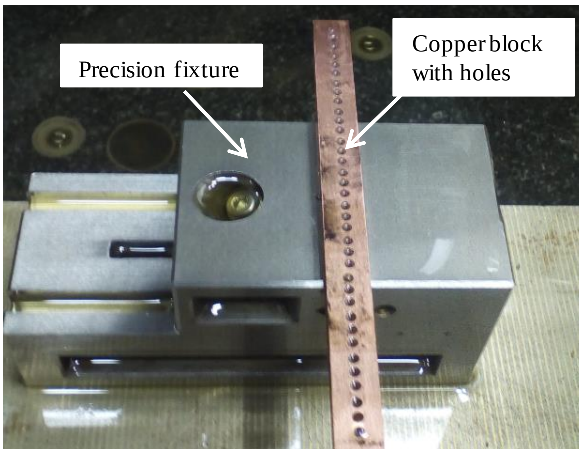
Precision fixture
Copper block with holes

Figure 60: Copper block after the machining of the holes.

III.7.5.3. Generation of the discharge

For the generation of a single discharge between the Cu and SKD11, three alternatives were considered: to build an electrical circuit, to use the generator of the machine tool and the use of a bipolar power source. Finally, the last alternative was considered. The set-up is illustrated in Figure 61.

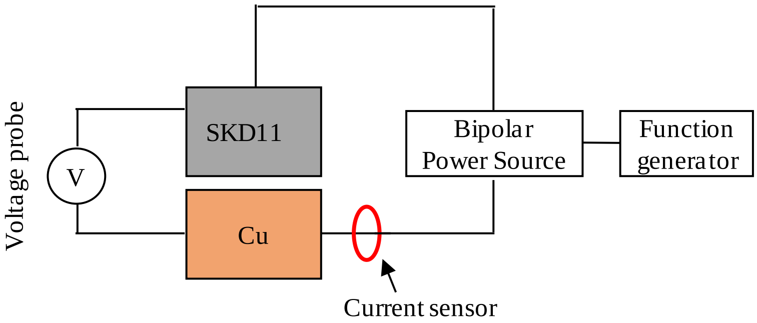
Voltage probe
V
SKD11
Cu
Bipolar Power Source
Function generator
Current sensor

Figure 61: Discharge generation set-up for the analysis of the discharge delay time.

For discharge delay time data acquisition, each discharge was recorded by an oscilloscope. Figure 62 shows an example in which the t_d value was of 65.61 µs.

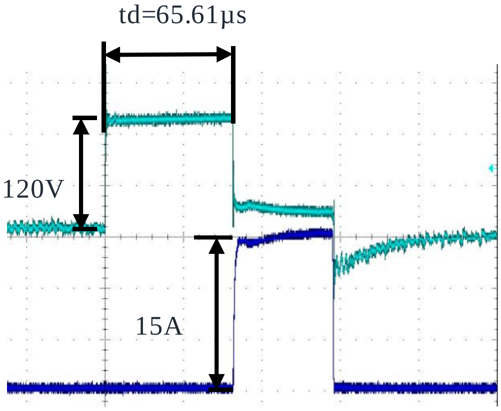

Figure 62: Example of a discharge waveforms for the case of no coating without holes.

III.7.5.4. Results and discussion

Figure 63 shows the Laue plot obtained for each electrode, and Figure 64 shows the average discharge delay time, $t_{d,ave}$. Results represent the trend of the distribution of the discharge delay time in order to analyze the influence of electrode design on the occurrence of probability of side surface discharges.

Results show that for both electrode with holes and coated electrode, the discharge delay time increases. Moreover, although the discharge delay time was significantly longer in the case of coated electrode, discharges occurred. This means that with a 5 µm epoxy layer, perfect insulation cannot be achieved. Hence, even though the probability of discharge occurrence is significantly low on the side surface, the debris particles can be removed by discharge which is ignited through the resin coating layer.

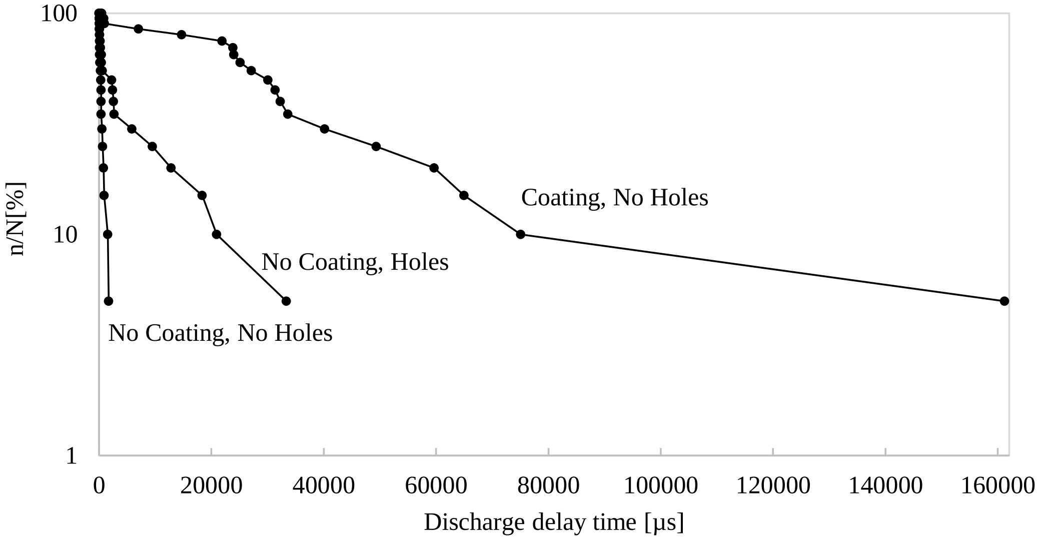

Figure 63: Distribution of the discharge delay time.

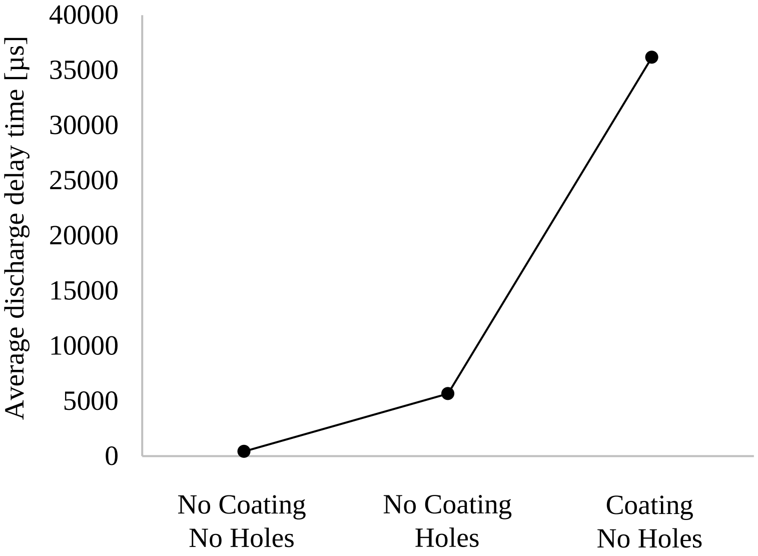

Figure 64: Relation between proposed electrode designs and average discharge delay time.

It can therefore be concluded that the two proposed electrodes, under the same conditions, are effective for reducing side surface discharges.

III.7.6. Strategy for optimal machining

From the results above, it can be concluded that both proposed electrodes are effective for improving the machining performance of SiC. The resin coating on the foil electrode is effective for reducing kerf loss. However, the thickness of the resin coating layer should be thinner than the gap width. Furthermore, the thickness should be thin enough to enable certain level of side surface discharge. Otherwise, the debris particles in the side gap cannot be removed, resulting in the deformation of the foil electrode. In addition, combined with jump motion of the tool electrode, optimal machining results can be achieved.

III.8. Conclusions

In the present work, attempts were made to improve SiC slicing by foil electrode. The main goal was improving kerf width accuracy by considering the influence of the occurrence probability of side surface discharge on the kerf width and machining performance. Two foil electrodes were proposed: an electrode with holes and an electrode with an insulation layer on the side surface. The effectiveness of both foil electrodes was confirmed by a series of cutting experiments and by a study on the distribution of the discharge delay time by the Laue plot. It was concluded that:

- Using a foil electrode with holes, cutting speed increased and tool wear decreased. As a reason, the chip pocketing effect of holes improved flushing and cooling conditions, thereby the machining stability improved and the thermal load on the foil electrode decreased.
- Kerf loss was reduced when the side surface of the foil electrode was coated with a resin coating layer of 5 µm in thickness. Thicker layers of 10 µm and 22 µm resulted in curved kerfs due to collision between the tool and workpiece.
- The fact that the electric insulation of the resin coating layer of 5 µm in thickness was not perfect indicates that the foil electrode surface should not be fully insulated.
- The lowest kerf loss and highest MRR were obtained when jump motion of the tool electrode was used. This indicates that debris concentration in the gap width has significant influence on the machining performance.
- From the analysis of the distribution of the discharge delay time by the Laue Plot, it was concluded that making holes and coating the electrode surface with a 5 µm resin coating layer result in a longer discharge delay time. Hence, it was verified that both techniques can decrease the kerf width.

Although this work is focused on SiC slicing, it is expected that the chip pocketing effect of holes can enhance the flushing conditions in other machining jobs. Hence, this work has driven the research work presented in Chapter IV. In this case the objective is to improve the machining stability and thus, the machining time, in the EDM'ing of high-aspect ratio slots.

Chapter IV: Improvement of EDM performance in high-aspect ratio slot machining

IV. IMPROVEMENT OF EDM PERFORMANCE IN HIGH-ASPECT RATIO SLOT MACHINING

Machining of high-aspect ratio slots is a common operation in industry, particularly in the mold and die and aerospace sectors. Considering that in EDM material hardness is not a limitation and that EDM can fulfil strict geometrical requirements, EDM is a competitive solution in the machining of high-aspect ratio slot. However, due to debris accumulation in the narrow gap, machining stability at high depths cannot be guaranteed, and material removal rate decreases drastically with machining depth. Taking as background the conclusions obtained in Chapter III, the present work includes original findings about the influence of machining holes on flushing efficiency in high-aspect ratio slot machining.

IV.1. Introduction

The present work was developed in the facilities of the department of Mechanical Engineering of the Faculty of Engineering of Bilbao of the University of the Basque Country by the support of Professor Kunieda and Doctor Zhao of the University of Tokyo.

As described in Section II.2.2, the manufacturing of deep slots is a common operation in industry, with special focus on two sectors: mold and die industry and aerospace industry. Nevertheless, even if EDM is a competitive solution it is not an effortless operation. In this application, due to the small discharge area, there is a high concentration of discharges in the bottom section of the electrode and as machining depth increases, the evacuation of debris becomes more difficult. Thus, those two factors set limits to the material removal rate.

The main objective of the present study is to enhance the flushing conditions in the narrow gap, and thus, improve MRR. With this purpose a specially designed multi-holed electrode is proposed. The main idea for electrode design, is based on the findings of the work described in Chapter III. In that work, it was found that in the application of EDM technology for SiC slicing using foil electrode if the slicing was conducted by feeding the thin foil electrode in Z direction, the cutting speed could be improved by 23% when using an electrode with holes.

Consequently, the objective of the experiments carried out in the present Chapter, is to assess the improvement in performance, if any, of the EDM process of high-aspect ratio slots when a specially designed electrode is used. The new electrode has a number of holes in its lateral faces that are expected to contribute to effective debris evacuation during the machining process.

IV.2. Main equipment and machine tools used

In this section, a description of the main equipment and machine tools used is included:

- The experiments were carried out under industrial conditions on an ONA CS300 sinking EDM machine. Table 8 shows the machine tool used and its main specifications. The generator of the machine tool used in the experiments is an iso-energetic generator. This means that during the machining process the generator attempts to maintain I and t_{on} at constant values. Moreover, in order to avoid inefficient discharges, such as arc and short-circuits, the pulse generator controls the t_{off} value.

Table 8: ONA CS300 SEDM machine main specifications.

ONA CS300		
Y-axis travel (mm)	400	
Z-axis travel (mm)	300	
C-axis. Max. suspension weight in static conditions (kg)	50	
C-axis. Max. suspension weight in dynamic conditions (kg)	12	
Table size (mm)	550x400	
Max. workpiece weight (kg)	800	
Machine tank dimensions (mm)	900x500x300	

Table 9: ONA PRIMA E250. WEDM machine main specifications.

ONA PRIMA E250 Specifications		
X-axis travel (mm)	350	
Y-axis travel (mm)	250	
Z-axis travel (mm)	200	
U-axis travel (mm)	80	
V-axis travel (mm)	80	
Max. workpiece dimensions (mm)	910x680x200	
Max. workpiece weight (kg)	500	
Max. cutting angle (°)	30	
Wire diameter (mm)	0.1-0.3	

- The electrode material was supplied in a rectangular sheet of 0.8 mm in thickens. Hence, the graphite was cut by WEDM before each experiment. The WEDM used was an ONA PRIMA E250, Table 9 shows the specifications.
- The workpiece material was F114 structural steel and the electrode material was POCO EDM-3®. The dimensions of the electrode were 0.8 mm in thickness and 50 mm in length.
- For electrode measurements two equipment were used: a profile projector Mitutoyo PJ-3000F, see Table 10, for the measurements of electrode edge radius and a Leica DCM 3D optical surface metrology system, see Table 11, for electrode lateral wear measurement.
- For analysing the discharges in the working gap, a high-frequency oscilloscope was used, DPO 5034B Digital Phosphor Oscilloscope, Tektronix Inc. [102]. The current signal was obtained using a CWT Rogowski Current Transducers (Power Electronic Measurement Ltd. [103]), and the voltage signal was obtained by using a High Voltage differential probe [102].

Table 10: Mitutoyo PJ-3000F profile projector [104].

Mitutoyo PJ-3000F profile projector		
Projected image	Inverted image	
Objectives	10x, 100x	
Counter illumination	2-stage brightness switch, Hear-absorbing filter	
Surface illumination	Vertical illumination with a half-reflection mirror	

Table 11: Leica DCM 3D optical surface metrology system [105].

Leica DCM 3D optical surface metrology system		
Measuring principle	Dual Core Optical Imaging Profilometry (Confocal and Interferometry) non-contact, 3D	DCM 3D Leica
Objectives	5x, 10x, 20x, 50x, 100x	
Measuring software	LeicaScan LeicaMap	
Axis	X, Y, Z	

IV.3. Improvement of EDM performance in high-aspect ratio slot machining using multi-holed electrodes

IV.3.1. Proposed multi-holed electrode

The main contribution of the present work is the use of a multi-holed electrode for the improvement of machining performance of high-aspect ratio slot machining.

For the machining of the holes on the graphite electrode, three possible alternatives were considered: SEDM, laser and conventional machining. In this work holes were machine by SEDM due to the availability in the laboratory. The electrode used was a copper round bars. Figure 65 illustrates an electrode after hole machining.

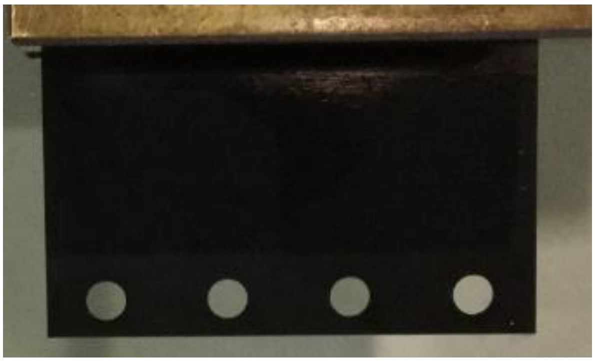

Figure 65. Specially designed graphite electrode for slot machining.

With the objective of enhancing the flushing condition of the narrow gap, three effects were studied: the effect of flushing holes diameters, positioning of the flushing holes, and geometry of the flushing cavity. In this Section the effectiveness of machining flushing holes on the electrode has been verified through a series of machining experiments as well as with a study of the optimum design.

IV.3.2. Test definition and methodology

Since the objective was to test the efficiency of the new electrode design, the conditions of the EDM process were not manipulated during this study. Instead, they were taken from a previous research study [25] in which optimization of process variables for the EDM machining of high-aspect ratio slots was addressed by using DoE technique. In the present study material removal rate is a priority, thus, the machining conditions that results in higher material removal rate were considered, see Table 12.

Table 12: Machining and experimental conditions.

Working fluid	EDM oil
Polarity (electrode)	+
U_0 (V)	120
I (A)	48
t_{on} (μs)	89
t_{off} (μs)	179
SV (V)	57

With the aim of studying the repeatability of the process and given that in industry the same electrode is used for machining a set of slots, in the present work 5 slots were machined for each experimental condition.

IV.3.3. Influence of hole diameter

In order to study the impact of the diameter of the flushing holes on machining performance, three different electrode designs were compared: conventionally used electrode (without holes), electrode with holes of 2 mm, and electrode with holes of 4 mm. Figure 66 shows a scheme of the electrodes. In both cases the reduction in the area of the electrode material was maintained constant.

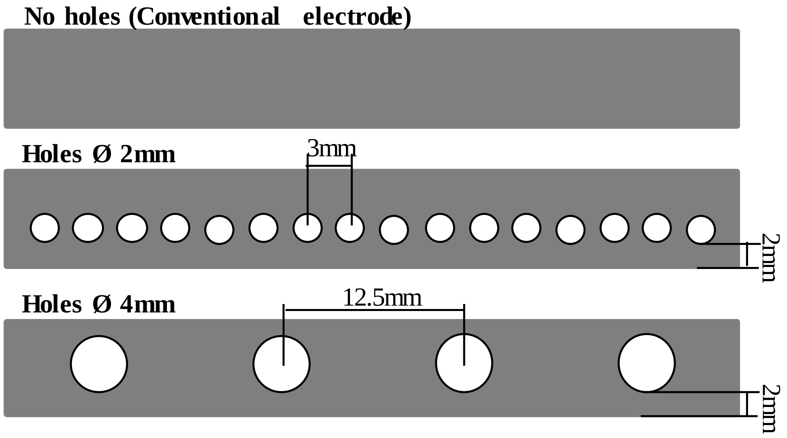

Figure 66: Test definition for analysing the effect of holes.

In order to compare the results, a machining depth of 6.5 mm was considered, which is a reasonable machining depth in the machining of the lateral faces of NGVs.

IV.3.4. Influence of positioning of holes in the electrode

In addition, the influence of the position of the flushing holes with respect to the discharge area was investigated. In this case, the diameter of the flushing holes was 4 mm and the machining depth was maintained 6.5 mm. Figure 67 shows the scheme of the electrode designs compared.

Additionally, machining flushing holes to a distance of 1 mm from discharge area was considered. However, due to the poor machining conditions, the cycle of 5 slots was not completed.

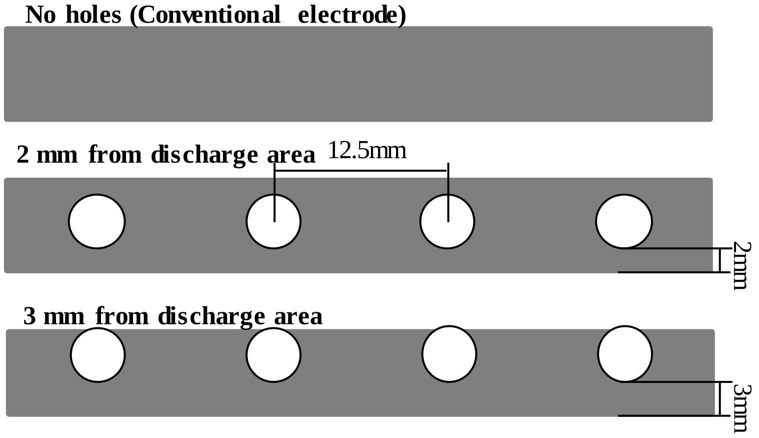
No holes (Conventional electrode)
2 mm from discharge area
12.5mm
2mm
3 mm from discharge area
3mm

Figure 67: Test definition for analysing the influence of positioning of the holes in the electrode.

IV.3.5. Influence of hole geometry

As discussed, an increase in the machining depth implies greater difficulties in terms of flushing conditions and debris evacuation. Therefore, in order to determine the optimum electrode design, two electrode designs were proposed when machining at a depth of 10 mm. The electrode designs compared are shown in Figure 68. The main objective was to understand which design — two rows of flushing holes in staggered rows or a pocket-flushing cavity — results in better machining performance.

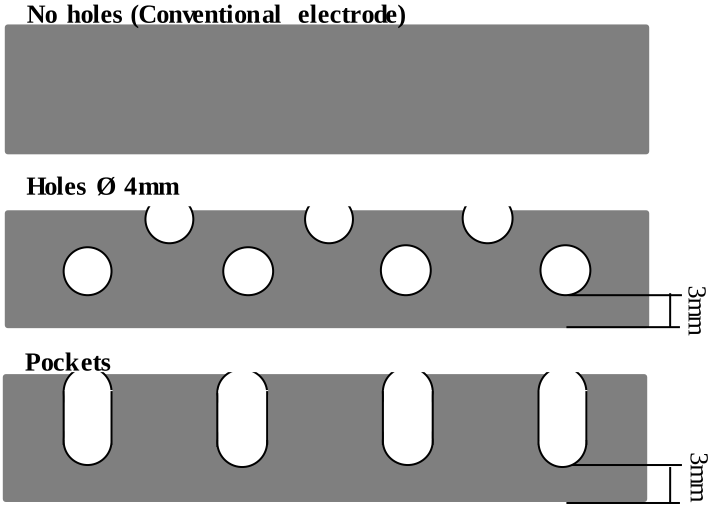
No holes (Conventional electrode)
Holes Ø 4mm
3mm
Pockets
3mm

Figure 68: Test definition for improving hole geometry.

Additionally, the influence of the chip pocketing effect of pockets on machining time was studied at a depth of 15 mm and 25 mm.

IV.3.6. Process outputs

With the aim of analysing the effect of flushing holes on the machining performance, the machining time and the electrode wear were compared.

When machining high-aspect ratio slots, an increase in machining depth causes the process to lose stability, whilst the rate of material removal decreases. This indicates that the rate of material removal is not constant throughout the process. Hence, in the present work machining time was considered as an output parameter, which refers to the average time of the five slots. Moreover, the standard deviation was represented.

Electrode wear was characterized by three outputs: electrode edge radius, lost length of electrode, and electrode lateral wear. Figure 69 illustrates the outputs measured for characterizing electrode wear. Measurements of edge radius and length loss were taken after each slot, whilst lateral wear of the electrode was measured after completing the machining of the 5 slots.

Electrode edge radius represents the average radius of both edges and it was measured using a profile projector, Table 10. Electrode length loss was measured in the machine tool by comparing the length of the electrode both before and after each operation. The measurement was taken at three points and the average value was represented. Moreover, with the objective of analysing the concavity effect of the electrode, the lateral section of the electrode was measured using a 3D optical surface metrology system, Table 11.

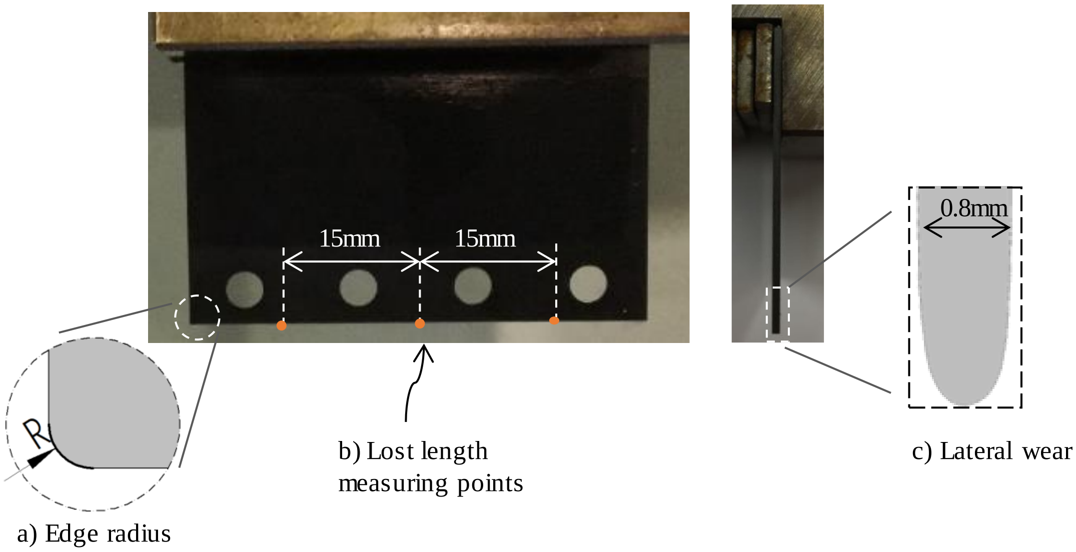

Figure 69: Characterization of electrode wear. a) Edge radius; b) Length loss; c) Lateral wear.

IV.3.7. Results and discussion

As explained in the previous section, various electrode designs have been considered in this study, so that three different effects could be analysed: effect of flushing hole diameter, effect of flushing hole position from the discharge gap and effect of flushing hole geometry.

In this section each effect is discussed separately in terms of machining time, electrode wear radius and electrode lost length. Results regarding lateral electrode wear are also considered.

IV.3.7.1. Effect of the diameter of the flushing holes machined on the electrode

This section compares the machining performance of a conventionally used electrode (No holes), electrode with holes of 2 mm (Holes Ø 2 mm) and electrode with holes of 4 mm (Holes Ø 4 mm). As mentioned previously, the area reduction of the electrode was maintained constant in both combinations. As explained before, the pre-set machining depth for each slot was 6.5 mm.

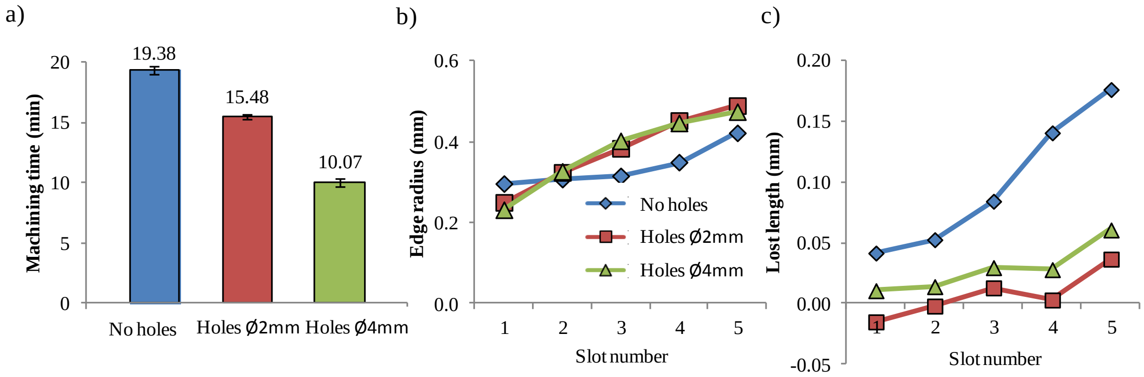

Figure 70: Influence of flushing hole diameter in terms of: a) Machining time, b) Edge radius, c) Length loss.

Figure 70.a shows the average machine time as well as the standard deviation between the five slots of the machined cycle. The impact of holes on the machining time is clear, at the sight of the improvement in machining time. With holes of 2 mm in diameter the improvement is 20% and for holes of 4 mm the improvement is 48%. This is attributed to the chip pocketing effect of holes, which improves the flushing conditions in a narrow gap. It is therefore clear that the strategy of machining holes in the electrode yields considerable benefits in terms of productivity.

Electrode wear is also of primary importance in this type of EDM operation. Figure 70.b shows the evolution of electrode edge radius during the experiments with the different electrode geometries. As previously observed by Mohri *et al.* [14] the increase in corner radius occurs at the early stages of machining. In the experiments the maximum change in radius occurs during the machining of the first slot. This is because discharge concentration — which leads to an increase in local electrode temperature — is higher at sharp edges. No significant differences were observed between the different experiments in terms of evolution of edge radius. However, it should be noted that significant differences are observed in the evolution of electrode lost length (see Figure 70.c). The use of the electrode with flushing holes leads to wear being reduced by 65%, regardless of the diameter of flushing holes used. Therefore, it appears that loss of electrode length is directly related to machining time.

IV.3.7.2. Effect of the position of flushing holes with respect to discharge area

In this section the influence of the position of the flushing holes with respect to the discharge area is analyzed. The experiments aimed to compare the machining performance when using a conventional electrode (No holes), an electrode with flushing holes of 4 mm diameter at a distance of 2 mm from the discharge area (2 mm) and an electrode with flushing holes of 4 mm diameter at a distance of 3 mm from the discharge area (3 mm). An additional test was conducted with holes at a distance of 1 mm from the discharge area. In this case, the machining destabilizes ones the holes were inside the slot, at a depth of 5 mm. Consequently, the results were similar with the results when the conventional electrode was used. Therefore, results have not included in the discussion.

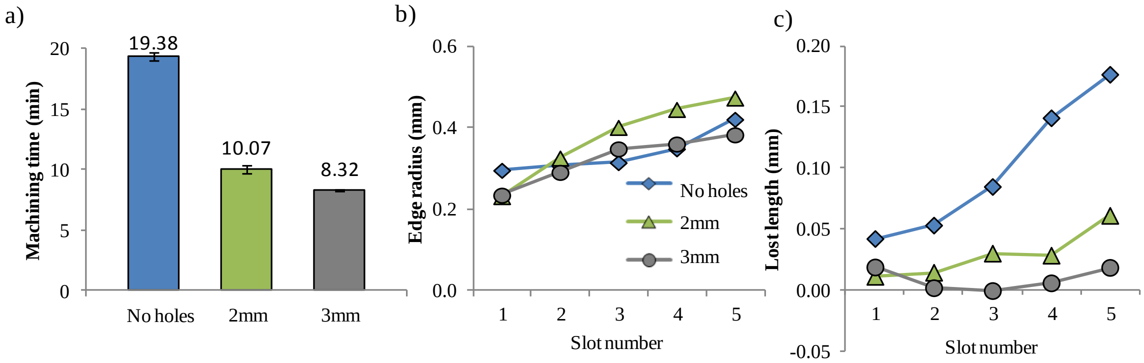

Figure 71: Influence of position of flushing holes from discharge area in terms of: a) Machining time, b) Edge radius, c) Lost length.

The data plotted in Figure 71.a indicate that machining time can be improved by machining the flushing holes of the electrode at a distance of 3 mm from the discharge area. In fact, an improvement of 57% is achieved when compared with the machining time consumed by the electrode with no holes. Even when comparing with the results in Figure 70 an improvement of 17% was observed. This effect was attributed to the enhancement of flushing conditions. Moreover, upon inspection of the displacement of the machine axis when machining a single slot, see Figure 72, it can be concluded that the machining process is very stable with this new configuration.

Figure 72 shows the evolution of machining time versus slot depth for three different electrode geometries: with no holes, with holes at 2 mm from electrode edge and with holes at 3 mm from electrode edge. According to the results, machining becomes unstable at a machining depth of 4mm when the conventional electrode is used. At that depth, the electrode retracts, and the material removal rate decreases dramatically. Stability is increased by locating holes at 2 mm from electrode edge, but the same effect of electrode retraction is observed when flushing holes are completely inside the slot. When holes are located at 3 mm from electrode edge, stability is ensured all along the operation. The issue of stability will be further discussed in the following section (see Figure 74).

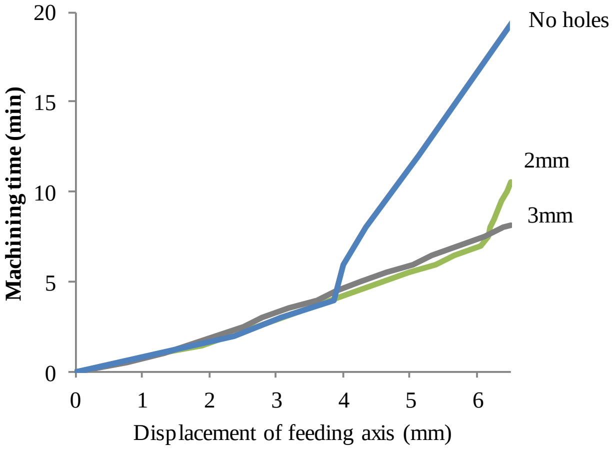

Figure 72: Comparison of the displacement of feeding axis vs. machining time with the three different electrode designs.

In terms of electrode wear at the edge radius (see Figure 71.b), no remarkable differences have been found. However, Figure 71.c clearly indicates that loss of electrode length decreases when flushing holes are machined at a distance of 3 mm from the edge of the electrode, which maintains the relationship with the machining time. A longer machining time means that the electrode is exposed for a longer time to high temperatures and, given that the area of discharge is small, this can have a considerable impact on electrode wear.

IV.3.7.3. Effect of flushing hole geometry

From the results described above it was concluded that machining stability could be guaranteed for a depth of 6.5 mm if the holes penetrate the entire depth of the machining operation (see Figure 72). In this section, a machining depth of 10 mm was chosen, and two electrode designs were proposed: two staggered rows of holes of 4 mm diameter (2 rows of holes) and open holes (Pockets). The main goal was to understand whether the holes need to penetrate the entire machining depth in order to enhance machining performance.

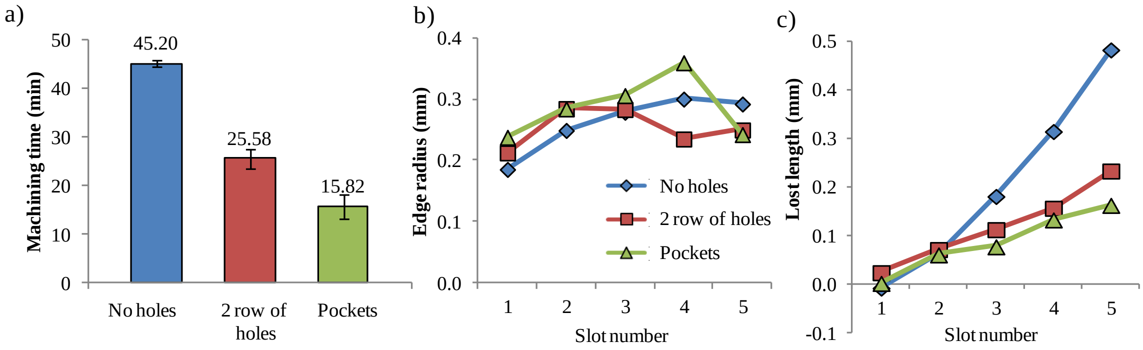

Figure 73: Influence of flushing hole geometry in terms of: a) Machining time, b) Edge radius, c) Lost length.

Figure 73.a represents machining time for the three experiments. Both staggered rows and pockets dramatically reduce machining time, but the best performance was obtained with the pockets design. With the electrode with two staggered rows of holes the improvement was 43% and with pockets this improvement was 65%. The reason for this, as observed in Figure 10, is that after the first row of holes is positioned inside the slot, there is a decrease in stability and hence, in material removal. In contrast, stability is ensured throughout the entire machining depth when using the electrode with pockets.

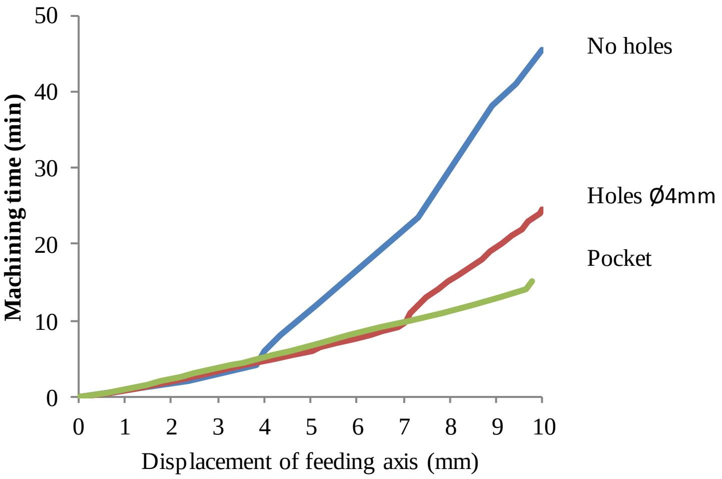

Figure 74: Comparison of the displacement of feeding axis vs. machining time with three different electrode designs.

With respect to electrode wear (Figure 73.b and c), a similar behaviour to that observed in the previous experiments can be noticed: no significant differences were recorded in the development of wear at the edge radius, but the loss in electrode length was reduced by 66% when using the proposed new designs. Moreover, a decrease of electrode edge radius is observed in Figure 73.b after consecutive slots had been machined. This may be due to slight variations between measurements and the possible attachment of material to the edge radius.

IV.3.7.4. Lateral wear of electrode

During machining, the discharges were concentrated on the bottom area of the electrode. However, some discharges also occurred on its lateral surfaces, causing concavity to appear in the wear pattern of the electrode. These discharges reduce the width of the electrode, which can be observed near to the discharge area. In order to analyse this effect, the electrode lateral wear was measured after the machining of the set of 5 slots in the cases of machining with the conventional electrode, with the electrode with 2 mm diameter holes, and with the electrode of 4 mm diameter holes.

Figure 75 shows the results obtained, together with an image depicting the wear pattern in a conventional electrode. The results show that the lateral wear only occurred at the tip. At 0.5 mm from the electrode tip the reduction of the electrode was 0.187 mm and when holes were used this reduction was 0.03 mm and 0.132 mm respectively.

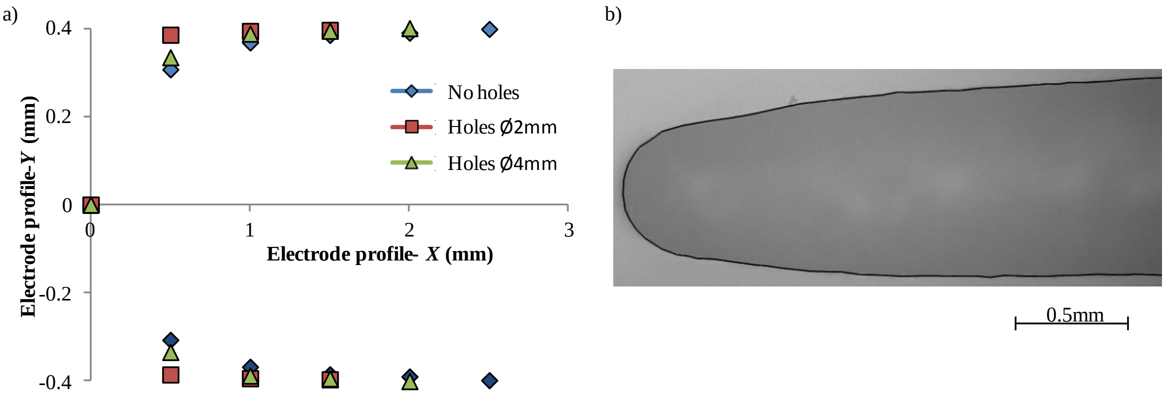

Figure 75: Example of electrode lateral wear for a machining depth of 6.5 mm. a) Electrode lateral wear for the different electrodes b) Microphotograph of worn electrode (Conventional, No holes).

It can be concluded that the concavity effect can be improved by flushing holes, whilst no firm conclusions can be drawn with respect to the various electrode designs.

IV.3.8. Optimum electrode combination

As already discussed (see Figure 72 and Figure 74), as the machining depth increases, accumulation of debris increases, and if an electrode without holes is used the process loses stability and the machining time starts to increase.

In previous sections it was concluded that machining stability can be guaranteed when the flushing pockets penetrate the whole depth of the slot to be machined on the electrode, which in turn results in considerable improvements in machining time.

Therefore, in order to understand the machining phenomena at greater depths, two extra experiments were conducted using an electrode with flushing pockets: at a machining depth of 15 mm and at a machining depth of 25 mm.

Figure 76 compares the average machining time and standard deviation at various machining depths. The results indicate that flushing pockets are also effective even at very high machining depths. Results show that a slight decrease of material removal rate is observed after the machining of 10 mm depth slot. Variations of removal rate when the depth increases (for instance, the slight speed increase after 15 mm) are too small to be considered since they are within the limits of repeatability of the experiment. Hence, the machining stability can be guaranteed at high depths.

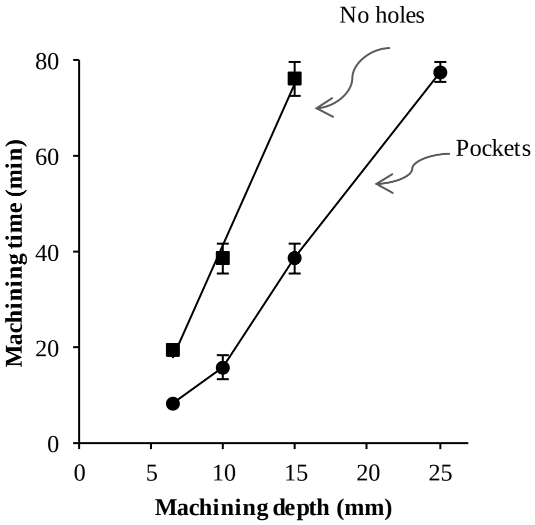

Figure 76: Improvement in machining time at different depths using the electrode with flushing pockets.

It is likely that this improved stability comes from the fact that debris removal from the working gap is much more successful when pockets are machined on the electrode. In order to confirm this possibility, an analysis of process signals is presented in the next section.

IV.4. Analysis of discharges in the working gap

In order to understand the reason for the improvement in machining time with an electrode with flushing pockets, a basic analysis of process parameters was carried out. A high-frequency oscilloscope was used for obtaining the waveforms of current and voltage during machining. The sampling rate was 1 MHz and the recording time was 4 s. In the present study, the same machining parameters, as shown in Table 12, have been used. The machining conditions recorded are those presented in Figure 77.

As explained in Section IV.3.2, the generator of the sinking EDM machine tool used in the experiments is an iso-energetic generator, fitted with an adaptive control that avoids inefficient discharges by controlling discharge interval time value. In the present work, the machining performance was analysed through a quantitative study of the main discharge parameters: duty cycle, discharge frequency, t_d, and t_{off}.

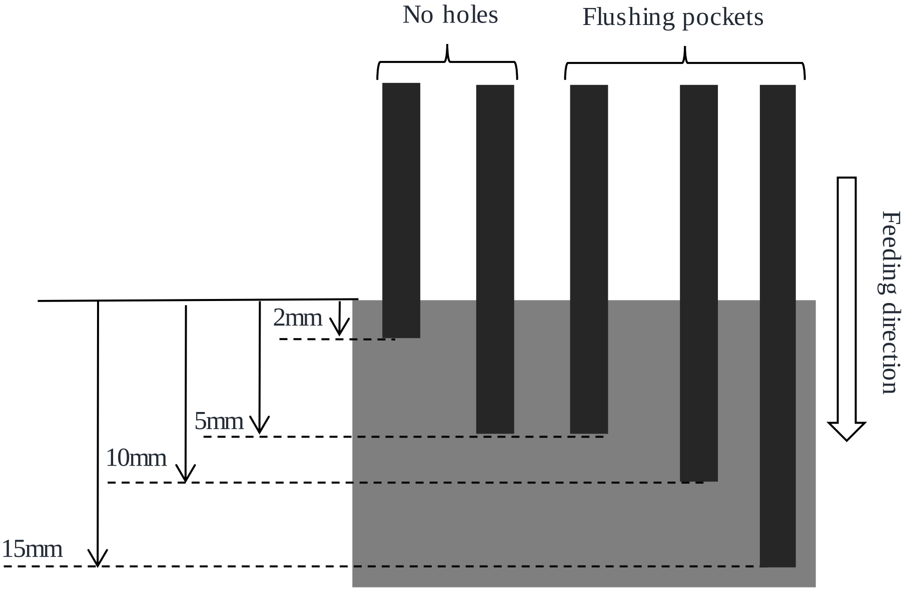

Figure 77: Machining conditions in which machining parameters were recorded.

The duty cycle refers to the ratio between the total discharge time ($\sum t_{on}$) and the total recording time, which was 4 s. In order to eliminate any possible noise generated during acquisition of the signal, a discharge is deemed to have occurred when the discharge current is higher than 30 A and discharge time higher than 50 µs. The results are shown in Figure 78.

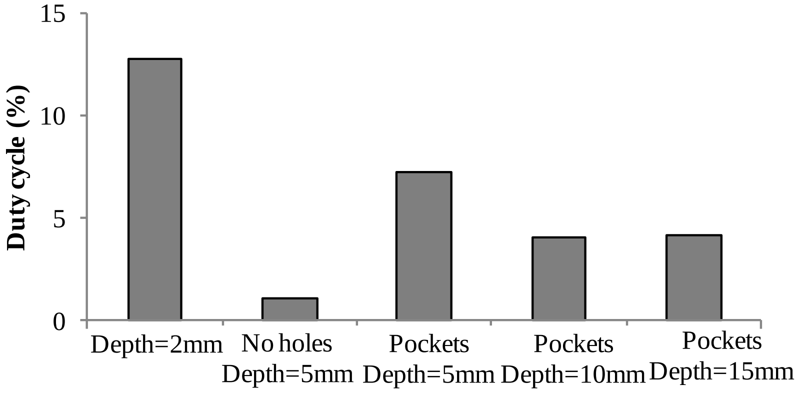

Figure 78: Effect of flushing holes on duty cycle (%) at different machining depths.

A higher machining rate indicates a more stable, and hence, more efficient machining process, which can also be defined as better flushing conditions in the narrow gap. As shown in Figure 78, at the beginning of the machining process, at a machining depth of 2 mm, the process is stable as there is no debris accumulation problem. However, with an increasing machining depth, at 5mm for instance, the difference between the electrode without holes and with flushing pockets becomes clear. Even when machining deeper slots (10 mm and 15 mm), the machining time ratio is kept at acceptable values if compared with those of a conventional electrode at 5mm depth. It must be explained here that experiments with the conventional electrode (no holes) were also carried out at 10 mm depth. However, the EDM process becomes completely unstable. For this reason, it was decided not to plot these results.

In terms of discharge frequency, two outputs were analysed, as shown in Figure 79: average frequency and frequency during machining. The former refers to discharge frequency, which takes into account the recording of the machining time by the oscilloscope, whilst in the latter the time at which the electrode is retracted by the generator is not considered. The results show that at the beginning of each operation, in which the flushing conditions were optimum, there was no retraction of the electrode. However, as the machining progresses, retraction of the electrode occurs. Moreover, the discharge frequency results also confirm the improvement in machining conditions when using an electrode with flushing pockets.

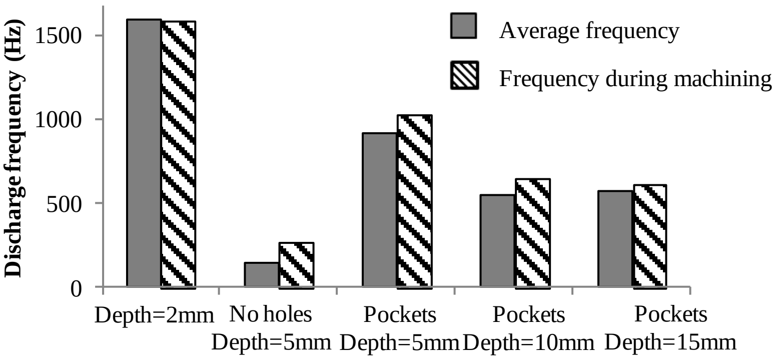

Figure 79: Effect of flushing holes on discharge frequency at different machining depths.

Furthermore, as explained in Section 2, the machine generator adapts the preset value of discharge off-time in order to avoid inefficient discharges (such as arc and short-circuits), the decrease of discharge frequency when no holes are used can be used as indicator of machining instability.

A further discharge parameter that provides useful information about machining stability is the discharge delay time. It refers to the time interval between the application of voltage and the dielectric breakdown and it is affected by debris concentration, gap width, discharge area, and surface profile [99] [100][101].

Figure 80 compares t_d values in the five situations. In the analysis of the data, a discharge is assumed to occur if the voltage reaches 100 V and the discharge delay time is longer than 2 µs.

Figure 80 a. represents the percentage of discharges classified by the duration of discharge delay time. Values of discharge delay time have been represented only up to 1000 µs. This is the reason why the summation of percentages for the conventional electrode does not reach 100%. In order to understand this effect, Figure 80 b. supports this statement. Results show that most of the discharges for the conventional electrode exhibit delay time well over 1000 µs.

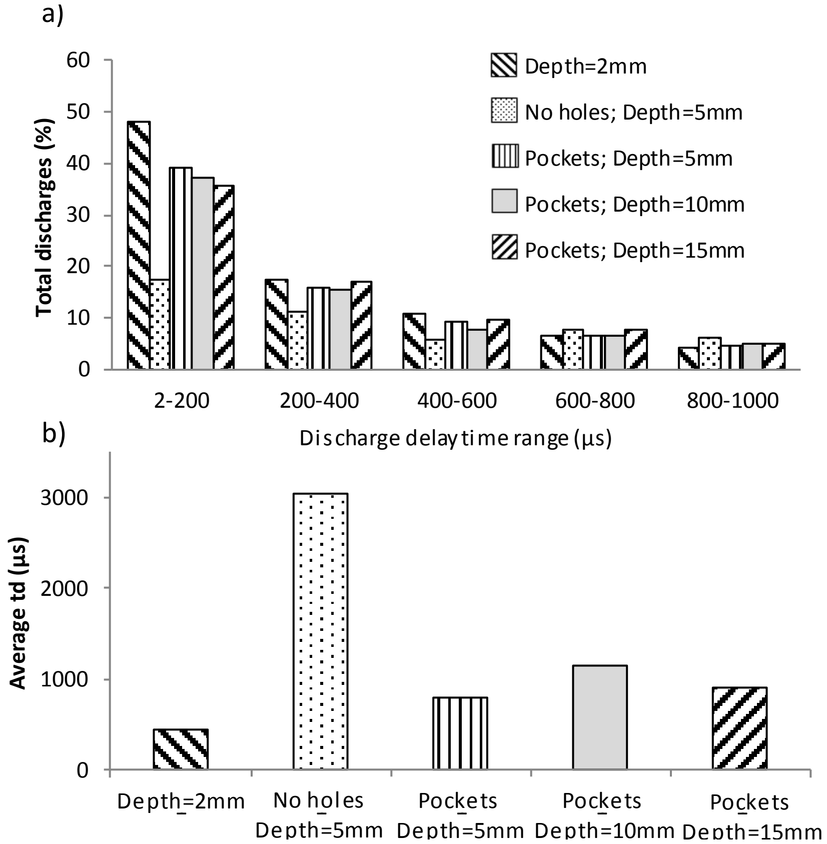

Figure 80: Discharge delay time at different machining depths for the different electrode geometries. a) Percentage of total discharges (up to 1000 ms); b) average values.

Results of the early stage of machining, at a depth of 2 mm show that the clear majority of discharges are generated with a delay time between 2 µs to 200 µs and then the percentage decreases. A clear situation of unstable machining is represented by the electrode with no holes at a machining depth of 5mm. In this case a uniform pattern of the percentage of t_d is observed as well as a much higher value of average t_d. The longer t_d values during unstable machining are related with the longer time for the recovery of the dielectric breakdown strength, as shown in Figure 81.

Another way of representing the results of t_d is the previously described Laue Plot, Chapter III Section 7.5. It shows the percentage of discharges, n/N, that does not break down until time t. Results are shown in Figure 82.

When flushing pockets are used, even though longer t_d values are observed, results show similar behaviour compared with the early stage of machining. The similarities between them indicate that stable machining can be achieved even at high machining depths with the right choice of holes on the electrode. Figure 81 shows the average values of discharge t_{off} obtained for each machining case studied.

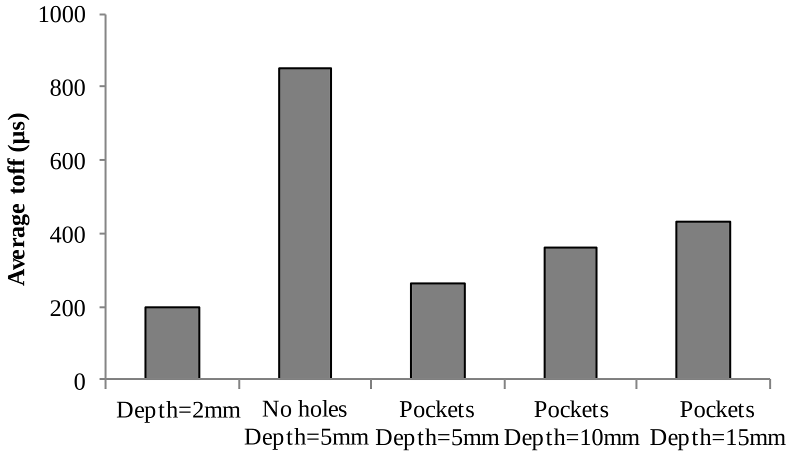

Figure 81: Average value of t_{off} at different machining depths.

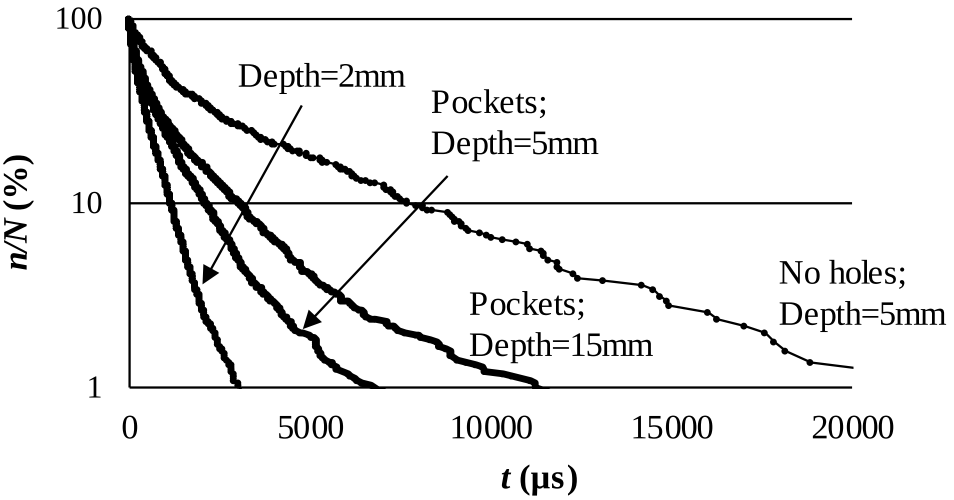

Figure 82: Distribution of t_d by the representation of the Laue Plot.

From Figure 80 and Figure 81 it can be concluded that when using an optimum configuration of flushing pockets, the values of t_d and t_{off} exhibit similar patterns. Also, it is particularly relevant that, using the information provided by the above experiments, machining depth becomes not a limitation when the optimum configuration of pockets is arranged on the lateral faces of the electrode.

IV.5. Conclusions

The most important and original findings of the present work are related to the geometry and the position of the holes machined on the electrode lateral faces for efficient flushing in slot EDM'ing. A remarkable and original finding is that continuous pockets or open holes are much better than the separated or closed holes. Furthermore, the paper shows that a sudden change in material removal rate occurs when the vacant spaces of the holes are sunk in the slot. This new contribution can be applied in both aerospace and dye and mold industries.

On the basis of the current findings, the following conclusions are drawn:

- Through the machining of holes of 4 mm in diameter in the electrode, a reduction of 57% in machining time is achievable when EDM machining a high-aspect ratio slot of 6.5 mm due to the chip pocketing effect of holes. Moreover, a reduction in the loss of electrode length is possible.
- When machining 10 mm depth slots, the process time can be reduced by 65% when an electrode with pockets is used. This is because the process does not loss stability along the machining depth.
- In terms of electrode wear, it was concluded that machining time is the predominant factor in terms of loss of electrode length, whilst no firm conclusions can be drawn with respect to electrode radius edge and lateral wear.
- Machining stability can be guaranteed if the flushing pockets machined on the electrode penetrate the entire machining depth. This was confirmed by the machining of a 25 mm depth slot.
- Higher discharge frequency, duty cycle, and shorter discharge delay time and discharge off time values were observed when using the electrode with pockets. This is compatible with the experimental results.
- No marked differences in terms of discharge properties were observed between machining depths of 10 mm and 15 mm, which indicates that, in terms of process stability, flushing pockets are effective at any machining depth.
- Future work will focus on how these findings can be applied to other electrode geometries in which debris evacuation is difficult.

As described by Figure 69, in this type of operations, in which the electrode has a simple geometry and the machining path is only in one axis, the definition of electrode wear has no special difficulties. However, those measurement indicators cannot be used for the definition of electrode wear in the machining of multi-axis operations, for example when machining a blisk. This last fact has driven the development of a methodology for the definition of electrode wear and gap width distribution that can be used in complex operations as well as in simple operations. The methodology is fully presented in Chapter V. Furthermore, with the objective of obtaining information of electrode wear patterns with electrode geometry, the methodology has been put in practice in the machining of different applications.

Chapter V: Determination of electrode wear and gap in multi-stage EDM

V. DETERMINATION OF ELECTRODE WEAR AND GAP IN MULTI-STAGE EDM

Multi-axis EDM has become a feasible solution in the manufacturing of complex geometry parts for the aerospace and energy industry. In EDM, the final workpiece is principally affected by electrode wear and gap width. Machine tool manufacturers provide limited information concerning both features, in which they do not consider the electrode geometry and electrode path. Thus, nowadays, previous highly time and cost consuming trial-and-error strategies are necessary for the machining of complex free form geometries. It is believed that a further understanding of electrode wear and gap width distribution patterns related with electrode geometry and machining path could enhance the electrode design and improve the process efficiency. Hence, the present section proposes an easy-to-put in practice electrode wear and gap width indicators, for those cases in which the average definition of wear is not enough.

V.1. Introduction

The present work was developed in the facilities of the department of Mechanical Engineering of the Faculty of Engineering of Bilbao of the University of the Basque Country.

As described in the revision of the State of the art, Section II.2.3, due to the need to enhance aerodynamic performance of aircraft engines, there is a high demand for the manufacturing of complex free form geometries, such as blade integrated disks (blisks) or impellers. In those cases, the available wear information is very generic and limited. Manufacturers of EDM machine and electrode materials usually specify the volumetric wear, front wear and corner wear [106]. Although this data could be enough for a first approach in many standard EDM jobs, when the application requires complex electrode shapes and trajectories, it becomes difficult to convert that wear information into useful criteria for the electrode design process. Thus, the present Chapter proposes a methodology for electrode wear and gap width measurement, that can be used in complex EDM jobs.

The methodology is described in Section V.3. Then, in Section V.4, the effectiveness of the method has been verified by the analysis of electrode wear and gap width of a shrouded blisk. This geometry was chosen due to its geometrical complexity and the multi-axis electrode feeding path. In Section V.5, the methodology has been used for gaining information when machining a V-shape electrode. For finishing, in Section V.6, a brief description of electrode wear and gap width pattern in the machining of a cross-section electrode has been described.

V.2. Main equipment and machine tools used

In this section, a description of the main equipment and machine tools used is presented:

- The experiments were carried out on an ONA CS300 sinking EDM machine, Table 8.
- The electrodes were cut by WEDM, the machine tool was an ONA PRIMA E250 WEDM machine, Table 9.
- For electrode profile measurement, three different measuring equipment were used: a Coordinate Measuring machine ZEISS MC 850 (Table 13), a profile projector Mitutoyo PJ-3000F (Table 10) and a Leica DCM 3D optical surface metrology system (Table 11).

Table 13: ZEISS MC 850 Coordinate Measuring Machine.

ZEISS MC 850 Coordinate Measuring Machine		
X-axis travel (mm)	850	
Y-axis travel (mm)	1200	
Z-axis travel (mm)	600	
Measurements by contact		
Measurement software	Holos/ Calypso	
Minimum probe diameter (mm)	0.5	

- After the measurement of the workpiece and electrode, information related with electrode wear and gap width was calculated using a Computer-Aided Design (CAD) software as described below. In the present study NX® PLM software of Siemens was used [107].

V.3. Proposed methodology for electrode wear and gap width definition

As explained, determination of gap values and wear pattern is critical in the design stage of electrodes for EDM of aerospace complex cavities. In this section, the proposed experimental methodology for wear pattern and gap width value determination in multi-stage EDM is presented.

The methodology takes into consideration different aspects by the indictors proposed. However, it should be kept in mind, that electrode geometry and machining path will determine the use of the indicators and the analysis procedure. The main methodology considers the multi-stage EDM process as a whole to record wear and gap information taking into account:

- The integral electrode geometry. The method does not only consider the front and corner wear.

- The complete EDM sequence. Applications in aerospace and energy gas turbine components usually involve different electrode shapes and trajectories. This composition of movements must be analysed in several time frames.
- EDM technology strategy. Consecutive operations of roughing, semi-finishing and finishing are planned in the proposed applications for turbine components. Hence, wear and gap data should be required for each of them.

Wear indicators have been proposed as shown in Figure 83.

- E_{wa}: Electrode wear area. This indicator evaluates the wear along different sections of the electrode over the time. It is an enhancement of the usual volumetric wear value and it can be obtained by measuring E_{wa} in different time frames of the complete EDM sequence.
- E_{ll} *(j)*: Electrode lost length. Profile of the worn electrode projected on the *YZ* reference plane (see Figure 83). This indicator provides the electrode wear at different points of the electrode profile (taking as reference the initial electrode geometry) for a specific time frame.
- E_{wd} *(i)*: Electrode wear distribution. Profile of the worn electrode projected on the *ZX* reference plane (see Figure 83).

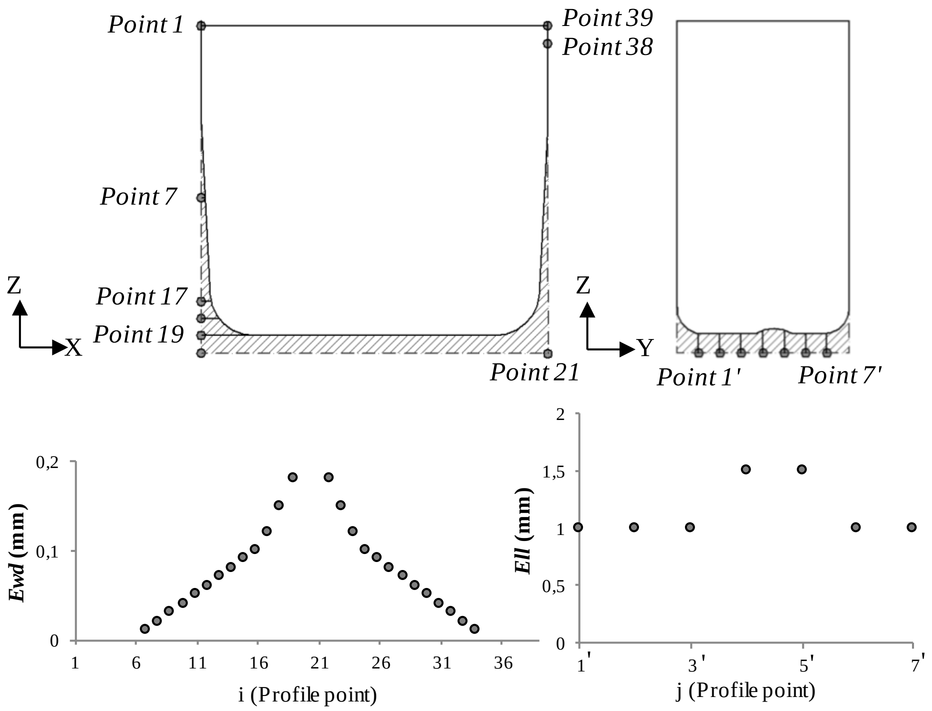

Figure 83: Proposal of functions for representing the of electrode wear.

For the measurement of E_{wa} and E_{wd} (i), the first step is to measure the section of the electrode before and after EDM'ing. For reliable results, the measuring expanded uncertainty must be below 5 µm. Then, the data obtained are processed, for instance, using a CAD software. The number of sections to be measured is conditioned by electrode geometry and electrode feeding path.

For determination of E_{ll} (j), the observation of electrode length is required. *Z* axis coordinates of different points of the bottom section of the electrode are compared before and after EDM'ing. In this case, the measuring expanded uncertainty must be below 5 µm.

Optimum electrode design requires not only knowledge of wear patterns, but also accurate knowledge of gap width distribution. Following, a methodology for the definition of gap width distribution, G_w, is presented.

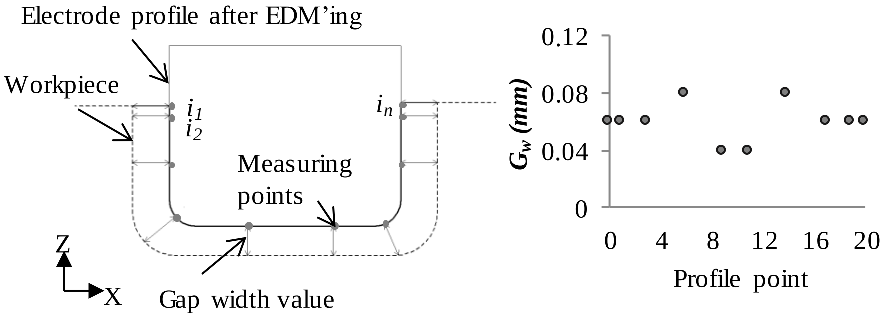

Figure 84: Proposal of functions for representing the gap width value.

For the definition of G_w two profiles need to be measured: electrode profile after EDM'ing and the final geometry of the EDM'ed workpiece. In both cases, the measuring expanded uncertainty must not exceed 5 µm. When working with complex geometries, the direct observation of the workpiece profile may be impossible. Therefore, it is proposed to extract a slice of the workpiece. The data obtained must then be processed, for instance using a CAD software. G_w is a function that represents gap value in different points of electrode for each step time. An example is shown in Figure 84.

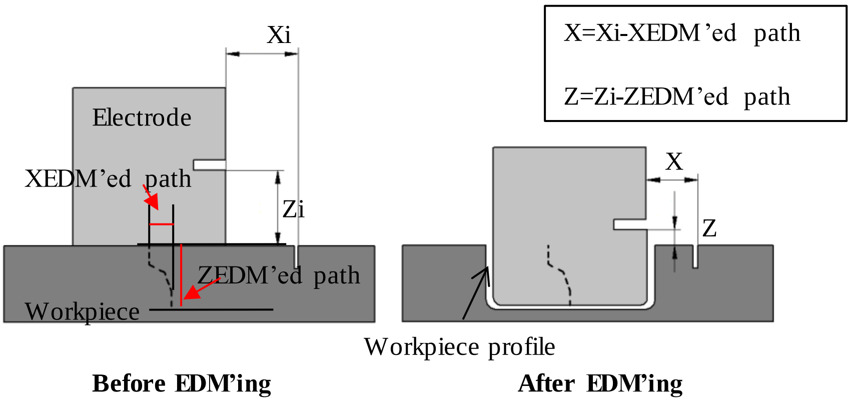

Figure 85: Example of electrode and workpiece positioning technique.

The main challenge for an accurate G_w measurement, is the correct positioning of both profiles on the *XZ* plane. For this matter, the definition of a reference in the workpiece and in the electrode is required. This reference will depend on electrode geometry, measuring instrument and

EDM'ing path. An example in which the positioning on the XZ plane has been carried out by using references machined in the electrode and workpiece is shown in Figure 85.

Furthermore, when working with symmetric geometries, or when there is discharging in both laterals of the electrode, only a reference for the positioning of Z axis is necessary. This can be done under the assumption of symmetry, this is, gap width is the same in both sides of the electrode. In this case Eq. 13 can be employed, and an example is shown in Figure 86.

$$G_{wi} = G_{wj} = \frac{Workpiece(Xi) - Electrode(Xi)}{\frac{1}{\cos(\alpha_i)} + \frac{1}{\cos(\alpha_j)}} \qquad \text{Eq. 13}$$

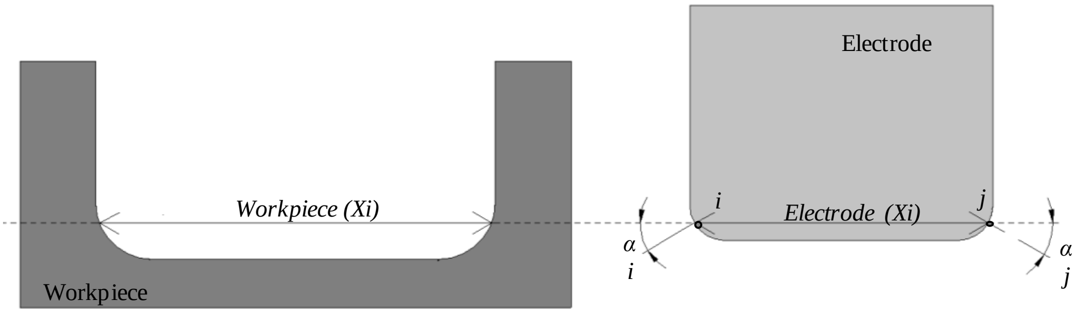

Figure 86: Example of calculation G_w in symmetric geometries. The reference used is on Z axis.

As highlighted at the beginning, the electrode geometry, feeding path and the required information will determine the indicators to use and the number of points to be measured. Hence, the proposed methodology should be modified in terms of the EDM jobs to study. Considering this assumption, three different EDM jobs have been analysed by the proposed methodology.

V.4. Case study: Shrouded blisk machining

The methodology proposed in the present Chapter has been applied to determine electrode wear and gap width values in the EDM'ing of a shrouded blisk. A blisk is monolithic part found on aerospace engines, which combines both blades and disk on a single piece. The main benefit is that it eliminates the join between them, which is the mayor source of cracks [37].

V.4.1. Experimental set-up and procedure

The methodology presented in this paper has been applied to determine electrode wear and gap width values in the EDM'ing of a shrouded blisk. Both electrode and EDM path have been obtained using the methodology proposed by Ayesta *et al.* [37]. They proposed an objective function based on the maximization of the minimum distance between electrode and workpiece which calculates the feeding paths. Furthermore, they proposed a simple electrode design modification guideline that should be used for obtaining the final electrode design and electrode feeding path. Figure 87 shows the workpiece to be machined, the electrode and the feeding path. It should be clarified, that in the real industrial EDM job, the electrode feeding path is interpolated in 3 axis, *XZC*. However, for simplicity, in the present work two axis have been interpolated *XZ*.

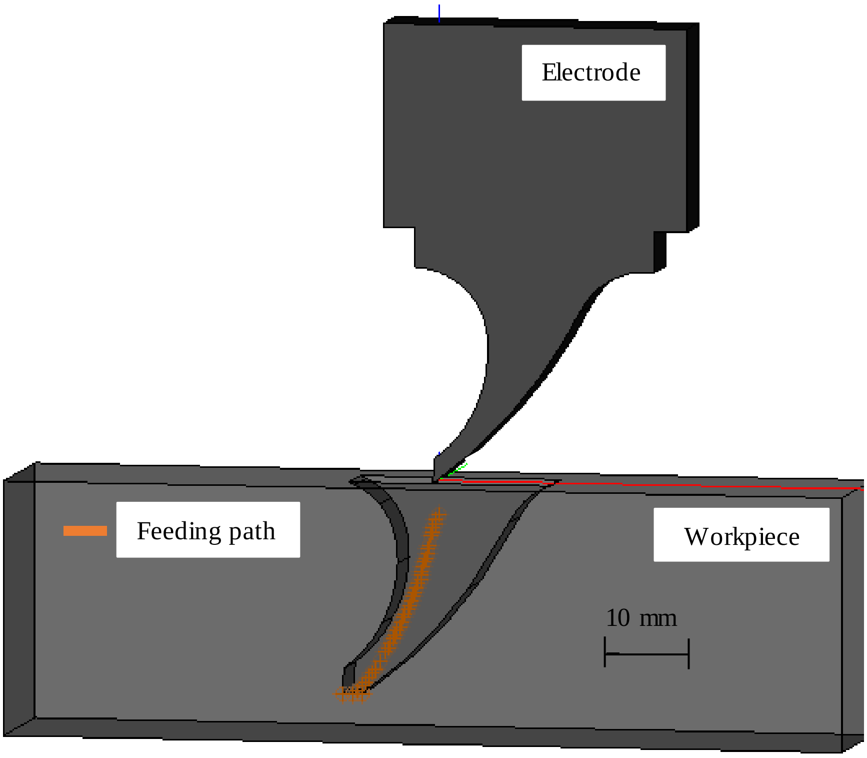

Figure 87: Scheme of the workpiece, electrode and feeding path.

The electrodes have been manufactured in POCO EDM-200® isotropic superfine graphite. It is a graphite that provides good strength, surface finish and wear resistance, and its main properties are shown in Table 14.

Table 14: Graphite properties. POCO EDM-200® [108].

	Poco EDM 200®
Average particle size (µm)	10
Flexural Strength (bar)	620
Compressive Strength (bar)	1070
Hardness (shore)	68
Electrical Resistivity (µOhm-mm)	15000

As mentioned in Section V.2, the experimental work was carried out on an ONA CS300 industrial sinking EDM machine and workpiece material was F114 structural steel.

In order to observe the variations of wear pattern and gap width as a function of the type of EDM operation, four different sets of EDM parameters indexed by final roughness were studied. Table 15 collects all the data relating regimens and electrical parameters for the experiments. The experimental procedure includes regimens ranging from finishing operations (VDI 28) to roughing (VDI 39) and semi-roughing (VDI 32 and VDI 36) have also been considered. The conversion between VDI class and R_a is defined by Eq. 14 [109].

$$VDI\ class = 20\ log_{10}(10\ Ra) \qquad \text{Eq. 14}$$

Table 15: Parameter settings of the test.

	VDI 28 **Ra. 2.5 µm**	**VDI 32** **Ra. 4 µm**	**VDI 36** **Ra. 6.3 µm**	**VDI 39** **Ra. 9 µm**
I (A)	6	18	18	36
U_0 (V)	200	160	160	120
t_{on} (µs)	50	25	100	200
Pre-set t_{off} (µs)	6.4	5	13	25
SV (V)	30	30	30	20

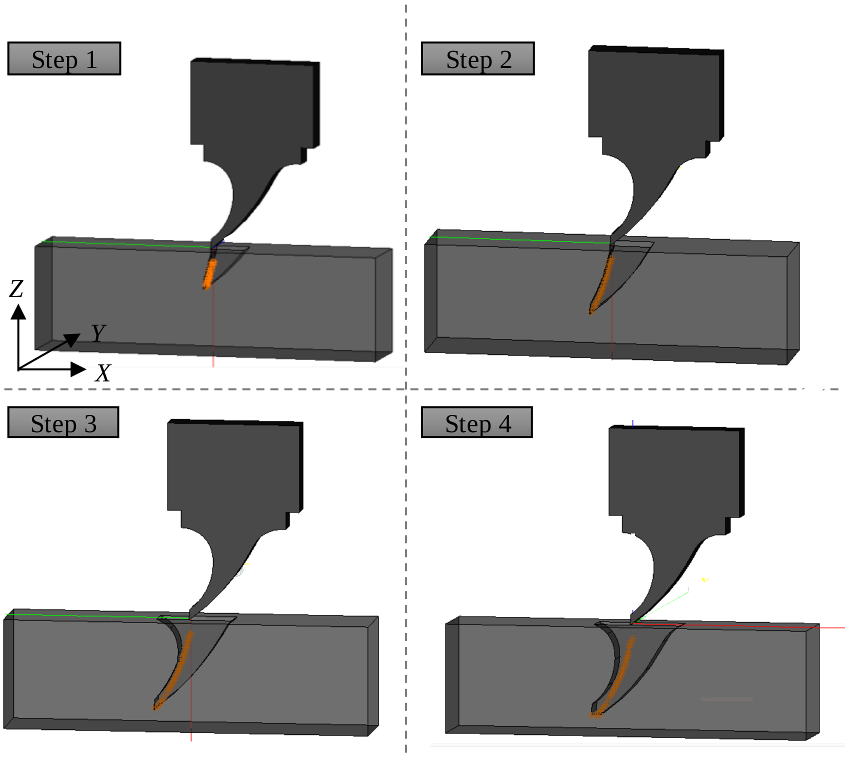

Figure 88: Electrode path of each step analysed.

Measurement of both electrode wear and gap width value were carried out following the methodology proposed in Section V.3. Electrode wear and gap width were studied at four different steps of the EDM sequence, see Figure 88.

E_{wa}, was obtained on three sections (section A, B and C, see Figure 89). The profile of the worn electrode on the ZX plane, E_{wd} (i) was analysed on section A. And finally, the profile of the worn electrode on the ZY plane, E_{ll} (j), was studied on sections C', B', A, B and C (see Figure 89). Values for E_{wa} and E_{wd} (i) were measured on a ZEISS WMM 850 Coordinate Measuring Machine. For the case of E_{ll} (j), electrode tip before and after the test was observed on a Mitutoyo PJ-3000F profile projector.

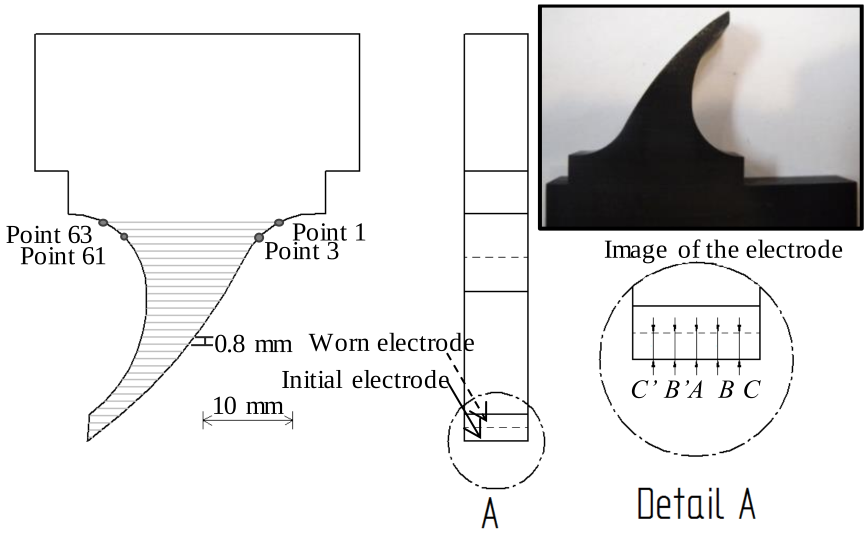

Figure 89: Electrode design and nomenclature employed.

Data required for gap width distribution were obtained both from the worn electrode (central section measured using a coordinate measuring machine) and from a 0.5mm thick slice of the final EDM'ed cavity, Figure 90 shows an example of a slice, which was measured on a 3D optical surface metrology system Leica DCM 3D. Both profiles, were imported to the CAD software for G_w measurement. Figure 91 shows an example of this method.

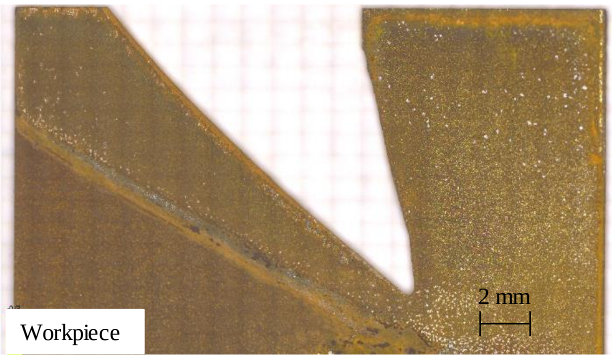

Figure 90: Example of a 0.5 mm thickness slice of the workpiece. Step 2.

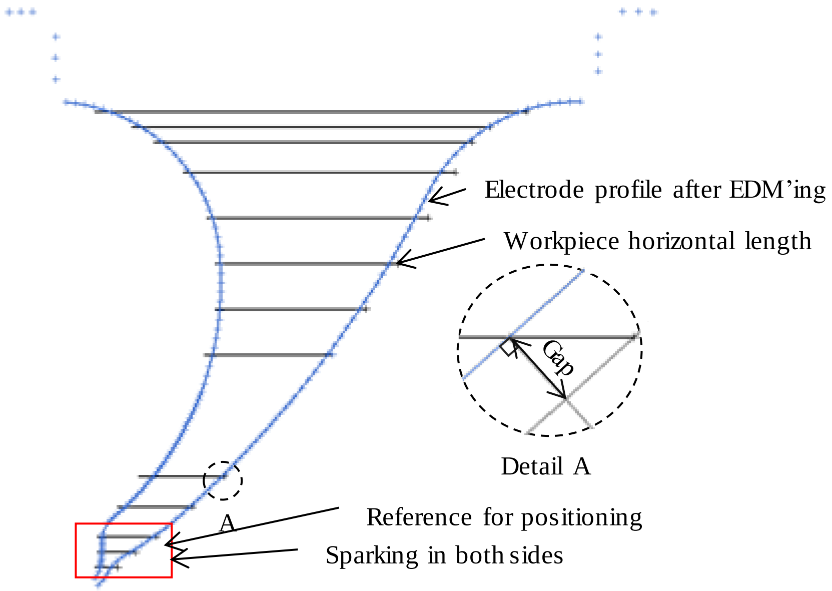
Electrode profile after EDM'ing
Workpiece horizontal length
Gap
Detail A
A
Reference for positioning
Sparking in both sides

Figure 91: *Z* axis defined by external references and *X* defined by Eq. 13 in the points highlight.

V.4.2. Discussion of results

In this Section the electrode wear and gap width results will be discussed in detail by the use of the indicators proposed in Section V.3.

V.4.2.1. Wear pattern indicators

Figure 92 shows the evolution of E_{wa} as a function of machining time for the different set of EDM parameters studied. Here machining time refers to the total time for completing the electrode programmed path. The plotted results correspond to the average of the three measured sections.

Analyzing the results, it is observed that E_{wa} follows a linear trend with R^2 higher than 0.9 for the four EDM parameter settings. The first result to be noticed is related to the absolute value of E_{wa}. When looking at roughing parameters, it can be observed that, for a similar operation time, higher wear is related to lower energy set of parameters (VDI 32). For instance, after 150 min operation, E_{wa} increases from 1.004 mm^2 in the case of VDI 39 up to 10.164 mm^2 in the case of VDI 32, which means a growth of as much as ten times. In the experiments, t_{on} in VDI 32 is 25 µs, taking a value of 200 µs for VDI 39. This result is sound with the well-known fact that higher t_{on} is related to less electrode wear, already commented in the revision of the State of the art.

When taking a look at the results obtained in the finishing regimes, higher absolute values of wear are found. However, EDM operation time is much higher in this case: since the material removal rate of the regime is very low, a longer time is required to remove a similar amount of part material.

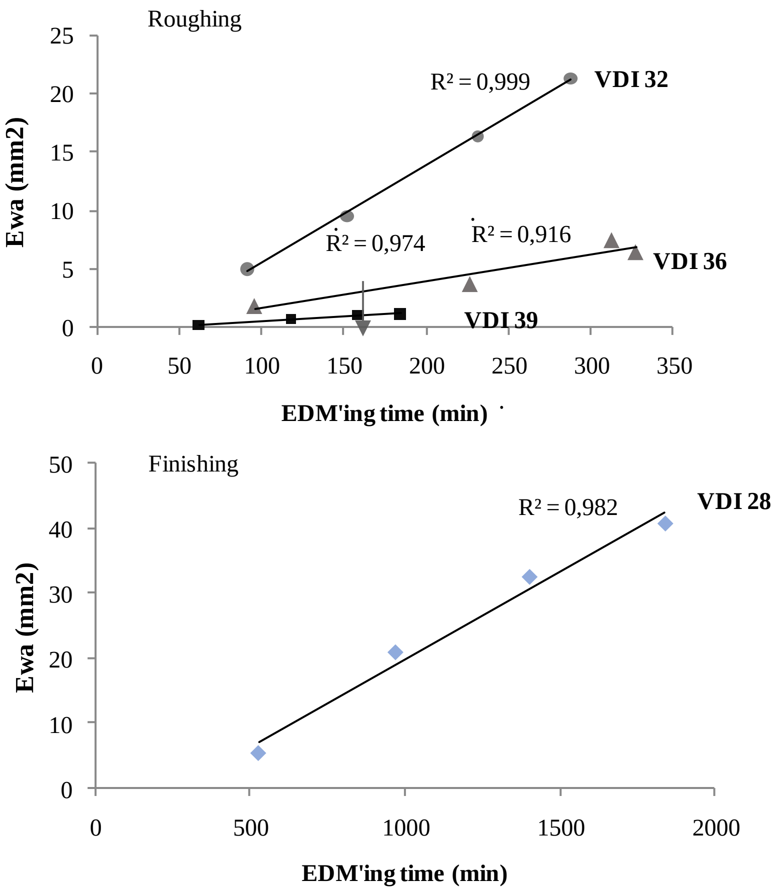

Figure 92: E_{wa} (mm^2) as a function of machining time and EDM regime. Above: Roughing regimens. Below: Finishing regimens.

Results for the electrode lost length E_{ll} are plotted in Figure 93. Results are presented as average values together with the standard deviation, so that scattering of results can be known. When the standard deviation is smaller than 0.04 mm the deviation bar has not been drawn.

E_{ll} follows quite similar pattern as E_{wa} does, results depending linearly on machining time. When analyzing results of VDI 39 and VDI 36, it is noticed that higher electrode lost length per minute is obtained when working with VDI 39, but lower electrode wear area per minute is observed. This indicates that with VDI 39, the electrode wear is concentrated on the tip of the electrode, but for the case of VDI 36 electrode wear is distributed along electrode profile. For the case of VDI 39 electrode wear lost length per min is of 6.6 µm and for VDI 36 the reduction is to 2.4 µm. In terms of electrode wear area, for VDI 39 is of 0.007 mm^2/min and for VDI 36 0.023 mm^2/min. This means, that if the objective is to obtain a depth cut on the workpiece VDI 36 is more suitable. Nevertheless, if the objective is to obtain better results in the profile without considering the tip of the electrode, VDI 39 is more suitable. Moreover, deviation results show that highest values are observed with finishing parameters, VDI 28.

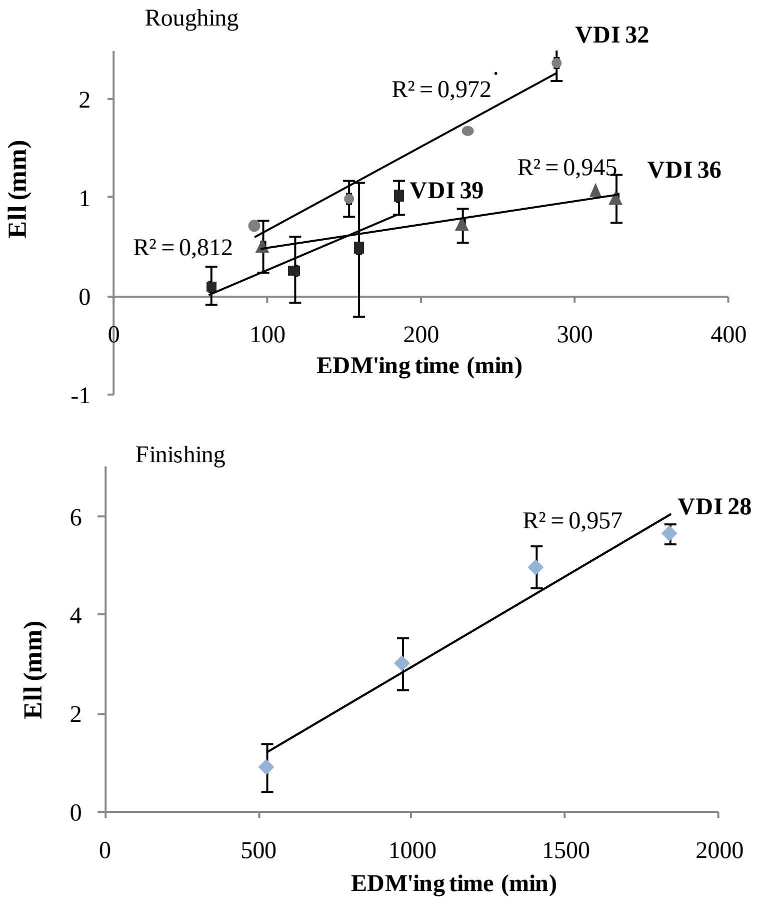

Figure 93: E_{ll} (mm^2) as a function of machining time and EDM regime. Above: Roughing regimens. Below: Finishing regimens.

A deeper insight into the geometry of wear is provided by the results of E_{wd} *(i)*. The objective of analysing E_{wd} *(i)* is to understand the parts of the electrode that suffer more during the erosion. A high value of E_{wd} means that at that point the electrode has suffered more degradation than at those for which the value of E_{wd} is lower.

Figure 94 shows the results of electrode wear distribution obtained for VDI 39, VDI 36, VDI 32 and VDI 28. Although the value of E_{wd} varies with the machining parameters, the curves shows the same trend but with different values.

Hence, from Figure 94 is concluded that electrode wear distribution is conditioned by the electrode path and its value by the erosion regimen. This is because the discharge probability along electrode is dependent on the electrode geometry as well as the erosion path. Those results highlight the interest of defining the discharge region in order to foreseen electrode wear distribution and take into consideration in the electrode design phase.

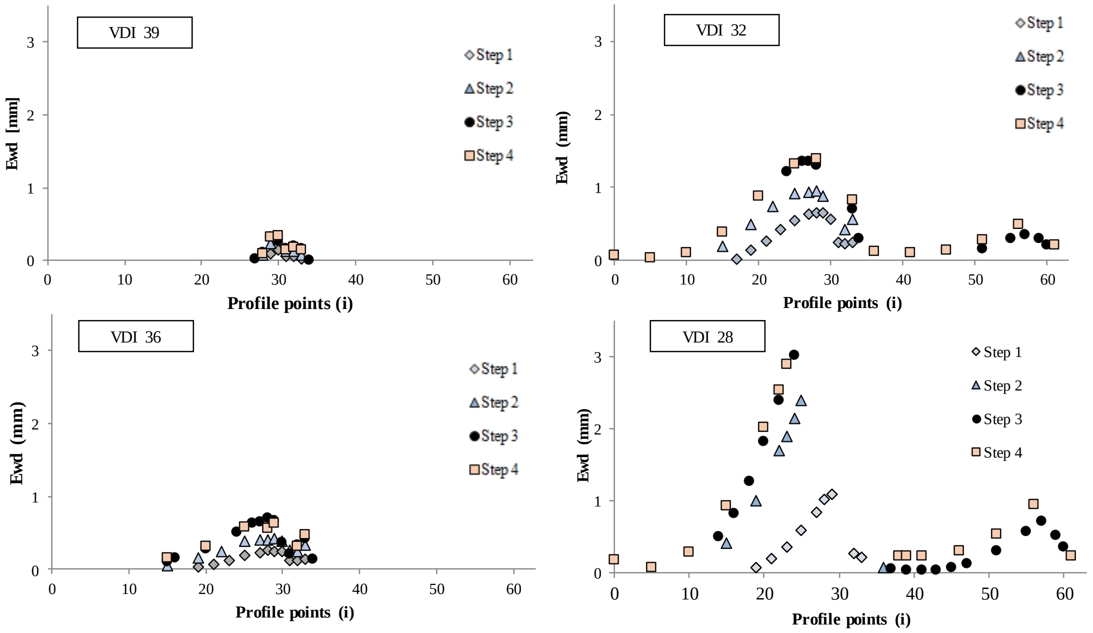

Figure 94: Results of E_{wd} (mm) for the studied regimens.

V.4.2.2. Non-uniform wear pattern and material build-up

When analysing electrode wear, non-uniform wear patterns and material build-up were observed in the tip of the electrode, Detail A of Figure 89. Those results have been presented in Figure 95, which are photos obtained from the profile projector.

With respect to results for VDI 28, from step 1 to step 2 electrode wear is concentrated in the middle, which results in an irregular workpiece geometry. Then, electrode wear, although its value is higher, becomes more uniform. With regards to VDI 32 and VDI 36, tips are generated in different sections of the electrode and they disappear at the end of the machining path. For the case of VDI 39, the corners tend to round, and material build-up is observed in step 2 and step 3. Overall, it has been concluded that finishing the machining path with movement in *X* axis, not only can improve final roughness, but also the uniformity of the workpiece.

However, even though the most prominent electrode region for material build-up is the tip of the electrode, in other regions material build-up was also observed. Figure 96 shows an example in which the initial electrode profile and the worn electrode profile have been compared. In this case, grey colour represents electrode wear and red material build-up.

As shown in Figure 96, two regions (A and B) were observed. The former is due to the effect of the wedge and the latter is due to debris concentration, because due to the electrode path debris that were generated in the upper profile may tend to gather in that area. When analysing the results, for the case of VDI 36 material build-up occurred in region B after the erosion path (steps 1, 2 and 3). For the case of VDI 39, material build-up occurred in both regions also after machining steps 1, 2 and 3. This it is related with the long pulse t_{on}.

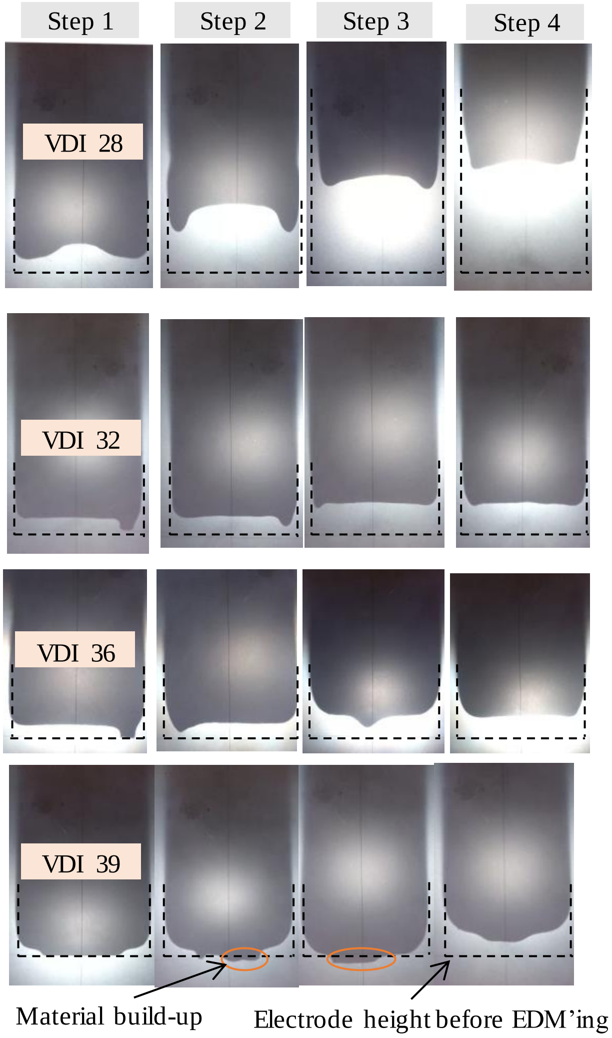

Figure 95: Observation of 'Detail A' of Figure 89 after EDM'ing.

As already explained in Chapter II, the phenomenon of material build-up observed during the experiments can be used, as described by Mohri *et al.* [39] and Maradia *et al.* [38][40] and others, to create a carbonaceous protective layer in such a way that electrode wear is prevented by this layer. This idea has been successfully applied in cylindric electrodes. However, the above results show a certain unpredictability of the geometry of the carbonaceous layer for complex geometry electrodes. It was concluded that the generated layer is also function of the machining path, which determines the actual regions where discharging occur, and of electrode geometry. Hence, in order to predict the regions where material build-up occurs and if zero-wear strategies need to be implemented, further research work must be carried out on this field.

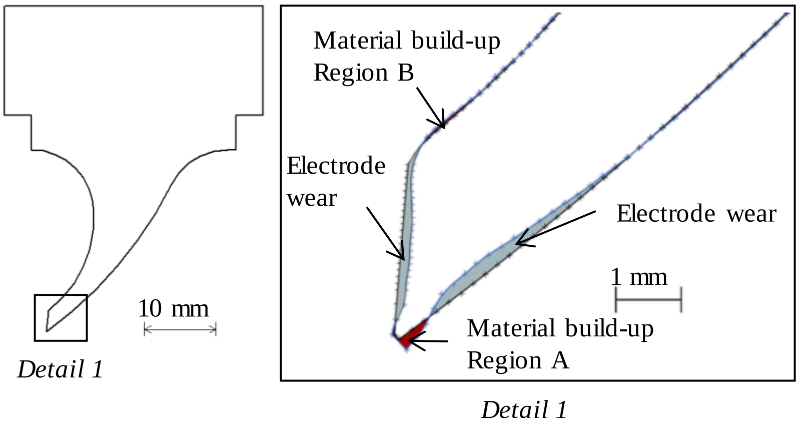

Figure 96: Regions of material build-up when eroding with VDI 39.

V.4.2.3. Gap width indicators

For a proper electrode design, the estimation of the actual gap value is of high interest. Results of the present industrial case revealed that no matter the machining parameters, when working with complex geometries, the real gap value is not constant along the profile and the value is below the theoretical gap value provided by the machine manufactures. Figure 97 confirmed the above statement. Results represent the difference between the measured gap value and the theoretical value. Moreover, the deviation along the profile has been defined.

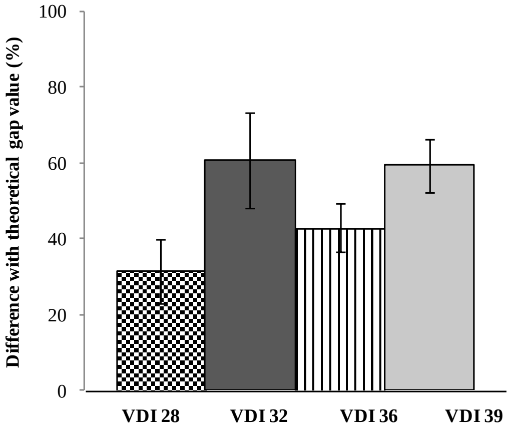

Figure 97: Representation of the gap width value and deviation with respect to the theoretical value.

Furthermore, Figure 98 represents the gap width distribution for VDI 28, VDI 32, VDI 36 and VDI 39 after the machining of each programmed step. With those graphs, the non-uniform gap width value along electrode profile is represented.

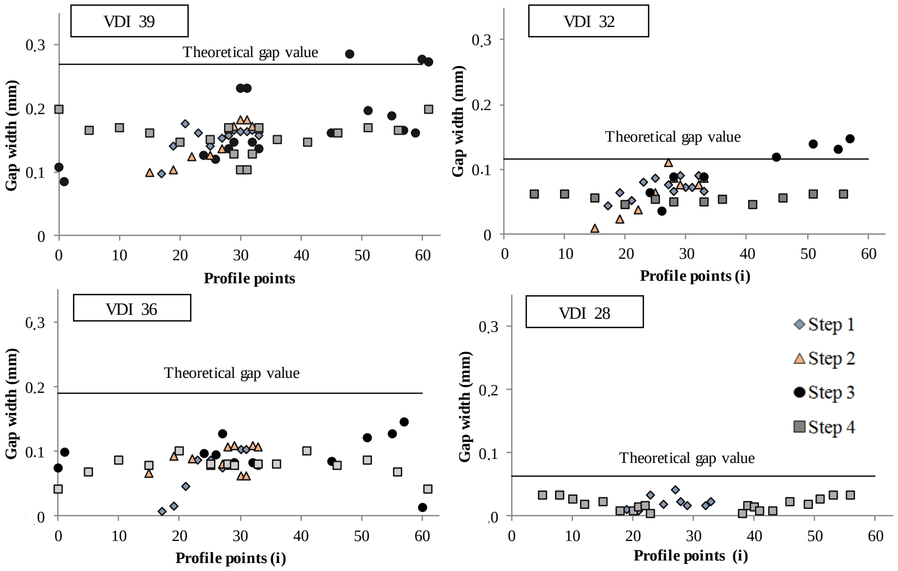

Figure 98: Results of G_w (mm) for the studied regimens.

V.5. Case study: V-shape wedge

Sharp edges are a common feature in parts machined in the die and mold industry as well as in aerospace industry. However, as observed in Section V.4.2.2 special attention should be paid for guaranteeing machining accuracy, because the electrode wear is not uniform along the profile and sharp edges tend to round rapidly [39].

Considering the high importance of those features, the present work sets out to gain knowledge of electrode wear and gap width distribution when machining by a V-shape electrode. The methodology followed for electrode wear and gap width measurement, is based on the methodology proposed in Section V.3. Nevertheless, as discussed in Section V.5.1, the indicators used have been modified for obtaining the information required on this type of applications.

V.5.1. Experimental procedure

Experiments were carried out on a ONA CS300 SEDM machine. The material used were F1414 for the workpiece and POCO EDM 200® for electrode. The electrode geometry was a V-shape electrode of 60 degrees and it was machining by WEDM. The machining parameters used in the trials are those for a regimen of VDI 38, Ra 8µm, and the EDM parameter settings are shown in Table 16.

Results of electrode wear and gap width were obtained at different machining depths: 0.5 mm, 1 mm, 2 mm and 4 mm. Furthermore, for testing results deviation, for he cases of 0.5 mm and 1 mm depth, 3 experiments were carried out.

Table 16: Parameter settings for an VDI 38.

	VDI 38 **Ra. 8µm**
Electrode polarity	+
I (A)	14
U_o (V)	120
t_{on} (µs)	200
Pre-set t_{off} (µs)	25
SV (V)	20

Electrode wear has been analysed by three indicators: previously described electrode wear area, E_{wa}, and electrode wear lost length, E_{ll}, and wedge radius, see Figure 99. The indicator of 'wedge radius' can be explained as a variation of the previously described E_{wd}, but, in the present case the measuring positions are concentrated in the wedges and not along the electrode profile. This approach is taken because the wedge is the part that will suffer more electrode wear.

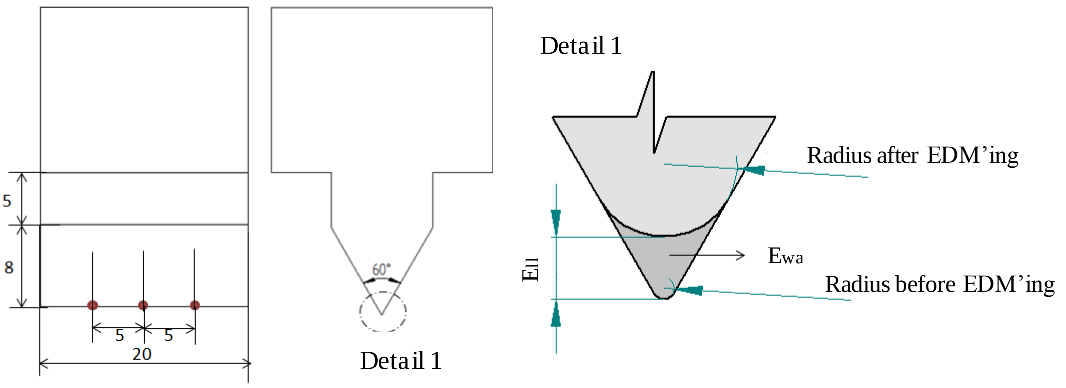

Figure 99: Electrode geometry in which the measured electrode wear indicators have been illustrated.

The measurements are taken in three different profiles of the electrode, which are: the middle profile and at 5 mm from the middle profile in both sides, check Figure 99.

- Wedge radius, E_r: Wedge radius has been calculated by measuring the electrode in the 3D optical surface metrology system Leica DCM 3D before and after erosion. Three profiles have been measured to ensure the uniform wedge wear along the electrode and to ensure the repeatability of the measurements. Figure 100 shows an example of result representation of the optical system.

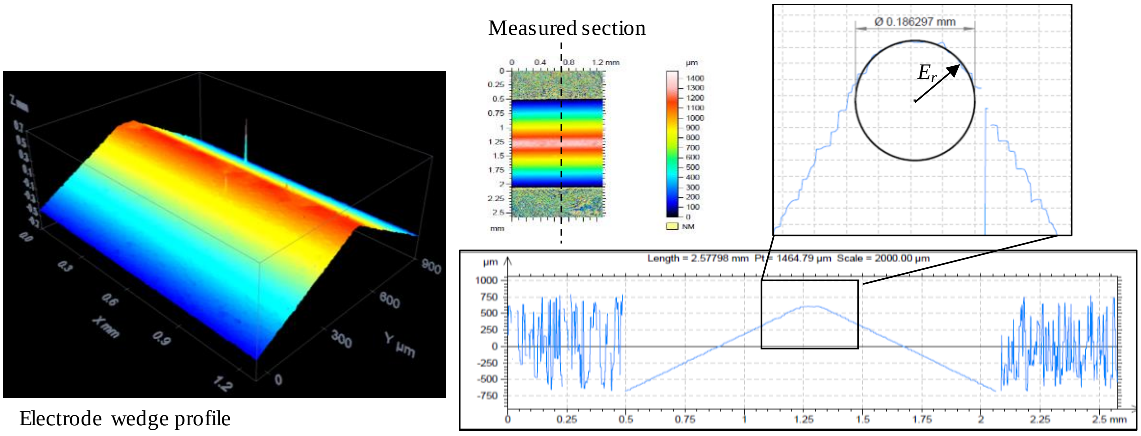

Figure 100: Example of a wedge radius after erosion (machining depth=0.5 mm).

- E_{ll}: Electrode lost length has been measured in the machine tool by comparing the length of the electrode both before and after each machining operation. In this case too, the measurement was carried out in three sections.
- E_{wa}: Electrode wear is measured only in the wedge, as it was previously observed that electrode wear does not occur, or it is not appreciable, at electrode walls. It has been measured in three sections is the optical system Leica DCM 3D. Firstly, the electrode profile before machining has been measured and then it has been compared with the electrode profile after machining. The software of the optical system compares both profiles and calculates the area change between them, which in this case corresponds to E_{wa} value. Figure 101 represents an example of one of the measurements.

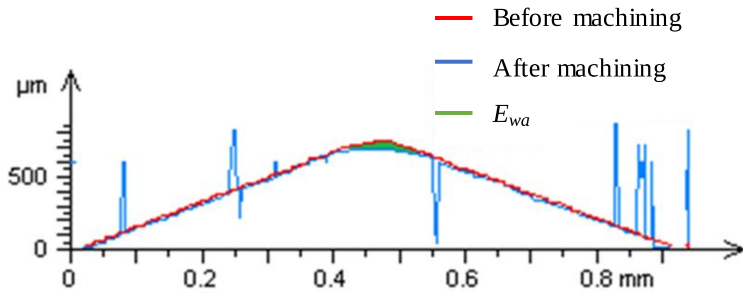

Figure 101: Example of the measurement of the electrode wear area, E_{wa}.

In terms of gap width measurement, G_w, symmetry has been used for electrode and workpiece superposition. The electrode profile after machining and the workpiece profile were obtained by the Leica DCM 3D system. Then, they were processed by NX9® CAD software.

In terms of gap width definition, the following information was obtained: G_w distribution along the profile, minimum gap width value, G_{wmin}, which represents the minimum distance between electrode profile and workpiece, and the maximum gap width value, G_{wmax}, which represents the maximum distance. Figure 102 shows an example of the superposition of both electrode and workpiece profiles.

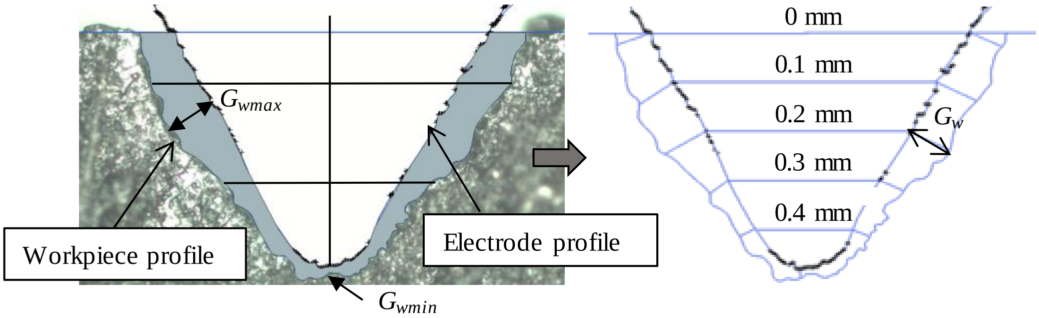

Figure 102: Example of the way to analyse gap width distribution, G_w.

V.5.2. Discussion of results

In this Section electrode wear and gap width results will be discussed in detail.

V.5.2.1. Wear pattern indicators

Figure 103 represents the wedge radius value after EDM'ing different machining depths: 0.5 mm, 1 mm, 2 mm and 4 mm. As expected, the maximum change of the radius occurs at the beginning of machining. Then, from 0.5 mm to 2 mm a slight increase of the wedge radius is observed. Then, the value can be considered constant. As Mohri *et al.* [39] also confirmed, results show that the discharge density at sharp edges is high and thus, the rounded of the electrode occurs at the early stage of machining. Then, the discharge density is more uniform, and the wedge suffers less wear, and thus the radius value does not suffer a considerable change.

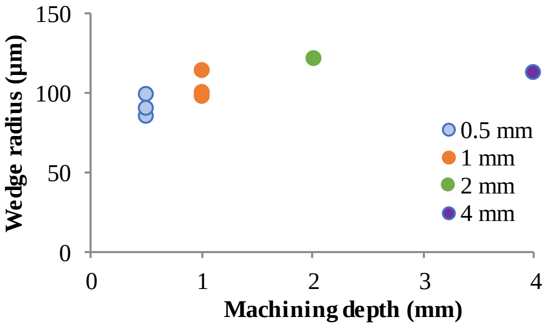

Figure 103: Electrode wear process. Wedge radius.

In terms of electrode lost length, Figure 104 shows the relation between E_{ll} with machining depth and with machining time. It is concluded, as also observed in the Case Study of Section V.4, that electrode lost length is a function of machining time. Moreover, even if electrode wear can be considered as linear, the more drastic change occurs when EDM'ing from 0 mm to 0.5 mm. This can be explained with results of Figure 103. In this case, the lost length is related with the rapid wear of the wedge.

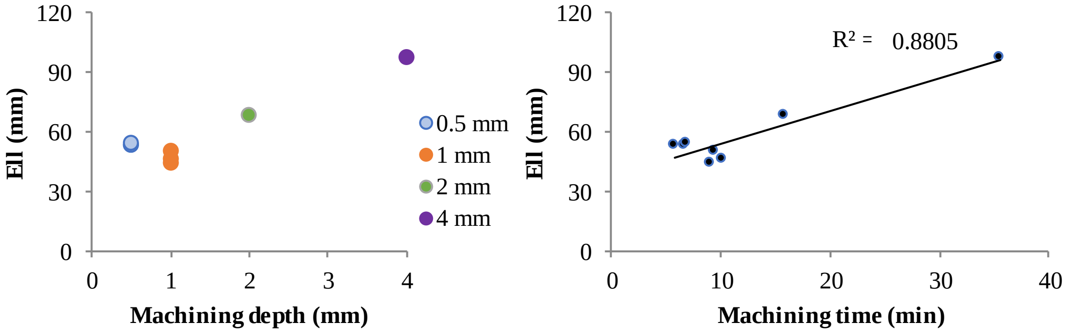

Figure 104: Electrode wear process. Electrode lost length.

With regards to electrode wear, E_{wa}, Figure 105 shows that electrode wear area is linearly dependent on machining time. In this case too, results ensemble with results obtained in Section V.4.

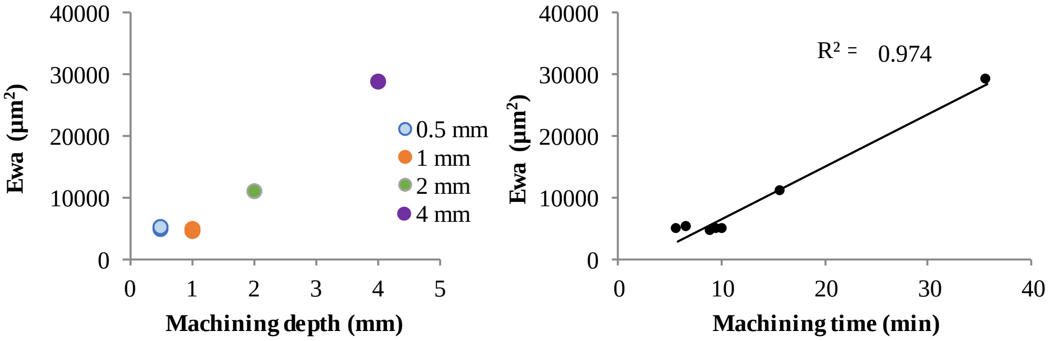

Figure 105: Electrode wear process. Electrode wear area.

V.5.2.2. Gap width indicators

Figure 106 represents the superposition of both electrode profile after machining and the achieved workpiece profile. Those images were then used for obtaining the data of gap width. It should be noticed that for a clearer result representation, the scale used for representing the gap between electrode and workpiece has been adapted to the machining depth.

Figure 107 represents the numerical results of the experiments of Figure 106. When analysing the results, it should be taken into consideration the variation related with the roughness value conditioned by the EDM parameters settings. In this case, R_a value is 8 µm, which means that the maximum height of the profile (R_t), which represents the distance between the highest and lowest points of the profile, is 64 µm. Thus, Figure 107 does not only present the gap width values but also the acceptable results variation. It should be clarified that the scale of *X* axis varies in each graph. Moreover, Figure 108 shows the average values obtained for each machining depth.

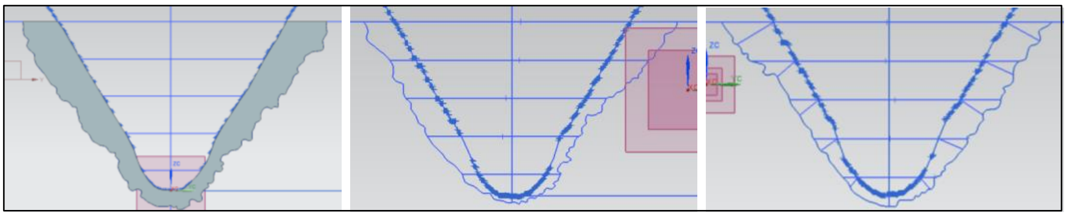

Machining depth= 0.5 mm

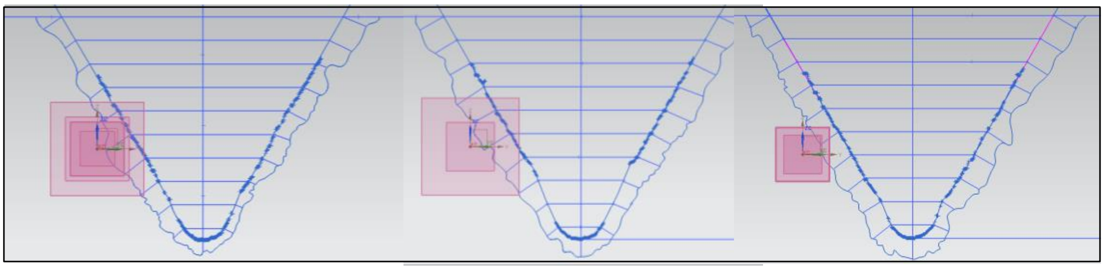

Machining depth= 1 mm

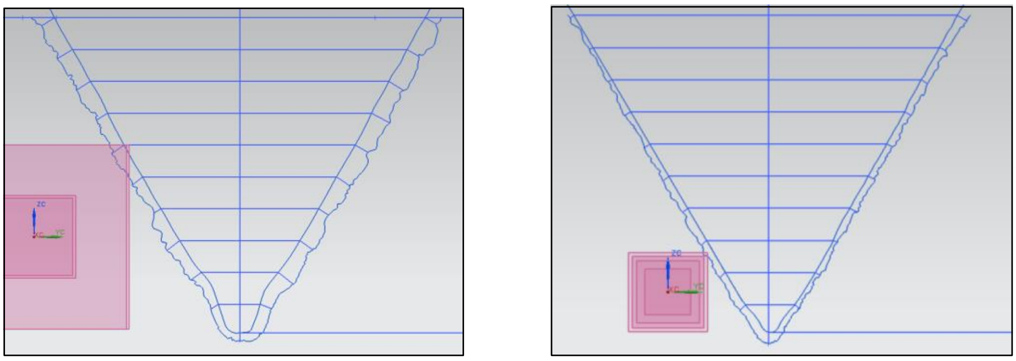

Machining depth= 2 mm

Machining depth= 4 mm

Figure 106: Superposition of electrode and workpiece profiles for gap width data acquisition.

From both Figures, Figure 107 and Figure 108, it is concluded that gap width is not constant along the profile. In the four cases, it is observed that gap width at the tip is narrower that at the top. One reason is that the flushing conditions are better at the top, and hence the machining discharge quality is better. The other reason is that a larger discharge area results in a higher probability of discharges to occur, widening the gap. Furthermore, the variation between gap width results is more pronounced with small machining depths, and the difference is getting smaller with the machining depth.

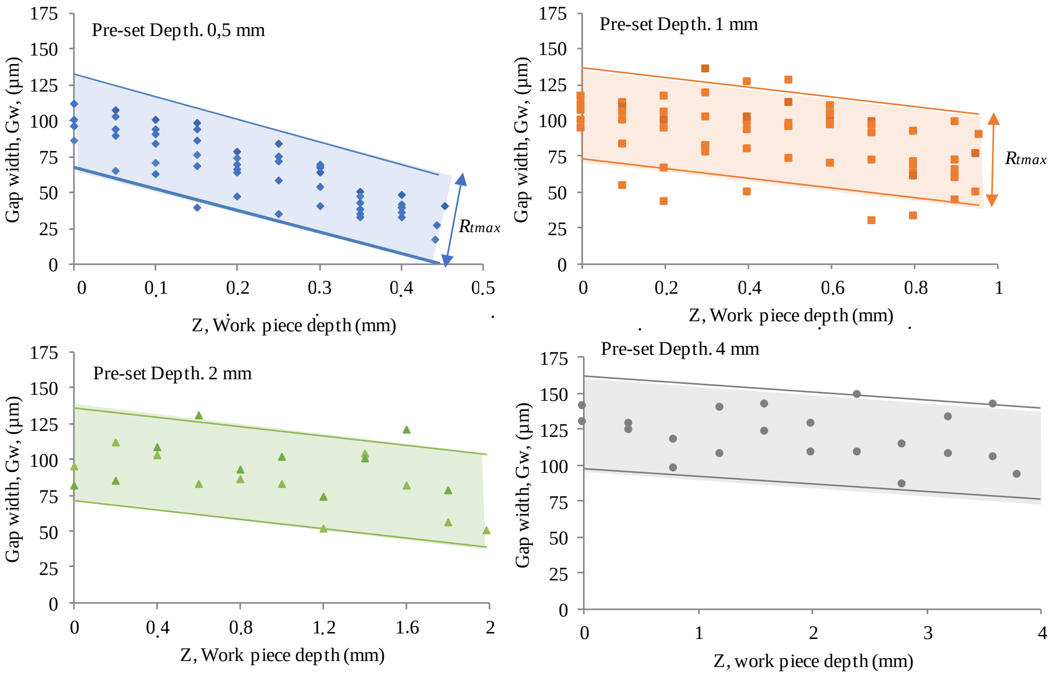

Figure 107: Gap width results representation with the corresponding deviation lines.

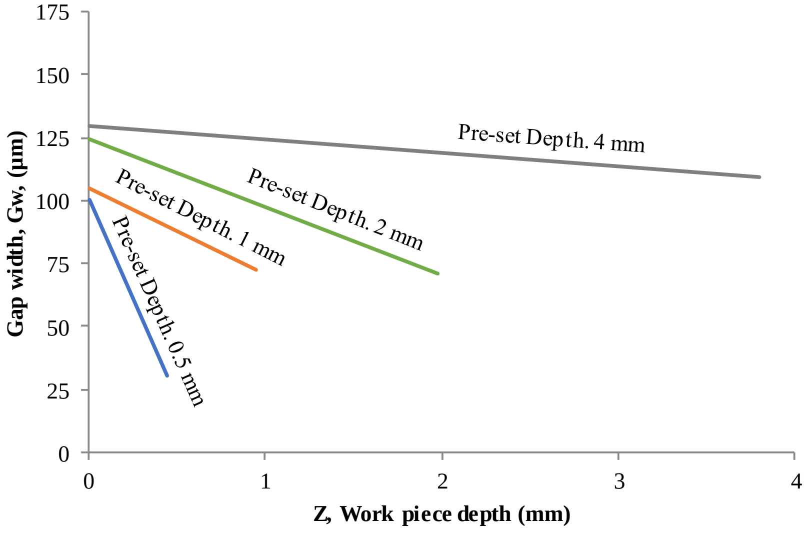

Figure 108: Representation gap width results by average value.

V.6. Case study: Square cross section electrode

In this section, by the methodology proposed in this Chapter, information of electrode wear and gap width patterns when machining with a square cross section electrode has been obtained. The information gathered will be used for developing the simulation model developed in Chapter VI.

V.6.1. Experimental set-up and procedure.

The electrodes have been manufactured in POCO-EDM 200® (Table 14), and structural steel has been used as the workpiece. The electrode has square cross section area of 20*20 mm and the feeding direction is the main axis.

The main objective of the present research works, was to analyse the electrode wear and gap width patterns in the initial machining stage time and the steady state is reached. Hence, results were gathered after different machining times, from 15 min to 4 h. The machining conditions were not varied, and they are presented in Table 17.

Table 17: Parameter settings for an VDI 39.

	VDI 39 **Ra. 9 µm**
Electrode polarity	+
***I* (A)**	30
U_0 (V)	120
t_{on} (µs)	200
Pre-set t_{off} (µs)	25
***SV* (V)**	20

Taking into consideration the electrode geometry and electrode path, electrode wear indicators used in the present work are: electrode lost length, E_{ll}, and edge radius, E_r. Figure 109 illustrates the indicators.

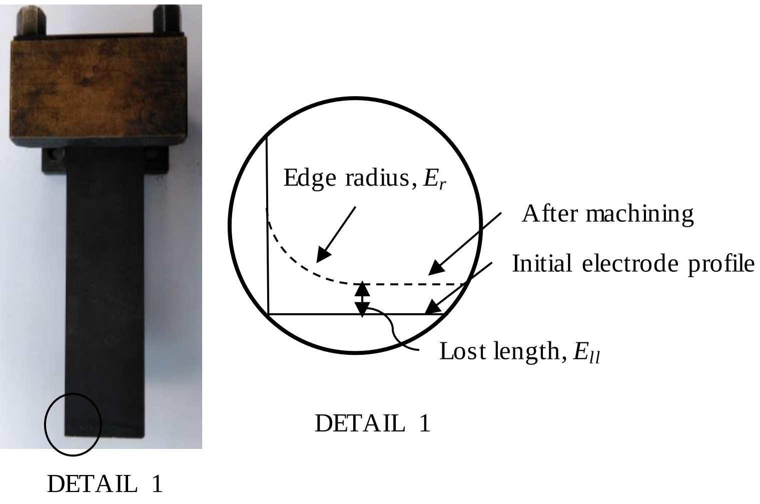

Figure 109: Representation of the indicators for electrode wear analysis.

The methodology for electrode wear and gap width measurement is described as follows:

- E_{ll}: Electrode lost length has been measured in the machine tool by comparing the length of the electrode both before and after machining. The measurements have been made at 5 different point and the average value as well as the deviation has been calculated. Figure 110 shows the measuring points.
- E_r: The edge radius of the electrode has been measured after each erosion by the 3D optical surface metrology system Leica DCM 3D. Measurements have been taken at 4 different points, see Figure 110.

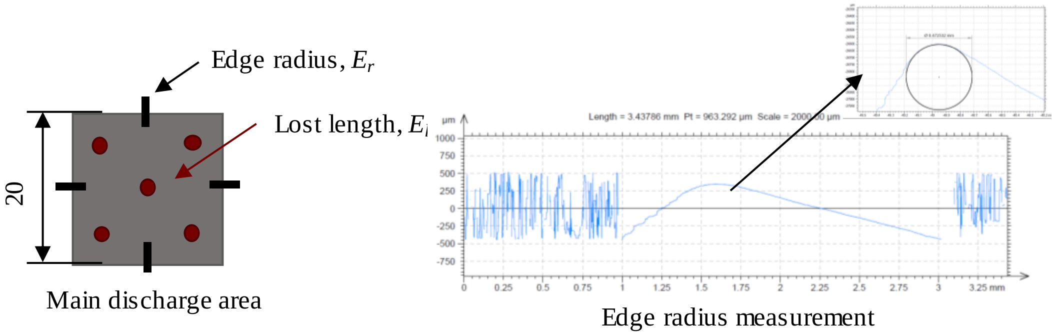
Edge radius, E_r
Lost length, E_l
20
Main discharge area
Length = 3.43786 mm Pt = 963.292 µm Scale = 2000.00 µm
µm
1000
750
500
250
0
-250
-500
-750
0
0.25
0.5
0.75
1
1.25
1.5
1.75
2
2.25
2.5
2.75
3
3.25 mm
Edge radius measurement

Figure 110: Representation of the outputs in terms of electrode wear.

- G_w: Gap width has been measured in the middle section of the electrode. The procedure is the same as in the previous two case studies. Figure 111 illustrats an example of the superposition of both electrode and workpiece profile in the CAD software.

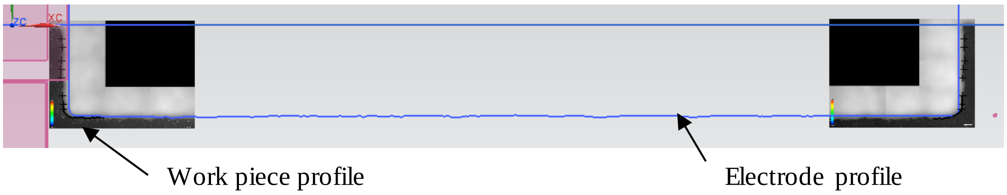
ZC
XC
Work piece profile
Electrode profile

Figure 111: Example of the superposition of both electrode and workpiece profiles.

V.6.2. Discussion of results

In this Section electrode wear and gap width results will be discussed in detail.

V.6.2.1. Wear pattern indicators

Figure 112 shows the results of E_r during the machining process, in which the average and the standard deviation have been represented.

From results, it is confirmed, as also explained previously, that edges get rounded rapidly at the beginning of machining, and then it becomes constant. It the present case it reaches a maximum value of 285-295 µm.

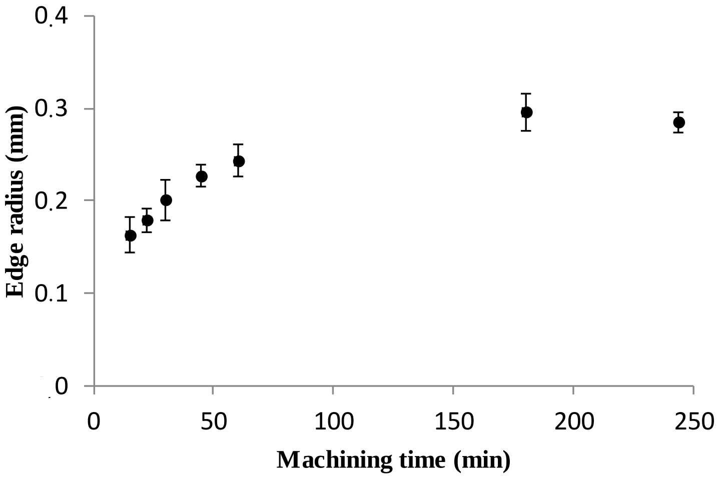

Figure 112: Cross section electrode. Edge radius, E_r, results.

With regard to electrode lost length, Figure 113 shows the the average results and the corresponding standard deviation. Negative results indicate that the electrode grows in length. Results show that at the beginning of machining, the electrode grows in length. This can be explained by the generation of an electrode wear layer on electrode surface due to long t_{on} value. Then, the layer is removed, and the electrode length starts to decrease linearly with machining time.

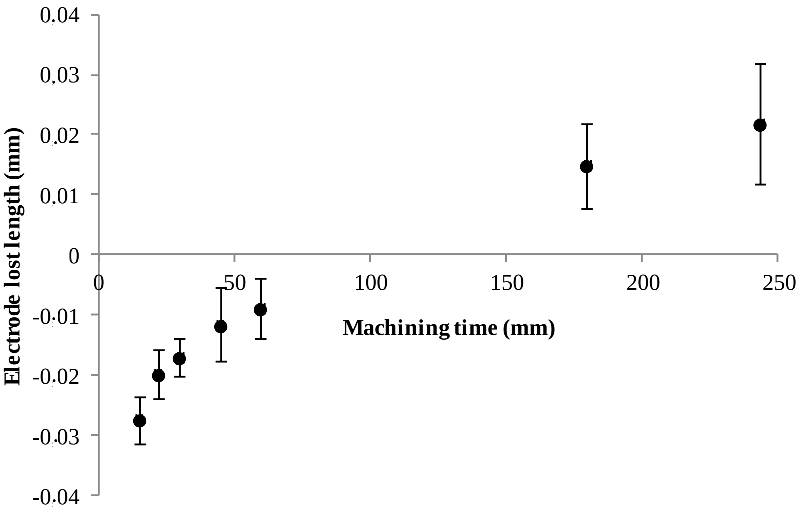

Figure 113: Cross section electrode. Electrode lost length, E_{ll}, results.

Considering that long discharges were used, the electrode growth observed at the steady state of machining can be explained by the material attachment phenomena described in Chapter II Section II.4.4. This layer is generated at the beginning, but as the machining process the layer is removed and the reduction in length of the electrode occurs.

V.6.2.1. Gap width profiles

Considering that the gap width is not constant along the profile, Figure 114 has been used for presenting the gap profile after different machining times. The graph represents the gap width at different points of the workpiece at 6 different machining stages: after 15 min of machining, 22 min, 30 min, 45 min and 60 min. Each stage has been represented by a different line. The red line, ‘theoretical gap value’, corresponds to the gap value provided by the machine tool manufacturer, and the deviation bar coloured in grey, represents the deviation attributed to the roughness of the workpiece.

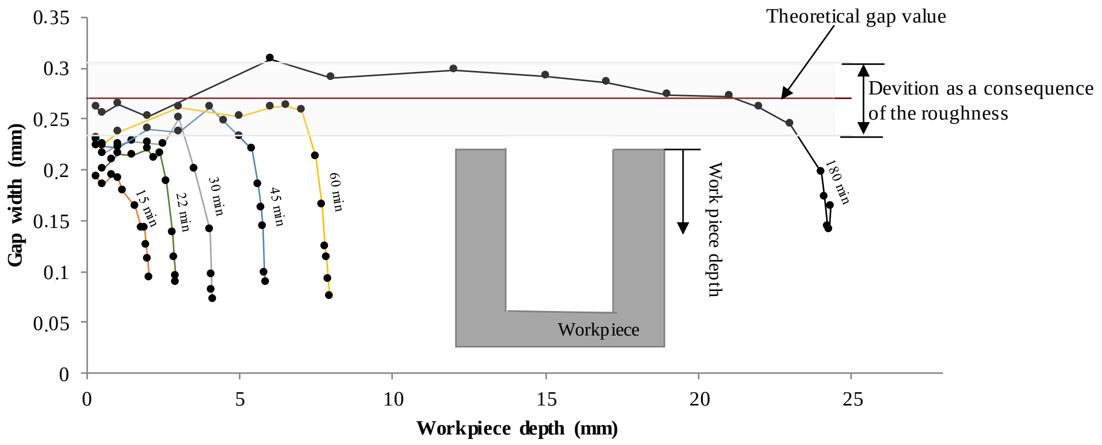

Figure 114: Cross section electrode. Electrode gap width profile representation at different machining stages.

Results indicate that until the steady state is reached, in the present case until 30 min machining time, the real gap width value is smaller than the theoretical gap value provided by the machine tool manufacturer. Furthermore, it is also observed, that for all the cases, the gap width is narrower at the bottom that at the top of the workpiece. This effect is attributed to the side surface discharges that enlarged the gap width. This phenomenon was also observed in Section V.5.

V.7. Conclusions

This research work proposes a methodology for studying electrode wear pattern and gap width value in multi-stage EDM of complex geometries. Regarding electrode wear, the methodology establishes different indicators for defining electrode worn geometry. Moreover, a procedure for gap width analysis is presented, as both factors need to be considered for an optimum electrode design.

The methodology proposed has been used for obtaining information in three different EDM jobs: the manufacturing of a shrouded blisk, the machining with a V-shape electrode and the machining with a cross section electrode.

From the experimental work, the following conclusion in terms of electrode wear and gap width patterns have been drawn:

- E_{wa} follows a linear trend with machining time. Moreover, it is concluded that the influence of machining time is higher when working with more energetic parameters.
- E_{ll} also follows a linear tendency with machining time. The maximum relative standard deviation occurs when working with the most energetic parameters setting. This was attributed to the uneven material build-up.
- E_{wd} distribution pattern is the same no matter the machining parameter setting even if the values differ. This phenomenon can bring improvement in electrode wear prediction.
- Edge radius, E_r, suffers a rapid rounded at the early stage of machining due to the high heat concentration at geometries with large curvature. Then, as the radius increases, no change of E_r with machining depth was observed.
- With regards to G_w value, if the steady state has not reached, the gap width value differs between 30-60% with respect to the theoretical values. Moreover, gap width is not constant along the electrode profile and narrower gap is observed at the bottom of the workpiece.

On the whole, it is concluded that the electrode wear pattern is conditioned by electrode geometry, electrode feeing path and machining conditions. This means that from experimental data the prediction of electrode wear is difficult or even impossible, as the number of EDM jobs is infinite.

Because of that, it is expected that the best solution for electrode wear prediction is the use of a simulation models that can give information to the EDM job designer. Therefore, in the next chapter a thermal simulation model that predicts the temperature distribution in the electrode has been developed. It is expected to use the model as a basis for the determination of electrode wear during continuous EDM.

Chapter VI: Thermal model for prediction of temperature distribution in the electrode

VI. A THERMAL MODEL FOR PREDICTION OF TEMPERATURE DISTRIBUTION IN THE ELECTRODE

As already explained in Chapter V, *EDM is a competitive machining alternative for the manufacturing of free form geometries, such as blisk and impellers. The main reason is because contrary to high-speed machining, material hardness and machinability do not set limits to the machining process. However, in EDM electrode wear occurs which conditions machining accuracy, as already discussed in Chapter* V. *Hence, prior to machining the final workpiece, trial-and-error strategies are necessary. This means that simulation of EDM process is not only relevant for the understanding of electrode wear phenomena, but also for improving the efficiency of EDM process. With both objectives in mind, the present work proposed a simulation model that predicts electrode temperature during machining. The main feature is that instead of simulating the temperature after the generation of each discharge, the model considers the energy generated during continuous EDM process and this energy is distributed over the electrode discharge area. This sets great value to the applicability of the model in industrial EDM jobs. Furthermore, the electrode temperature simulation model can be used as a basis for the determination of electrode wear during machining.*

VI.1. Introduction

The present work was developed in the facilities of the department of Mechanical Engineering of the Faculty of Engineering of Bilbao of the University of the Basque Country.

As pointed out in Chapter II, during EDM the material removal mechanism involves several effects; thermal, mechanical, chemical and electrics effects, which complicates the modelling of EDM process. Furthermore, in EDM the definition of the energy distribution of the discharges depends on different factors, which also difficulties the simulation of the process. Moreover, discharges occur at a high frequency, (10^3 -10^6 Hz) [7], which also set limits to the simulation, because simulation of each single discharge increases drastically computational time.

The main contribution of the present work is the development of a thermal model that predicts electrode temperature distribution during continuous EDM. In order to be applicable under practical EDM jobs without high computational cost, it is proposed to simulate the energy generated by the discharges, but without the resolution of single discharge simulation. The model is thought to be able to apply under industrial condition in the machining of complex EDM jobs, such as the machining of shrouded blisk or impellers.

Furthermore, combining the knowledge in terms of electrode wear acquired in the previous Chapters, especially in Chapter IV and Chapter V, with the thermal simulation of the electrode, a preliminary hypothesis for electrode wear prediction will be presented.

The Chapter is distributed as follows. Firstly, the algorithm and hypothesis used for developing the model are described, Section VI.2. Then, in Section VI.3, an inverse simulation method is proposed to define the fraction of energy absorbed by the electrode, F_E. The method is based on the comparison between the temperature measured experimentally with the temperatures of the model. Finally, in Section VI.4, by combining the knowledge acquired in terms of electrode wear and the temperature results, a preliminary hypothesis for wear based on electrode temperature is discussed.

At this point, it should be highlighted that recent publication of RWTH Aachen University confirmed the interest of simulation continuous EDM and the challenges that need to be faced for achieving the goal [60][110]. The main contributions of those publications are summarized in Section II.3.2.

VI.2. Principles of the thermal simulation model

The simulation model has been developed using the Finite element method (FEM) ANSYS® Mechanical APDL software [111]. This software is a powerful scripting language that allows to parameterize the model and automate common tasks. For simplicity, the model consists of a single solid that represents the electrode. The effect of the dielectric is taken into consideration by the convection coefficient, as detailed later on.

As the model is solved in solid phase, the heat transfer can be defined by the equation of the heat transfer described by Fourier [61]:

$$\rho C_p \frac{\partial T}{\partial t} = \Delta.(\lambda \Delta T) + \sum q \qquad \text{Eq.15}$$

Where, ρ is the density, C_p is the heat specific capacity, λ is the conductivity and q is the specific heat source.

The method faces two main challenges: the definition of the fraction of energy absorbed by the electrode, F_E, and the definition of the material removal criteria. The former is described in Section VI.3 and the latter in Section VI.4.

VI.2.1. Main algorithm of the electrode thermal model

Figure 115 shows the flowchart that summarize the simulation model, where $t_{working}$ is the working time and $t_{bakward}$ is the backward time. The working time is defined by the period in which discharges occurs without the rise of the electrode from the discharge position. The backward time is defined by period that involves the rise and lowering back of the electrode. Δt refers to the simulation time interval, which should be a value equal or smaller than $t_{bakward}$ and $t_{working}$. And $T_{model}(t, Z)$ refers to the temperature field of the electrode at a given time.

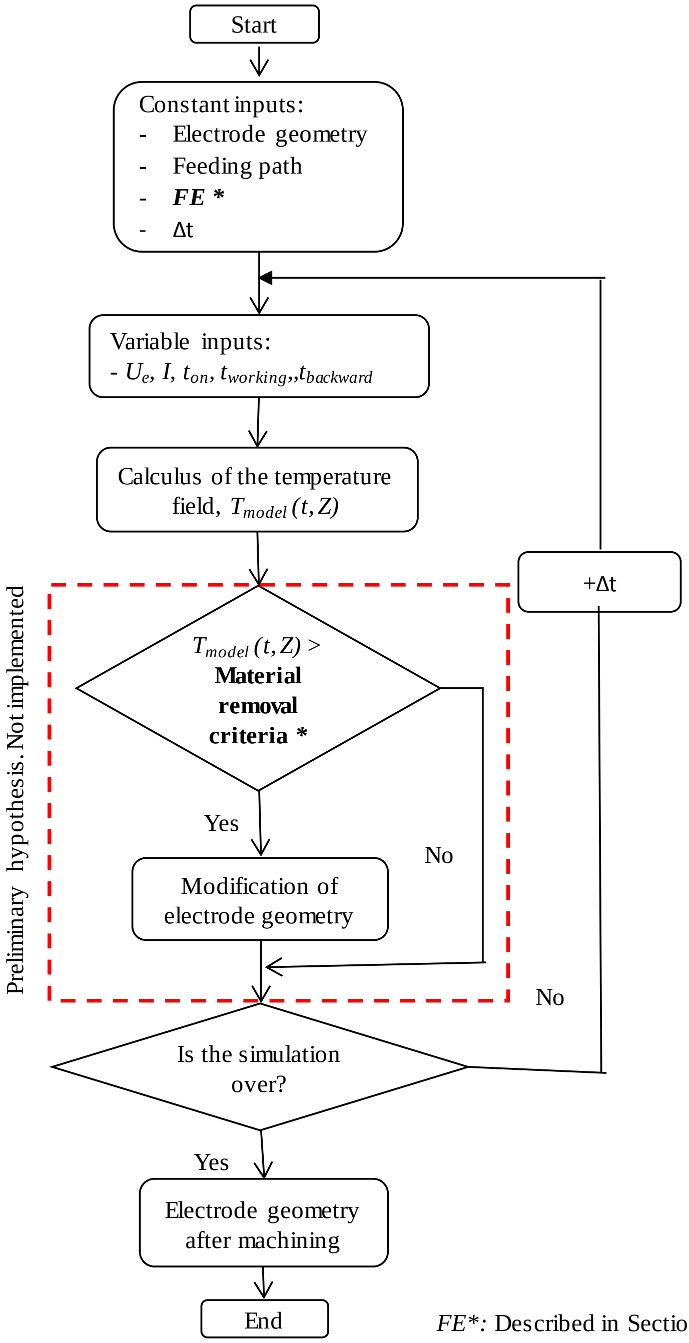
Start
Constant inputs:
- Electrode geometry
- Feeding path
- **FE ***
- Δt
Variable inputs:
- U_e, I, t_{on}, $t_{working}$,,$t_{backward}$
Calculus of the temperature field, $T_{model}(t,Z)$
$T_{model}(t,Z) >$ **Material removal criteria ***
Yes
No
Modification of electrode geometry
+Δt
No
Is the simulation over?
Yes
Electrode geometry after machining
End
Preliminary hypothesis. Not implemented

FE:* Described in Section VI.3

Material removal criteria*: Described in Section VI.4

Figure 115: Flowchart to predict electrode geometry after EDM process.

The sequence can be described as follows. Firstly, the electrode, the feeding path, F_E and Δt are defined. Then, at every Δt information regarding the machining parameters- I, t_{on}, $t_{backward}$ and $t_{working}$- is introduced. It is expected that once the steady state is reach $t_{backward}$ and $t_{working}$ values, will not vary if the machining regimen is not modified. Once the simulation has run for Δt the temperature field of the electrode will be known. The next step will be to apply the material removal criteria, and thus, simulate the electrode geometry change during machining. Nevertheless, as discussed in Section VI.4, it is only a preliminary hypothesis, which must be validated or discussed by future research work.

VI.2.2. Boundary conditions

Figure 116 shows a scheme of the boundary conditions of the developed mode.

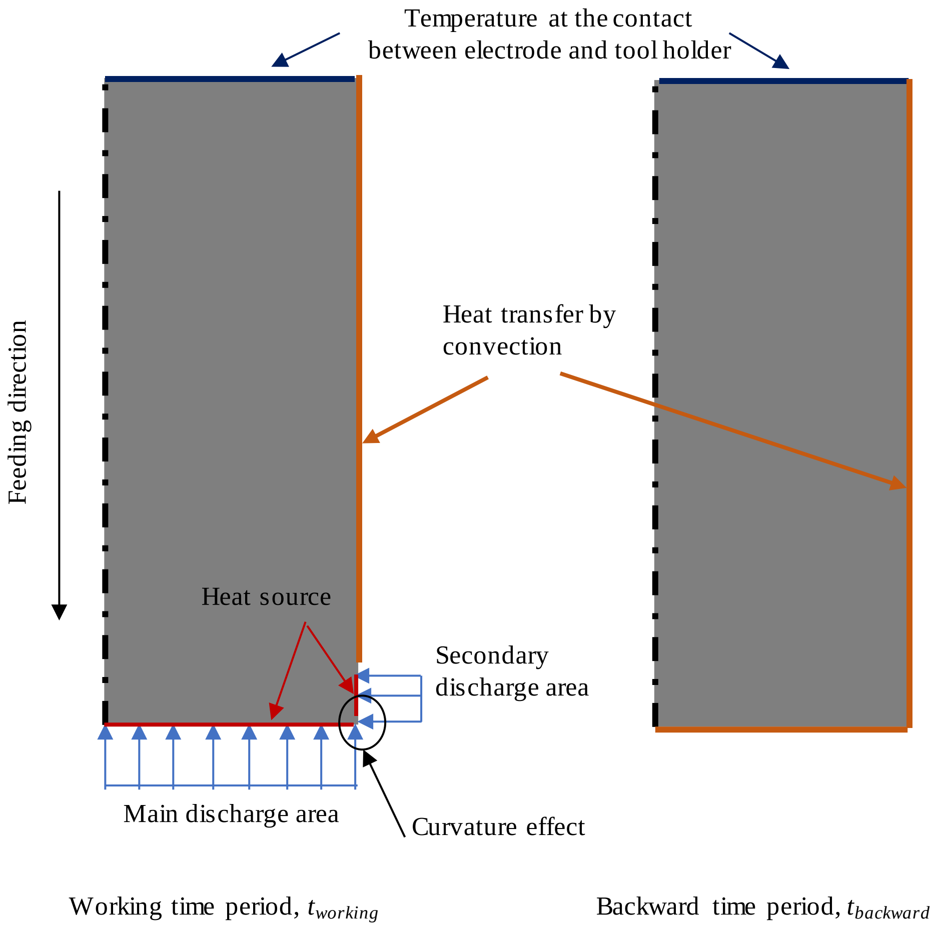
Temperature at the contact between electrode and tool holder
Feeding direction
Heat transfer by convection
Heat source
Secondary discharge area
Main discharge area
Curvature effect
Working time period, $t_{working}$
Backward time period, $t_{backward}$

Figure 116: Scheme that represents the boundary conditions.

Heat source application

As described, in EDM the heat is applied in very short time, measured in microseconds, at a localized spot. The simulation of the continuous discharges implies an extremely high computational cost. This is one of the main reason for the lack of research work in the simulation of continuous EDM jobs.

In order to be able to simulate industrial EDM jobs with an acceptable computational cost, the model proposes the application of the heat source generated during $t_{working}$ over the discharge area. Consequently, in the simulation sequence two main sequences are differentiated: the working time period, $t_{working}$, and the backward time period, $t_{backward}$. In the former, the heat source is applied, and in the latter, there is not heat source application, see Figure 117.

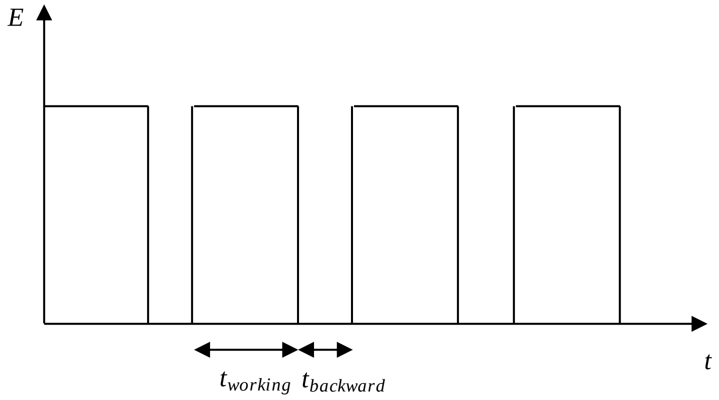

Figure 117: Scheme for illustrating the energy simulation method.

For simplify, the value of energy generated during each working time period is considered constant. Thus, the energy applied in the models is functions of the average values of: I, t_{on}, U_e, t_d and t_{off}. This way, the total energy generated during the $t_{working}$, $E_{working}$, is calculated as follow:

$$E_{working} = I.\,t_{on}.\,U_e.\frac{t_{working}}{t_{on} + t_{off} + t_d} \qquad \text{Eq. 16}$$

$E_{working}$ value corresponds to the total energy generated during the discharges, hence this value should be multiplied by the F_E coefficient for simulating the energy distributed to the electrode, E_E. Section VI.3 explains the procedure proposed for calculating F_E value.

Once the E_E is known, the energy is distributed into the discharge area. The energy is not distributed uniformly along electrode profile, but two effect are combined: the curvature effect, explained in Section VI.2.3, and the area effect, described in Section VI.2.4.

Heat transfer by convection

For simplicity, the model consists in a single solid that represents the electrode thus, the effect of the dielectric is taken into consideration by the convection coefficient.

Even if the dielectric of the tank is recirculating and connected to refrigerators, due to the discharges the temperature at the discharge gap is higher than in the parts in which discharges do not occur. Thus, for considering this effect two reference temperatures are considered: temperature in the gap, which is calculated experimentally in Section VI.3.2, and temperature of the dielectric of the tank, which due to the tank dimensions and the use of a refrigerator it is maintained constant.

VI.2.3. Method to consider the curvature effect

As observed in the results obtained in Chapter IV and Chapter V, electrode edges tend to wear rapidly and then the radius becomes constant. One explanation is that at the edges discharges occur more often per unit area, and thus, the temperature at the edges increase and electrode wear is higher. However, once the edge gets rounded the effect of discharge concentration does not occur and the electrode wear becomes more uniform along the discharge area. To consider this effect, as explained in the State of the Art, Kunieda *et al.* [45] modified the conventional reverse simulation method by an algorithm that compensate the error due to curvature.

Based on that publication, the proposed simulation model considers the curvature effect by modifying the energy distribution. With this purpose, the discharge area of the electrode is divided in different sections and according to its curvature, measured by radius, a coefficient β_i is assigned. At flat areas the value is 1 and at edges the value will vary from 1 to infinite according its radius. Figure 118 shows a graphical explanation of the coefficient.

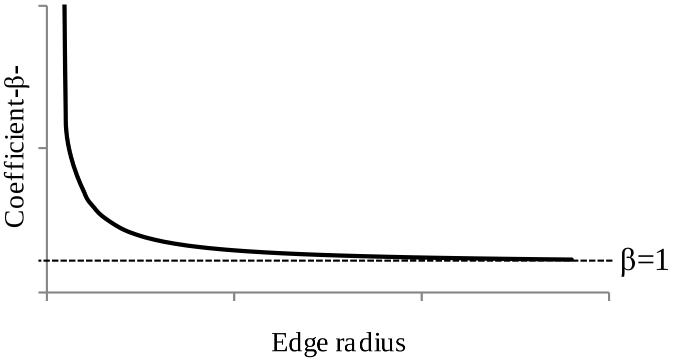

Figure 118: Example of the value of edge radius on the coefficient that consider the curvature effect.

Then, the energy at each section is calculated as follows:

$$E_{Ei} = \frac{E_E . \beta_i}{\sum_1^i \beta_i} \qquad \text{Eq. 17}$$

Where E_{Ei} refers to the heat input value that is applied in the electrode at section *i.*

VI.2.4. Method to consider the discharge area effect

During the EDM process the vast majority of the discharges occur at the main discharge area, but some side surface discharges also occur. This indicates that not all the heat input should be applied in the main discharge area.

For explaining the phenomena, the example of Figure 119 has been considered. Area *A1* refers to the main discharge area, *A2* refers are near the main discharge area and *A3* refers to the area in which side surface discharges occur.

The probability to a discharge to occur is the highest at *A1* and the less likely is at *A3*, as at this area the gap is wider than at the other two areas. Thus, the simulation model differentiates those regions in order to weight the energy transferred to each one.

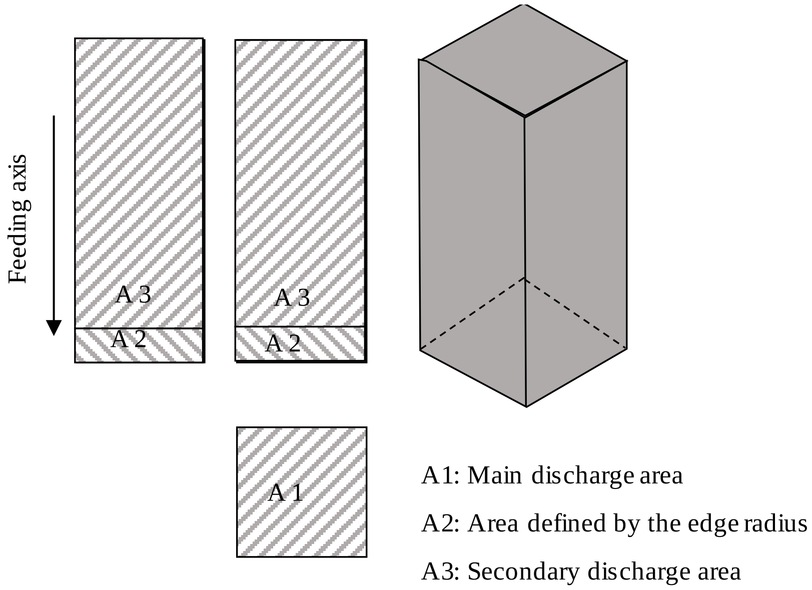
Feeding axis
A 3
A 2
A 3
A 2
A 1
A1: Main discharge area
A2: Area defined by the edge radius
A3: Secondary discharge area

Figure 119: Definition of the areas considered in the model for the application of the heat input.

VI.2.5. Graphite properties

An important input for the model are the properties of the graphite. For the heat transfer study, three are the main material properties that should be considered: the apparent density, the thermal conductivity and the heat capacity. Furthermore, with the objective of simulating electrode wear, the grain size should be considered.

Apparent density

The value of the apparent density will be considered constant, because the value is affected by temperatures up to 2000°C-3000°C [106] and those temperatures are not expected during the simulation. For the commonly used graphite electrode material, the value of apparent density is 1.81 g/cm^3 [112].

Thermal conductivity

The thermal conductivity of a material is a measure of its ability to conduct heat. A high thermal conductivity denotes a good heat conductor, while a low thermal conductivity indicates a good thermal insulator. As shown in Figure 120a. , thermal conductivity decreases with the increase of the temperature [106]. In the model the influence of thermal conductivity with temperature has been input as shown by Figure 120b.

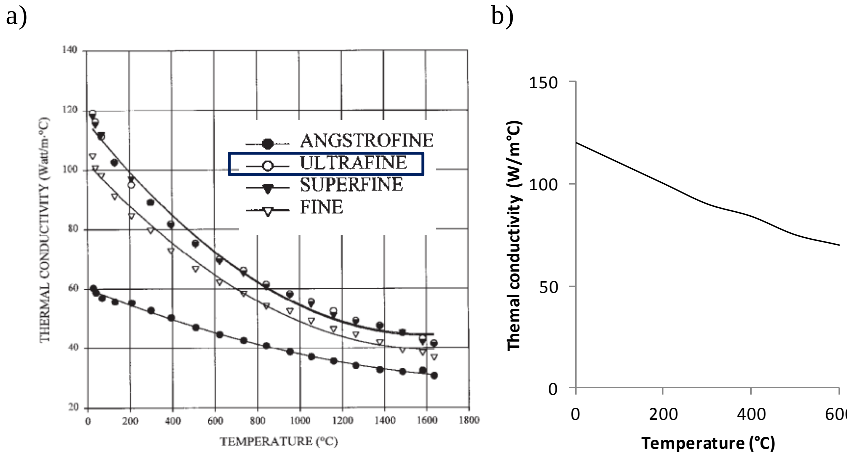
a)

b)

Figure 120: Thermal conductivity vs. temperature. a) Theoretical values [106]. b) Output for the model.

Heat capacity

Heat capacity is the quantity of heat required to raise the temperature of a unit mass of material 1K. With regards to graphite, it has been found that the values of heat capacity for all types of natural and manufactured are basically the same. Figure 121a. as shows the variation of heat capacity with temperature [106]. In the model the influence of heat capacity with temperature has been input as shown by Figure 121b.

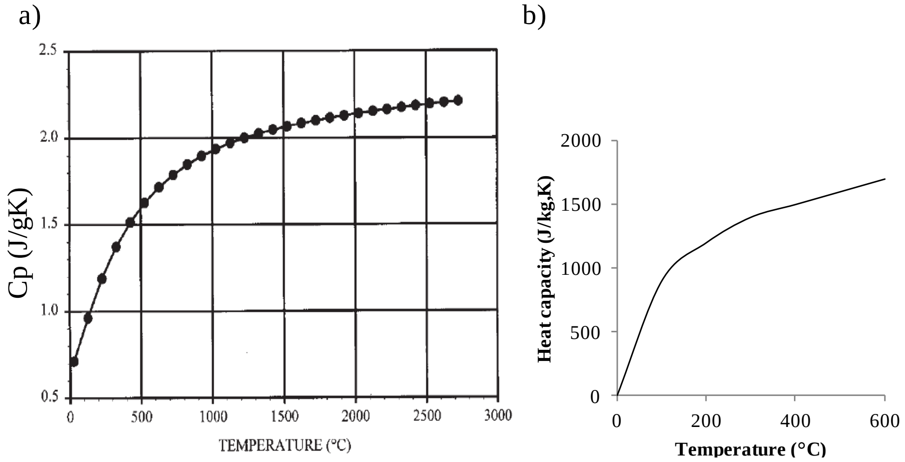
a)

b)

Figure 121: Heat capacity VS temperature. a. Theoretical values [106]. b. Output for the model.

Particle size

Furthermore, the particle average size of the electrode should be considered, as its value will condition the mesh size in the regions in which material removal is expected. It is recommended to define the mesh size of the regions near the discharge area with the graphite particles size value. This is because the main electrode wear mechanisms when graphite is used as electrode, is the detachment of graphite grains [113].

VI.3. Heat transfer definition during continuous EDM process

As discussed in Chapter II, energy distribution during EDM is a complex phenomenon and the existence of models for the determination of the energy fractions are limited, thus it remains an active topic of research.

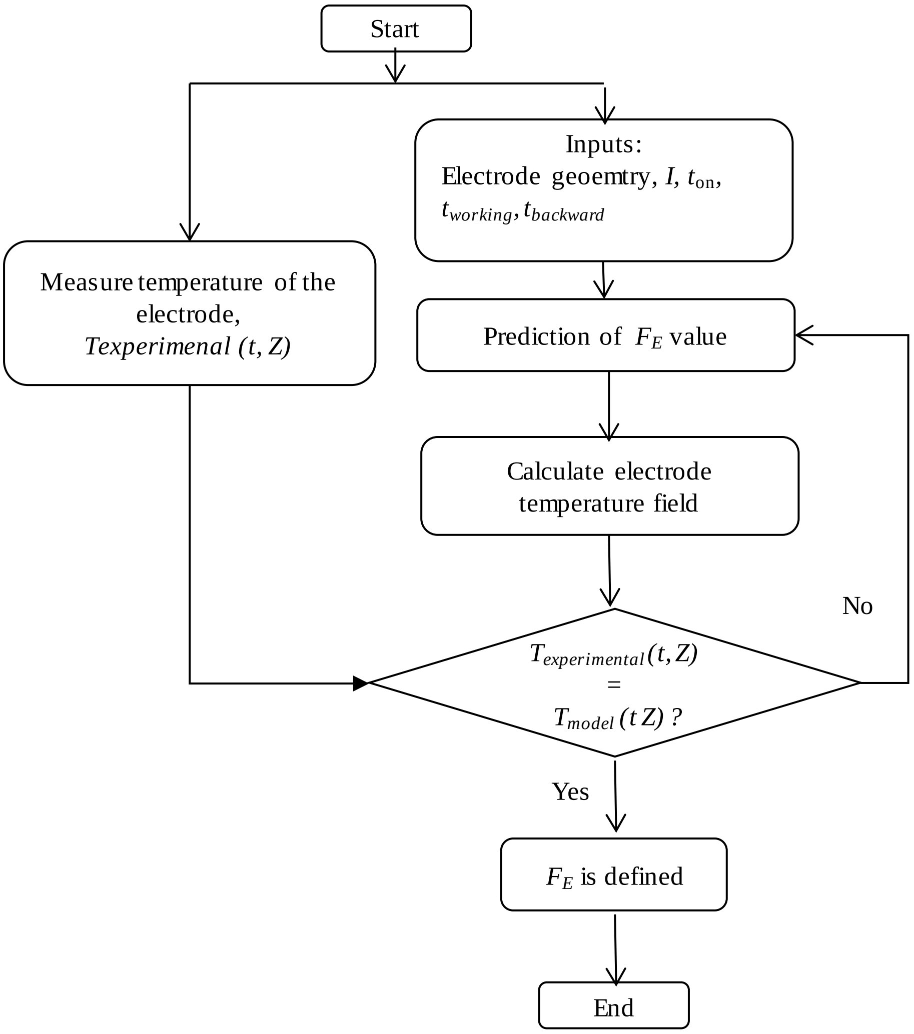
Start
Inputs:
Electrode geoemtry, I, t_{on}, $t_{working}$, $t_{backward}$
Measure temperature of the electrode, $Texperimenal\ (t, Z)$
Prediction of F_E value
Calculate electrode temperature field
No
$T_{experimental}(t, Z)$ = $T_{model}\ (t\ Z)$?
Yes
F_E is defined
End

Figure 122: Flowchart for F_E value determination.

The work presented in this Section has the objective of defining F_E value. For this matter, an inverse simulation model is proposed. Firstly, the temperatures of the electrode are measured experimentally and then results are compared with the temperatures of the model until the correct value of F_E is calculated. Figure 122 shows a simplification of the flowchart of the method use for the definition of F_E value. Where $T_{experimental}\ (t,Z)$ represents the experimentally measured temperature of the electrode and $T_{model}\ (t, Z)$ represents the temperature that is reached during the machining process.

VI.3.1. Experimental set-up

The experiments were carried out under industrial conditions on an ONA CS300 sinking EDM machine, Table 8. The materials used where graphite POCO EDM-200® for electrode and F114 structural steel for workpiece. As discussed in Section VI.2, the average grain size of the electrode should be considered for building the mesh, which in this case is of 10 µm. The main properties of the electrode are presented in Table 14.

The machining was carried out under the machining conditions of Table 18. Under those machining conditions, the following temperatures were measured: temperature of the electrode, temperature of the dialectic in the discharge gap, temperature of the dielectric that surrounds the electrode and temperature between electrode and tool holder.

Table 18: Machining and experimental conditions.

Working fluid	EDM oil
Polarity (electrode)	+
Ue (V)	120
I (A)	36
t_{on} (µs)	200
Pre-set t_{off} (µs)	25
SV (V)	20

For measuring the temperatures, thermocouples of type K and a sheath diameter of 0.5 mm were used. The technical data are described in Table 19. The temperatures were recorded by LabVIEW software [114].

During machining, current and voltage waveforms were recorded by a high-frequency oscilloscope for a posterior processing and determination of the actual EDM parameters. The data were processed by MathWorks® software.

Table 19: Main specification of the thermocouple used [115].

Reference	Application	
406-480	Thermocouple type K Sheath diameter 0.5mm Operation range: -100°C to 800°C Insulated Junction	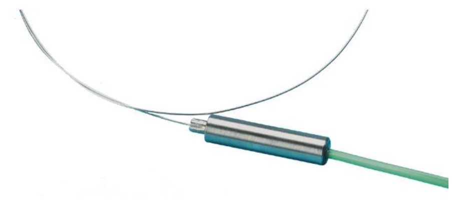

In the following paragraphs the experimental set-ups used for each temperature measurements are described.

Temperature measurement on tool electrode

Figure 123 illustrates the electrode temperature measurement set-up used for measuring the temperature of the electrode.

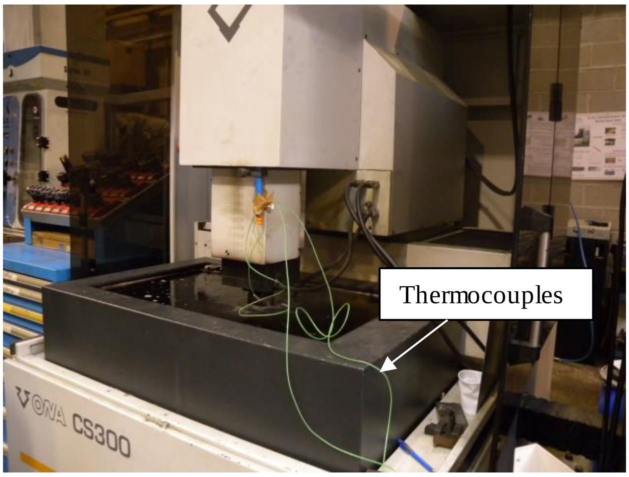

Figure 123: Set-up during the electrode temperature recording.

The temperature was measured at 2 mm from the discharge gap by two thermocouples, see Figure 124. The temperature signals were recorded at f=100 Hz. Nonetheless, considering that the discharge frequencies is much higher, the temperature recorded is not the maximum, but the average value.

For inserting the thermocouples two holes were machined, however, due to the strong heat conductivity of the graphite, the holes won’t be a source of measurement distortion [61]. The contact between the thermocouple and the electrode was ensured by inserting the thermocouples is the narrow hole made in the electrode and by attaching the thermocouple from the top of the electrode.

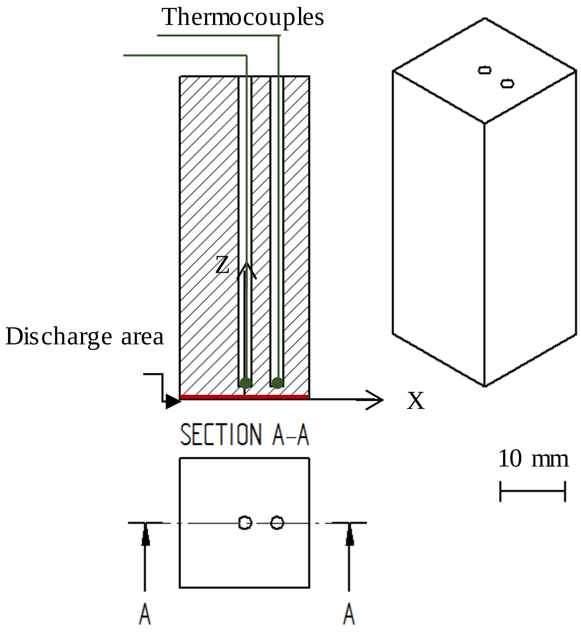

Figure 124: Scheme of thermocouple displacement.

Moreover, to guarantee that the thermocouple was in contact with the electrode, after the temperature recording the electrode was cut to see if there was contact between the electrode and the workpiece. Figure 125 shows an example of one of the sections, in which the contact between the thermocouple and the electrode is observed.

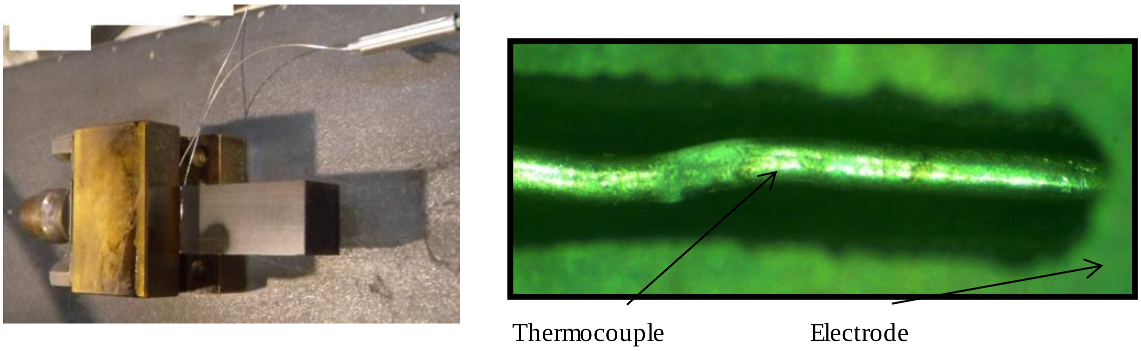

Electrode with the thermocouples

Figure 125: Example that shows the contact between electrode and workpiece.

Temperature measurement of the dielectric

The temperature of the dielectric that surrounds the electrode was measured by a thermocouple. In this case the recording frequency was set as f=10Hz. As is illustrated by Figure 126, a thermocouple was attached in one of the electrode walls. The thermocouple is in contact with the dielectric.

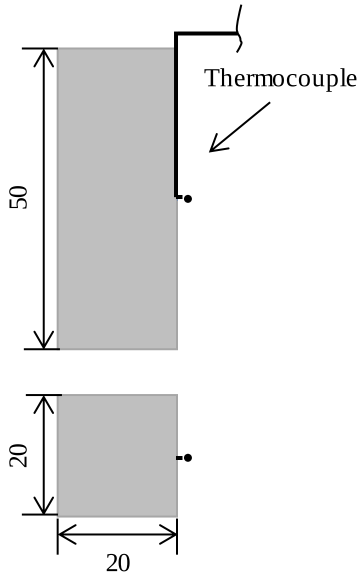

Figure 126: Experimental set-up for dielectric temperature measurement.

Temperature measurement of the dielectric in thedischarge gap

It is known that after continues discharges the temperature of the dielectric of the discharge gap increases due to the heat generated by the discharges. However, its direct measurement is a difficult task. In the present work, in order to measure its approximate value, a destructive experiment has been proposed.

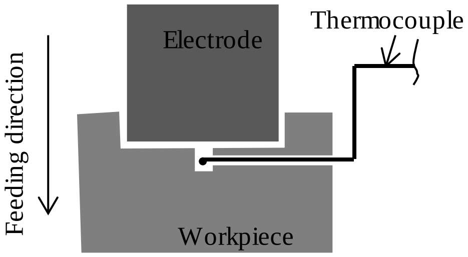

Figure 127: Experimental set-up for dielectric temperature measurement in the discharge gap.

As illustrated Figure 127, a thermocouple was inserted in the workpiece in which previously a couple of holes were machined. It was ensured that the thermocouple was in contact with the dielectric. Ones the set-up was ready the machining was started, and the temperatures were recorded until the thermocouple was destroyed by a discharge. It was considered that the temperature of the dielectric in the gap corresponds to the last average temperatures recorded.

Temperature measurement at the boundary between electrode and tool holder

As is well known, during machining the tool holder temperature increases. This temperature is not high, and due to the heat transfer and machine tool dimensions, after a couple of seconds of machining this temperature becomes constant. Its value was measured in order to verify the hypothesis.

VI.3.2. Temperature measurement results

In this section the temperatures recorded following the experimental set-ups described in Section VI.3.1 are shown.

Temperature of the electrode

The results of the temperature recorded on the electrode will be used for defining the fraction of the discharge energy absorbed by the electrode, F_E.

Figure 128 shows the temperature result of the electrode at 2 mm from the discharge gap during continuous machining. The higher temperature rise, as was expected, occurs after the first discharges are generated. Then the temperature rise becomes less prominent, and after 2-3 minutes of machining, the temperature becomes constant, which indicates that the steady state has been reached.

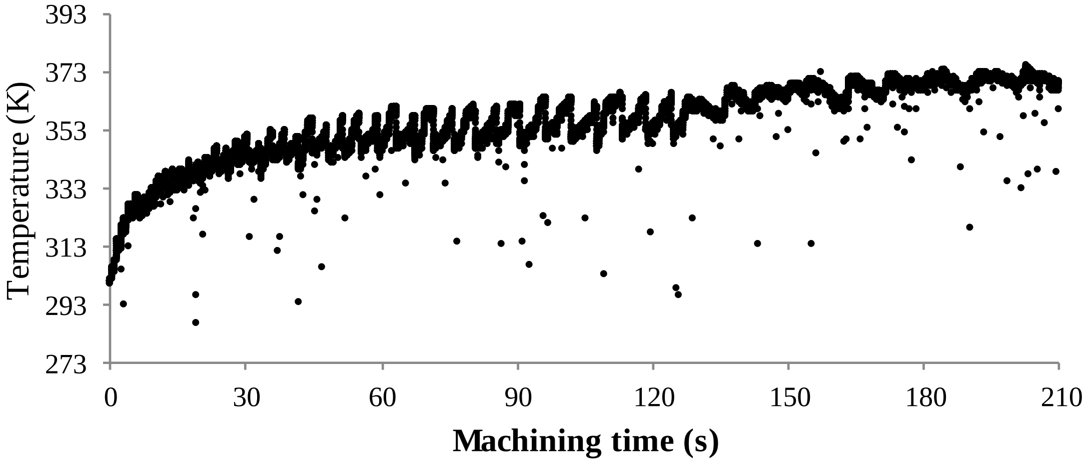

Figure 128: Temperature in the electrode at 2 mm form the discharge gap.

The up and downs of the temperature matches with the $t_{working}$ and $t_{backward}$ time measured. This demonstrates that the up and down of the electrode is not only effective in terms of flushing, but also in terms of electrode wear, as long $t_{backward}$ lowers the temperature of the electrode.

Temperature of the dielectric

As was expected, due to the heat conductivity of the electrode material, after several seconds, the temperature of the dielectric around the electrode is maintained constant. The value can be considered as 312 K, see Figure 129.

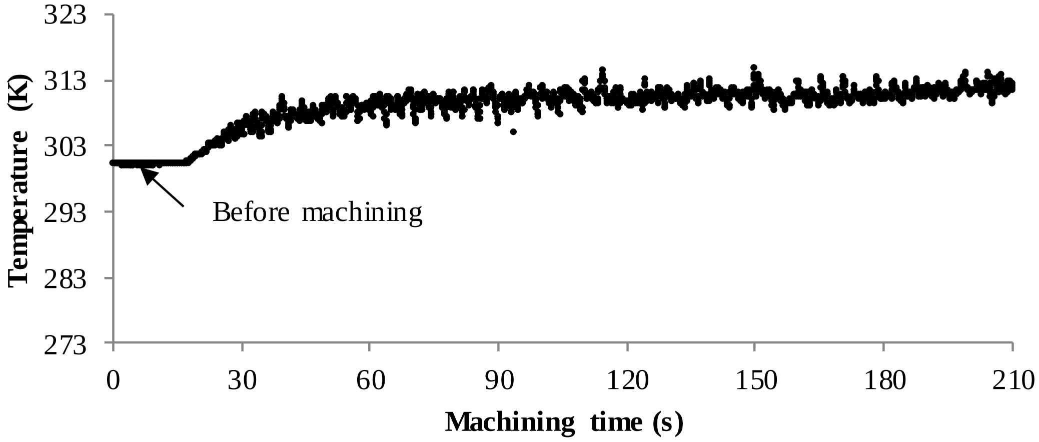

Figure 129: Temperature in the dielectric that is surrounding the electrode.

Temperature of the dielectric in the discharge gap

As is shown in Figure 130, the temperature of the dielectric in the discharge gap can be considered as 403 K.

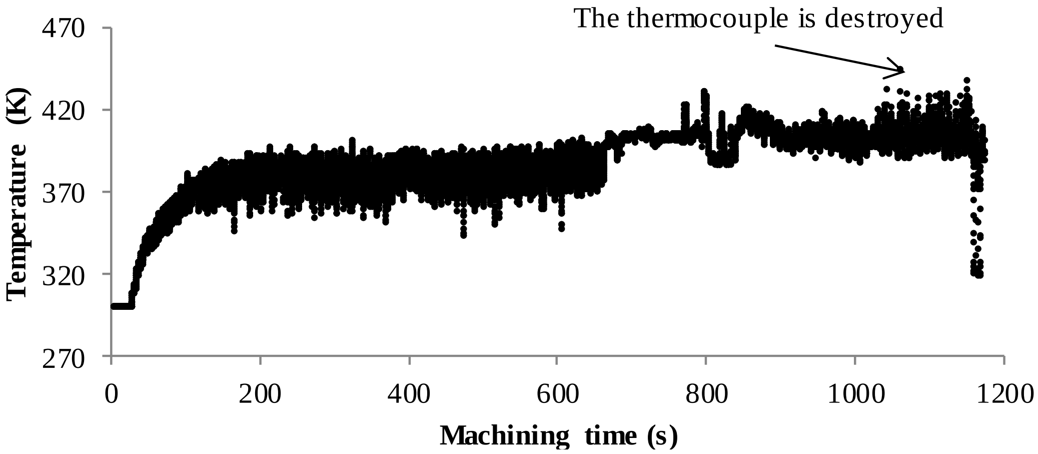

Figure 130: Temperature measurement for obtaining the temperature of the dielectric of the discharge gap.

Temperature measurement at the boundary between electrode and tool holder

Results of Figure 131 show that after a several seconds the temperature is become constant at 308K.

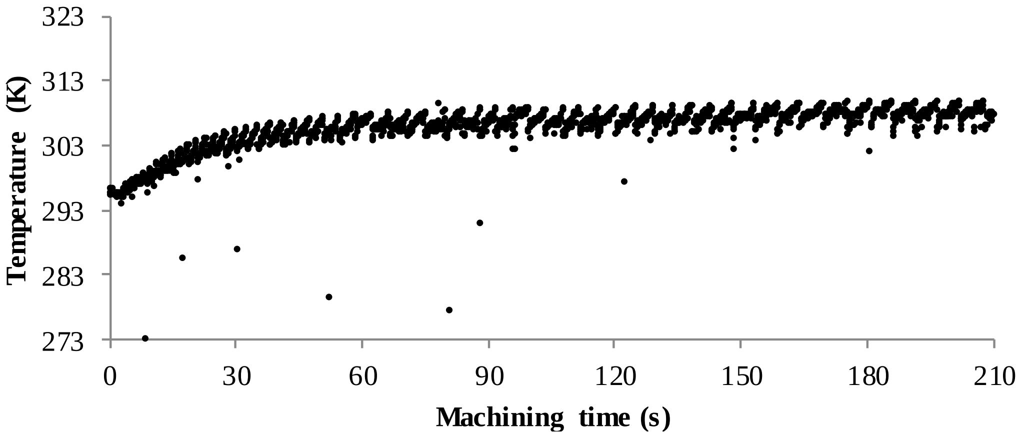

Figure 131: Temperature in the contact between electrode holder and electrode.

VI.3.3. Discussion of results

The temperature profiles obtained in the experimental work have been compared with the simulation temperature results to determinate F_E value. In order to validate the results two stages were compared: temperatures during machining, Figure 132, and the cooling of the electrode once the machining was stopped, Figure 133.

Figure 132 compares the experimental results with the simulated results when F_E is considered 0.08. As observed, both experimental and simulated results show similar values at the early stage of machining and at the steady state.

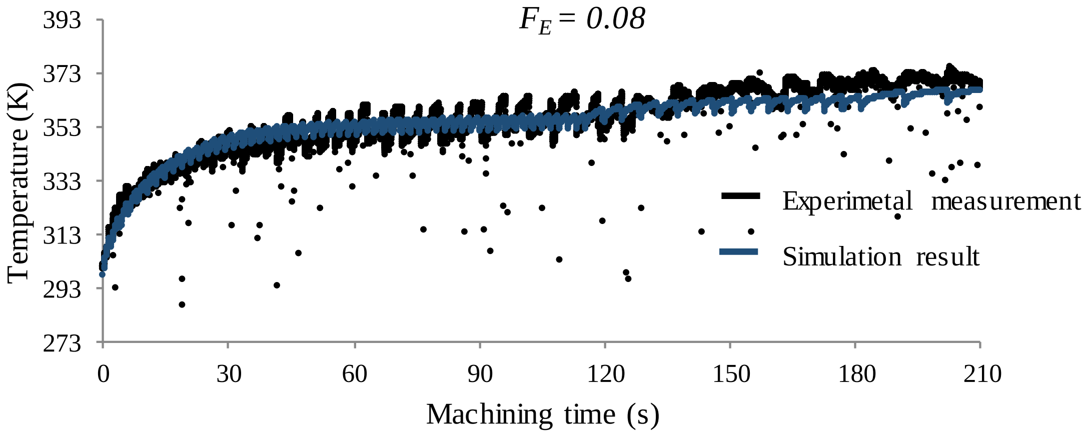

Figure 132: Temperature results. Experimental measurement vs. simulation result.

In addition, Figure 133 compares the electrode temperature decrease seconds after the machining is stop. In this case too, simulated results are in good agreement with the measured temperatures. These results confirm that the criteria followed for the boundary conditions, as described in Section VI.2.2, resembles reality.

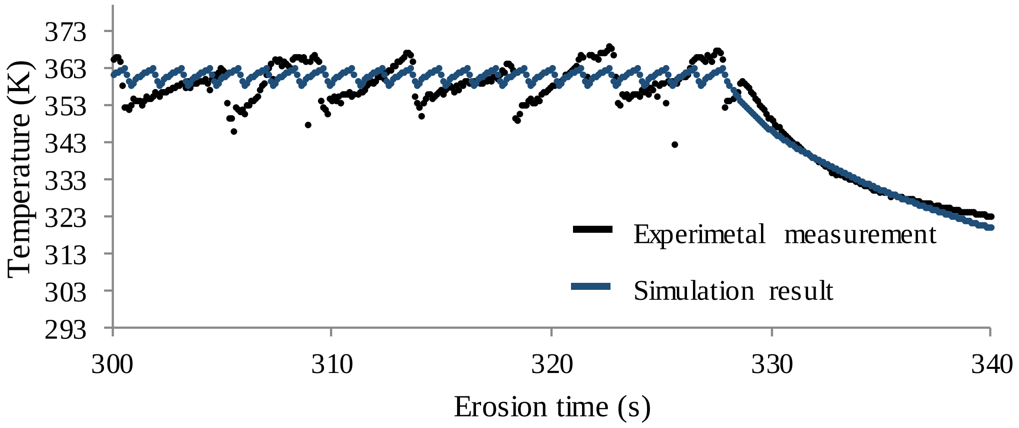

Figure 133: Temperature of the electrode after the machining was stopped. Experimental measurement vs. simulation result.

It should be noted, as described in Chapter II, that the energy distribution into the gap is dependent on the machining parameters used. For instance, regarding t_{on}, when short durations are used, most of the energy is dissipated into the dielectric and plasma, and thus, F_E is low. Nevertheless, with long durations it is believed that the plasma becomes self-sustaining and higher energy is distributed to both electrode and workpiece [84][49]. For instance, Oßwald *et al.* [60] concluded that when machining with copper electrode, F_E value could varied between 0 and 0.1 depending on the machining parameters used. Another example is the work of Sing [116]. He observed that when tungsten carbide was used as tool electrode F_E varied between 0.05 to 0.25 depending on the machining parameter. Figure 17 of Chapter II shows a comparison of energy distribution ratios found in the literature.

This highlight the importance of the developed simulation method for the calculation of F_E value. Because, even if the variability of F_E may not be considerable, if electrode temperature distribution wants to be simulated, the F_E value for the given discharge parameters should be calculated.

VI.4. Preliminary proposal: Electrode material removal criteria

From the conclusion of the experimental results presented in Chapter V, there is no doubt that a simulation model that predicts electrode wear during continuous EDM can bring improvements in the understanding and to the competitiveness of EDM process.

Based on the thermal simulation model described in Section VI.2 it is believed that the electrode geometrical change during EDM can be predicted by the definition of a material removal criteria based on local electrode temperature. With this objective in mind, in the present Section, a preliminary study in which the temperatures reached in the electrode are compared with the progress of electrode wear during machining is carried out. For this matter, the machining of a high-aspect ratio slot was chosen as case study.

Firstly, in Section VI.4.1, the experimental set-up for obtaining information for electrode wear patterns is described. Then, in Section VI.4.2, the results of both electrode wear and temperature field of the electrode are discussed. Finally, in Section VI.4.3 the conclusion drawn for the definition of a preliminary hypothesis for material removal criteria is discussed.

VI.4.1. Experimental set-up

VI.4.1.1. Experimental work

The experiments were carried out under industrial conditions on an ONA CS300 sinking EDM machine. The workpiece material was F114 structural steel and POCO EDM-3® for the electrode. The main properties of the graphite are shown in Table 20.

Table 20: Main specifications of POCO EDM-3® [108].

Average Particle Size (µm)	<5
Flexural Strength (psi)	13300
Compressive Strength (psi)	18100
Hardness (shore)	73
Electrical Resistivity (µOhm-in)	615

Figure 134 shows the electrode geometry used in the experiments, which corresponds to the one used in the work presented in Chapter IV.

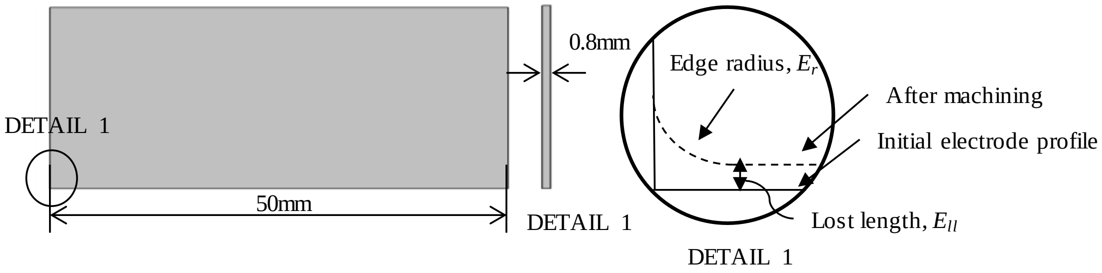

Figure 134: Electrode geometry and representation of electrode wear indicators.

The machining depth was set as 6.5 mm. The machining parameters were also maintained as in Chapter IV, see Table 12. It should be reminded that the generator of the machine tool used in the experiments is an iso-energetic generator. This indicates that during the machining process the generator attempts to maintain I and t_{on} at constant values. Furthermore, to avoid inefficient discharges, such as arc and short-circuits, the pulse generator controls the t_{off} value. Moreover, even if jump motion is not applied during the experiments, the generator adapts the values of the working time and backward time. Consequently, by a high-frequency oscilloscope the value of I, t_{on}, t_{off}, $t_{working}$ and $t_{backward}$ have been measured.

The electrode wear indicators used for analysis of electrode wear were: Electrode lost length, E_{ll} and the edge radius, E_r. For the analysis of the progress of both indicators during the machining of the slots, results were obtained at the following machining depths: 2 mm, 3 mm, 4 mm, 5 mm and 6.5 mm. Each experiment was performed with a new electrode.

VI.4.1.2. Definition of the simulation model

As explained by the flowchart of Figure 115 the data required for the model is: initial electrode geometry, information for defining the heat input- I, $t_{on,}$ t_{off} -, the coefficient of the heat transferred to the electrode, F_E, and $t_{working}$ and $t_{backward}$ times.

Once the initial electrode geometry is defined, the mesh must be built. As shown in Table 20, the average particle size of the graphite used in the experimental work is 5 µm, thus, as explained in Section VI.2.5 the minimum mesh size for building the mesh of the thermal model in regions near the discharge are must be below 5 µm.

Considering that the machining parameters conditioned the distribution of the energy [55][61], the data of F_E value for the current discharge parameters combination is essential for the simulation. Thus, the inverse simulation method described in Section VI.3 has been carried out, prior to the actual electrode temperature simulation with the actual electrode geometry. Following the simulation method, and the experimental set-up described in Section VI.3.1, it was concluded that the value of F_E is 0.14.

It should be mentioned, as described in Section VI.3.3, that the EDM parameters used for the machining of the slots are an especial set of parameters that are only used for the machining of those type of slots. However, the explanation of the method described in Section VI.3 was carried out with a commonly used combination of EDM parameter. This is the reason why the value of F_E differs from the value obtained when explaining the proposed methodology for the determination of F_E value. This again, highlight the importance of the developed simulation method for the calculation of F_E value.

In terms of the heat input definition, the waveforms of current and voltage were recorded for the proper definition of I, $t_{on,}$ $t_{off,}$ $t_{working}$ and $t_{backward}$. The data acquisition and processing were carried out according with the procedure followed in the analysis of discharges described in Chapter IV in Section IV.4

Furthermore, the curvature effect and the area effect described in Section VI.2.3 and VI.2.4 were also considered.

VI.4.2. Experimental results. Results discussion

The first thing to mention is that as concluded from the work described in Chapter IV, if electrode with pockets is not used, due to debris accumulation in the narrow gap, machining stability is affected, and after a certain machining depth, the feeding speed decreases drastically. For the present case, as illustrated Figure 135 , the machining stability is affected after 4 mm machining depth. This was corroborated by the machining of 5 slots in a row.

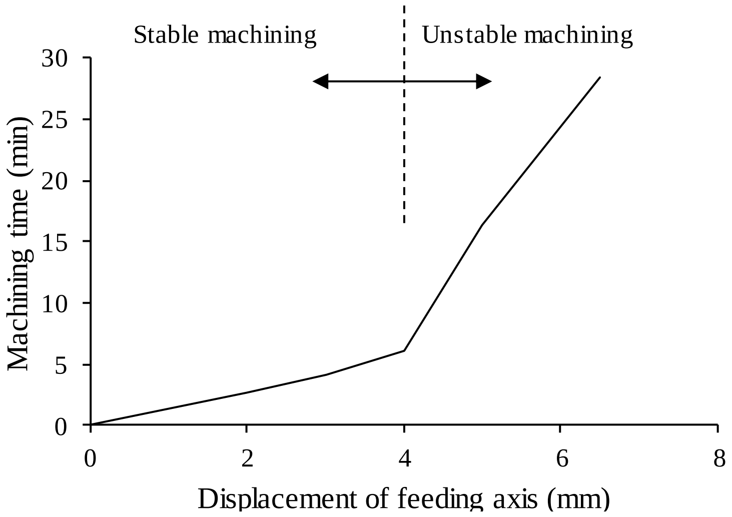

Figure 135: Feeding axis vs. machining time.

This indicates that during machining two different scenarios can be clearly classified: the stable machining and the unstable machining. Because of that, results will be discussed in terms of machining stability regions.

VI.4.2.1. Electrode wear indicators: E_{ll}

Figure 136 shows the results of E_{ll} progress during the machining of a slot of 6.5 mm. From results, the two stages, stable machining stage and unstable machining stage, can be distinguished. During stable machining E_{ll} has a negative value, which means that the electrode length grows. In other words, it means that material build-up occurs. However, during unstable machining the electrode lost length becomes positive, indicating that not only the generated material layer is removed but also, that electrode lost lengths occurs.

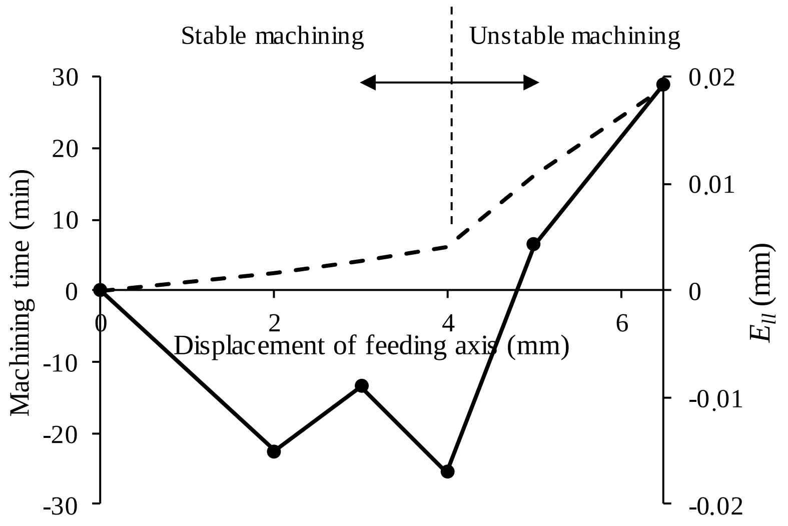

Figure 136: E_{ll} progress during the machining of a slot of 6.5 mm.

One of the factors that provokes the material build-up is the long t_{on} values [74][39]. However, the present results cannot only be explained by the t_{on} effect, because, the EDM generator automatically detects unstable conditions in the discharge gap and by the adaptive power control extents the t_{off} value and the $t_{backward}$ value maintaining constant the value of t_{on}. In brief, t_{on} value is the same in both stable and unstable regions.

This effect is clearly observed by a capture of the discharge signal during both stable and unstable machining. Figure 137.a illustrates an instant during stable machining and Figure 137.b during unstable machining. In both cases t_{on} value is the same, but the values of t_{off} and the $t_{backward}$ vary.

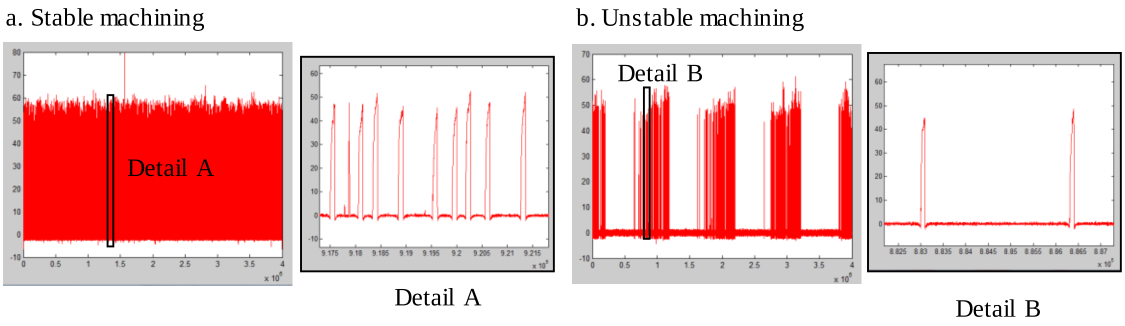
a. Stable machining

Detail A

b. Unstable machining

Detail B

Figure 137: Current waveform. a) Stable machining, b) Unstable machining.

A possible explanation for the generation of the material build-up, apart from the long t_{on} value, can be drawn from the results of the average temperature of the discharge area of the electrode. Results of the simulated electrode temperatures show that during stable machining, due to the high discharge frequency, the temperature of the electrode reaches 401 K, Figure 138.a shows the temperature distribution after 2 min of machining. Nevertheless, during unstable machining the discharge frequency decreases, resulting in a lower electrode temperature. Figure 138.b shows that during unstable machining the temperatures are around 319 K. This means that even if the local temperature resulting from a single discharge is the same in both cases, the average temperature of the surface varies considerably with the discharge frequency.

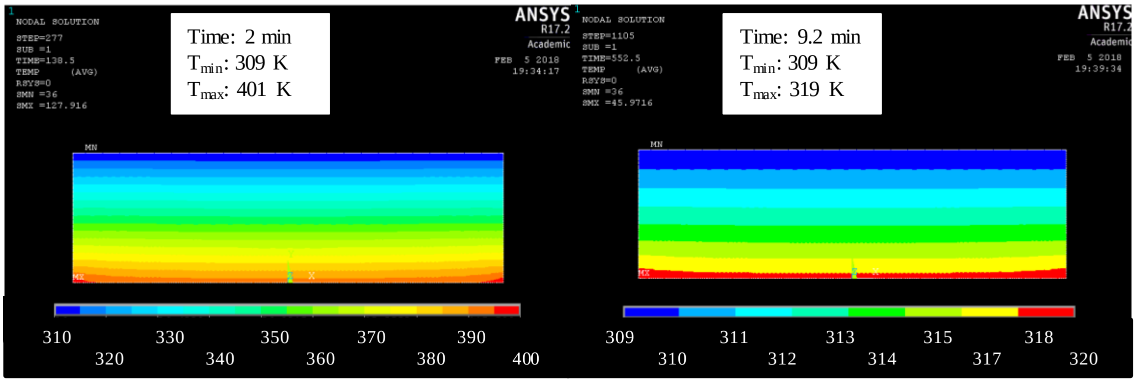
a. Stable machining

b. Unstable machining

NODAL SOLUTION
STEP=277
SUB =1
TIME=138.5
TEMP (AVG)
RSYS=0
SMN =36
SMX =127.916
Time: 2 min
T_{min}: 309 K
T_{max}: 401 K
ANSYS
R17.2
Academic
FEB 5 2018
19:34:17
MN
MX
310
320
330
340
350
360
370
380
390
400
NODAL SOLUTION
STEP=1105
SUB =1
TIME=552.5
TEMP (AVG)
RSYS=0
SMN =36
SMX =45.9716
Time: 9.2 min
T_{min}: 309 K
T_{max}: 319 K
ANSYS
R17.2
Academic
FEB 5 2018
19:39:34
MN
MX
309
310
311
312
313
314
315
317
318
320

Figure 138: Electrode temperature field. a) Stable machining, b) Unstable machining.

Consequently, a prior hypothesis drawn is that for the generation of a carbonaceous layer is that not only the temperatures of the discharge spot should be considered [40], but also the temperature distribution of the discharge area.

VI.4.2.1. Electrode wear indicators: E_r

Figure 136 shows the results of E_r progress during the machining of a slot of 6.5 mm. As expected, at the early stage of machining the edges get rounded until a certain value and then it is maintained constant. This effect was also observed in previous experimental works described in Chapter IV and Chapter V.

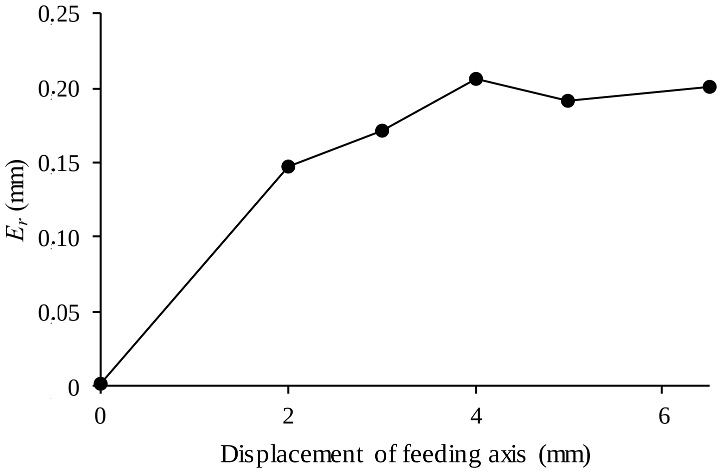

Figure 139: E_r progress during the machining of a slot of 6.5 mm.

The main reason is that at sharp edges there is higher concentration of discharges and thus, the grains of the edges will be easier to remove due to the higher temperatures at those points.

However, ones the edges get rounded, the energy is more uniform distributed along the discharge area. For instance, Figure 140 represents at early stage, in which discharges are concentrated at the edges. In this case, as discharges are concentrated at the corners, thus, much higher temperatures are observed at the edges than at flat areas.

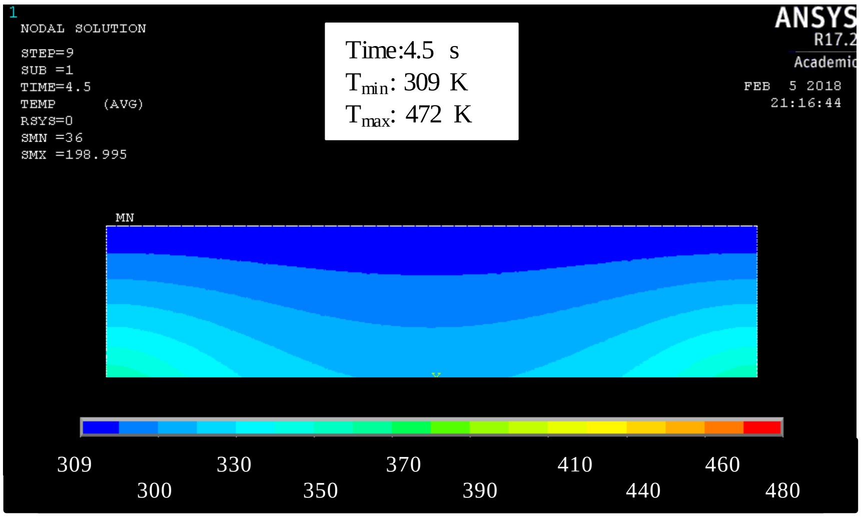

Figure 140: Electrode temperature field at early stage of machining.

VI.4.3. Material removal criteria hypothesis

From the preliminary work presented in this Section, it is expected that by the application of a material removal criteria to the proposed temperature simulation model, the electrode geometry change during machining can be simulated.

Observing both electrode wear results and temperature distribution results, it is expected that the material removal criteria can be a temperature value: an equivalent temperature for material removal, $T_{eq.removal}$ and equivalent temperature for material attachment, $T_{eq.attachment}$. If during the simulation, the temperature of the discharge area is higher than $T_{eq.attachment}$, material attachment will be simulated. However, if temperature is between $T_{eq.attachment}$ and $T_{eq.removal}$ material removal will be simulated. Furthermore, as described by Mohri *et al.* [39], the material attachment at edges is difficult to occur, thus at edges only the criteria of material removal should be applied.

VI.5. Conclusions

The present Chapter proposes a thermal model that predicts electrode temperatures during continuous machining. The simulation does not calculate the instant temperature generated for each discharge, but the average temperature of the discharge area by the sum of the energy of the total discharges. This feature, enables its applicability to practical EDM jobs with a reasonable computational cost.

As first step prior to the temperature simulation, there is the need to determine the energy absorbed by the electrode, F_E. For its calculation, the presented work proposed an inverse simulation method that compares temperature results obtained experimentally with simulated temperatures.

Moreover, a preliminary study has been carried out from which the hypothesis that electrode wear can be predicted by the temperature results is discussed.

Chapter VII: Conclusions and future works

VII. CONCLUSIONS AND FUTURE WORKS

In the present Chapter the main conclusions and the future works have been summarized.

VII.1. Conclusions

The present section summarizes the main conclusions drawn from the present PhD dissertation.

Approaches for the improvement of EDM cutting by foil electrode.

The present study is focused on the improvement of SiC slicing by foil electrode technique. The main goal of the work was improving kerf width accuracy by considering the influence of the occurrence probability of side surface discharges on the kerf width and machining performance. With those purposes, two foil electrodes were proposed: an electrode with holes and an electrode with an insulation layer on the side surface.

- Kerf loss was reduced when the side surface of the foil electrode was coated with a resin coating layer of 5 µm in thickness.
- Using a foil electrode with holes, cutting speed increased and tool wear decreased, due to the chip pocketing effect of holes.
- The lowest kerf loss and highest MRR were obtained when jump motion of the tool electrode was used.
- From the analysis of the distribution of the discharge delay time by the Laue Plot, it was concluded that making holes and coating the electrode surface with a 5 µm resin coating layer result in a longer discharge delay time.

Improvement of EDM performance in high-aspect ratio slots using multi-holed electrodes.

Due to debris accumulation in the narrow gap, the machining depth for stable machining is limited. The present study, proposed a multi-holed electrode that guaranties the machining stability when machining high-aspect ratio slots, by the improvement of the flushing conditions. The geometry and the position of the holes machined on the electrode lateral faces have been studied.

- Through the machining of holes of 4 mm in diameter in the electrode, a reduction of 57% in machining time was achievable when machining a high-aspect ratio slot of 6.5 mm due to the chip pocketing effect of holes.
- When machining 10 mm depth slots, the process time was reduced by 65% when an electrode with pockets was used. This is because the process does not loss stability along the machining depth.

- Machining stability can be guaranteed if the flushing pockets machined on the electrode penetrate the entire machining depth. This was confirmed by the machining of a 25 mm depth slot.
- Higher discharge frequency, duty cycle, and shorter discharge delay time and discharge off time values were observed when using the electrode with pockets.

Development of a methodology for the determination of electrode wear and gap in multi-stage EDM.

In this work, a methodology for studying electrode wear pattern and gap width in multi-stage EDM of complex geometries was developed. Regarding to electrode wear, the methodology establishes different indicators for defining the electrode worn geometry. Moreover, a procedure for gap width analysis was presented.

- E_{wa} follows a linear trend with machining time. Moreover, it was concluded that the influence of machining time is higher when working with more energetic parameters.
- E_{ll} also follows a linear tendency with machining time. The maximum relative standard deviation occurred when working with the most energetic parameter settings. This was attributed to the uneven material build-up.
- E_{wd} distribution pattern is the same no matter the machining parameter setting even if the values differ.
- The edge radius, E_r, suffers a rapid rounded at the early stage of machining due to the high heat concentration at geometries with large curvature. Then, as the radius increases, no change of E_r with machining depth was observed.
- With regards to G_w value, if the steady state has not reached, the gap width value differs between 30-60% with respect to the theoretical values. Moreover, gap width is not constant along the electrode profile and narrower gap was observed at the bottom of the workpiece.

Development of a thermal simulation model for prediction of temperature distribution in the electrode.

The work proposed a thermal simulation model, that predicts electrode temperature during machining. The main feature is that the model considers the energy generated during continuous EDM process and this energy is distributed over the electrode discharge area. This way, the computational cost is reduced, and the simulation can be applied in the study of industrial EDM jobs.

Furthermore, an inverse simulation method for the determination of the energy absorbed by the electrode was proposed. The methodology was followed for the determination of F_E value when machining with two diverse set of EDM parameters, resulting that the energy absorbed by the electrode is in the range of 10-15%. Results showed good agreement with the results provided in the scientific literature.

VII.2.Future works

The complexity of the EDM machining process makes necessary the constant research of the material removal process. From the work presented in the present dissertation, the following research interests can be highlighted.

To study the feasibility of using the foil electrode with holes as a running foil in SiC slicing.

In order to improve the efficiency of the process, a running foil electrode was successfully performed using a specially designed apparatus [117]. However, the large side surface area of the foil difficult the flushing conditions. Considering that the chip pocketing effect can improve the flushing conditions, and thus enhance the machining performance, it will be of high interest to use a foil with holes as a running foil electrode.

To test the proposed multi-holed electrode for the machining of high-aspect ratio slots under industrial conditions.

It was proved that the electrode with flushing pockets improves drastically the machining performance of the EDM'ing of high-aspect ratio slots. However, the manufacturing of the electrode may increase the cost of the final workpiece part. Hence, from an industrial point of view it will be of high interest to carry out an economical study on this matter.

Furthermore, it will be of high interest to study the feasibility of using multi-holed electrodes under industrial conditions: aeronautical workpiece materials, complex electrode designs and cutting-edge machine generator.

To study the applicability of multi-holed electrodes to other geometries.

The improvement of the flushing conditions by machining holes on the electrode was verified in two applications: the slicing of SiC and the machining of high-aspect ratio slots. It may seem likely that the technique of making holes on the electrode may also be applicable in other electrode geometries in which debris evacuation is difficult.

To apply the proposed electrode wear and gap width methodology in 4 axis machining jobs.

The feasibility of the proposed electrode wear and gap width methodology was proved by the manufacturing of a shrouded blisk that interpolates three axes. However, in the industry, more than 3 axes are interpolated for achieving the requires workpiece geometry. Hence, it will be interesting to analyse electrode wear and gap width distribution of a real industrial job.

Development of a thermal wear criteria to predict electrode geometry during machining.

Observing the electrode wear results and the electrode temperatures during machining, it was concluded that there should be an equivalent electrode temperature with which the electrode material removal can be defined.

Once the material removal criteria is defined and implemented in the simulation model, the electrode geometry change during machining will be predicted.

Implementation of the electrode simulation model in the electrode path generation algorithm.

An ambitious objective will be to implement the electrode simulation model in the electrode path generation algorithm developed by Ayesta *et al* [37]. This model will carry improvement in the industry, as the time-consuming trial-and-error strategies will be reduced.

References

REFERENCES

[1] Izquierdo B. Un modelo numérico para la determinación de las características de la descarga y el análisis del mecanismo de arranque de material en el proceso de electroerosión. PhD Thesis, University of the Basque Country, 2009. (Spanish)

[2] Rajurkar KP, Sundaram MM, Malshe AP. Review of Electrochemical and Electrodischarge Machining. Procedia CIRP 2013;6:13–26. doi:10.1016/j.procir.2013.03.002.

[3] Mohri N, Fukuzawa Y, Tani T, Saito N, Furutani K. Assisting Electrode Method for Machining Insulating Ceramics. CIRP Ann - Manuf Technol 1996;45:201–4. doi:10.1016/S0007-8506(07)63047-9.

[4] Fukuzawa Y, Mohri N, Gotoh H, Tani T. Three-dimensional machining of insulating ceramics materials with electrical discharge machining. Trans Nonferrous Met Soc China (English Ed 2009;19:s150–6. doi:10.1016/S1003-6326(10)60263-4.

[5] www.onaedm.com (Last access 12/2017).

[6] www.sodick.com (Last access 12/2016).

[7] Kunieda M, Lauwers B, Rajurkar KP, Schumacher BMAdvancing EDM through Fundamental Insight into the Process. CIRP Ann - Manuf Technol 2015;54:64–87.

[8] www.makino.com (Last access 12/2016).

[9] Neudeck PG. Silicon Carbide Electronic Devices 2001.

[10] Roccaforte F, Fiorenza P, Greco G, Vivona M, Lo Nigro R, Giannazzo F, et al. Recent advances on dielectrics technology for SiC and GaN power devices. Appl Surf Sci 2014;301:9–18. doi:10.1016/j.apsusc.2014.01.063.

[11] Matus LG, Powell JA, Petit JB, Park B. Development of Silicon Carbide Semiconductor Devices for High Temperature Applications 1991.

[12] Zhao Y. Development of Electrical Discharge Machining System for Cutting Single Crystal SiC. PhD Thesis, The University of Tokyo, 2015. (English)

[13] Ishikawa Y, Yao YZ, Sugawara Y, Sato K, Okamoto Y, Hayashi N, et al. Comparison of slicing-induced damage in hexagonal SiC by wire sawing with loose abrasive, wire sawing with fixed abrasive, and electric discharge machining. Jpn J Appl Phys 2014;53. doi:10.7567/JJAP.53.071301.

[14] www.mitsubishielectric.com (Last access 12/2016).

[15] Kimura A, Okamoto Y, Okada A, Ohya J, Yamauchi T. Fundamental study on multi-wire EDM slicing of SiC by wire electrode with track-shaped section. Procedia CIRP 2013;6:232–7. doi:10.1016/j.procir.2013.03.052.

[16] Kato T, Noro T, Takahashi H, Yamaguchi S, Arai K. Characterization of Electric Discharge Machining for Silicon Carbide Single Crystal. Mater Sci Forum 2009;600-603:855–8. doi:10.4028/www.scientific.net/MSF.600-603.855.

[17] Okamoto Y, Kimura A, Okada A, Uno Y, Ohya J, Yamauchi T. Challenge to Development of Functional Multi-Wire EDM Slicing Method Using Wire Electrode with Track-Shaped Section. Key Eng Mater 2012;523-524:287–92. doi:10.4028/www.scientific.net/KEM.523-524.287.

[18] Zhao Y, Kunieda M, Abe K. Study of EDM cutting of single crystal silicon carbide. Precis Eng 2014;38:92–9. doi:10.1016/j.precisioneng.2013.07.008.

[19] Zhao Y, Kunieda M, Abe K. Comparison on foil EDM characteristics of single crystal SiC between in deionized water and in EDM oil. Int J Adv Manuf Technol 2016. doi:10.1007/s00170-016-8412-z.

[20] Zhao Y, Kunieda M, Abe K. Challenge to EDM Slicing of Single Crystal SiC with Blade Electrode Utilizing a Reciprocating Worktable. Procedia CIRP 2016;42:185–90. doi:10.1016/j.procir.2016.02.268.

[21] Klocke F, Holsten M, Hensgen L, Klink a. Experimental Investigations on Sinking-EDM of Seal Slots in Gamma-TiAl. Procedia CIRP 2014;24:92–6. doi:10.1016/j.procir.2014.07.143.

[22] Ayesta I. Motor aeronautikoko piezen fabrikaziorako elektrohigadura teknologien optimizazioa eta garapena. PhD thesis, University of the Basque Country, 2015. (Basque language)

[23] Luo YF. An investigation into the actual EDM off-time in SEA machining. J Mater Process Technol 2010;74:61–8.

[24] Uhlmann E, Domingos DC. Development and Optimization of the Die-Sinking EDM-Technology for Machining the Nickel-based Alloy MAR-M247 for Turbine Components. Procedia CIRP 2013;6:180–5. doi:10.1016/j.procir.2013.03.102.

[25] Ayesta I, Izquierdo B, Sánchez JA, Ramos JM, Plaza S, Pombo I, et al. Influence of EDM parameters on slot machining in C1023 aeronautical alloy. Procedia CIRP 2013;6:129–34. doi:10.1016/j.procir.2013.03.059.

[26] Aas K. Performance of two graphite electrode qualities in EDM of seal slots in a jet engine turbine vane. J Mater Process Technol 2004;149:152–6. doi:10.1016/j.matprotec.2004.02.005.

[27] Klocke F, Holsten M, Welling D, Klink a., Perez R. Influence of Threshold Based Process Control on Sinking EDM of a High Aspect Ratio Geometry in a Gamma Titanium Aluminide. Procedia CIRP 2015;35:73–8. doi:10.1016/j.procir.2015.08.083.

[28] Obaciu G, Pisarciuc C, Klocke F, Klotz M. energy consumptions evaluation at electro discharge machining of polycrystalline diamond. Nonconv Technol Rev 2010;3:30–3.

[29] Uhlmann E, Domingos DC. Investigations on Vibration-assisted EDM-machining of Seal Slots in High-Temperature Resistant Materials for Turbine Components. Procedia CIRP 2013:71–6. doi:10.1016/j.procir.2013.03.019.

[30] Uhlmann E, Domingos DC. Investigations on vibration-assisted EDM-machining of seal slots in high-temperature resistant materials for turbine components-part II. Procedia CIRP 2016;6:71–6. doi:10.1016/j.procir.2013.03.019.

[31] Cetin S, Okada A, Uno Y. Electrode Jump Motion in Linear Motor Equipped Die-Sinking EDM. J Manuf Sci Eng 2003;125:809. doi:10.1115/1.1615793.

[32] Liao YS, Wu PS, Liang FY. Study of debris exclusion effect in linear motor equipped die-sinking EDM process. Procedia CIRP 2013;6:123–8. doi:10.1016/j.procir.2013.03.058.

[33] Caiazzo F, Cuccaro L, Fierro I, Petrone G, Alfieri V. Electrical Discharge Machining of René 108 DS Nickel Superalloy for Aerospace Turbine Blades. Procedia CIRP 2015;33:383–8. doi:10.1016/j.procir.2015.06.086.

[34] Klocke F, Klink A, Veselovac D, Aspinwall DK, Soo SL, Schmidt M, et al. Turbomachinery component manufacture by application of electrochemical, electro-physical and photonic processes. CIRP Ann - Manuf Technol 2014. doi:10.1016/j.cirp.2014.05.004.

[35] X. Wu, W. Zhao R Du. Tool path generation for machining shrouded turbine blisk. Procedia-American Soc Mech Eng 2004:795–802.

[36] Li Gang ZW-S. A special CAD/CAM software for electro-discharge machining of shrouded turbine blisks. J Shanghai Univ 2007;11:74–8.

[37] Ayesta I, Izquierdo B, Sanchez J a., Ramos JM, Plaza S, Pombo I, et al. Optimum electrode path generation for EDM manufacturing of aerospace components. Robot Comput Integr Manuf 2015;37:1–8. doi:10.1016/j.rcim.2015.04.003.

[38] Maradia U, Knaak R, Dal Busco W, Boccadoro M, Wegener K. A strategy for low electrode wear in meso-micro-EDM. Precis Eng 2015;42:302–10. doi:10.1016/j.precisioneng.2015.06.005.

[39] Mohri N. Electrode Wear Process in Electrical Discharge Machining 1995;44:165–8.

[40] Maradia U, Boccadoro M, Stirnimann J, Kuster F, Wegener K. Electrode wear protection mechanism in meso-micro-EDM. J Mater Process Technol 2015;223:22–33. doi:10.1016/j.jmatprotec.2015.03.039.

[41] Chen Y, Mahdavian S. Parametric study into erosion wear in a computer numerical controlled electro-discharge machining process. Wear 1999;236:350–4. doi:10.1016/S0043-1648(99)00304-X.

[42] Gostimirovic M, Kovac P, Skoric B, Sekulic M. Effect of electrical pulse parameters on the machining performance in EDM 2012;18:411–5.

[43] Tetsuro Itoh RM. Method and apparatus for sink-type electrical discharge machining with control of pyrographite buildup, 1994.

[44] Klocke F, Schwade M, Klink a., Veselovac D. Analysis of Material Removal Rate and Electrode Wear in Sinking EDM Roughing Strategies using Different Graphite Grades. Procedia CIRP 2013;6:163–7. doi:10.1016/j.procir.2013.03.079.

[45] Kunieda M, Kaneko Y, Natsu W. Reverse simulation of sinking EDM applicable to large curvatures. Precis Eng 2012;36:238–43. doi:10.1016/j.precisioneng.2011.10.003.

[46] Qu C, Natsu W, Kunieda M. Clarification of EDM Phenomena by Spectroscopic Analysis. J Adv Mech Des Syst Manuf 2012;6:908–15. doi:10.1299/jamdsm.6.908.

[47] Liao YS, Woo JC. The effects of machining settings on the behavior of pulse trains in the WEDM process. J Mater Process Technol 1997;71:433–9. doi:10.1016/S0924-0136(97)82076-6.

[48] Fazli Shahri HR, Mahdavinejad R, Ashjaee M, Abdullah A. A comparative investigation on temperature distribution in electric discharge machining process through analytical, numerical and experimental methods. Int J Mach Tools Manuf 2017;114:35–53. doi:10.1016/j.ijmachtools.2016.12.005.

[49] Maradia U, Wegener K. EDM Modelling and Simulation 2017.

[50] Boccadoro, M., Bonini, S. Method and apparatus for spark-erosion machining ofa workpiece. 2015 (US 2015/0069023 A1).

[51] Vinoth Kumar S, Pradeep Kumar M. Machining process parameter and surface integrity in conventional EDM and cryogenic EDM of Al-SiCp MMC. J Manuf Process 2015;20:70–8. doi:10.1016/j.jmapro.2015.07.007.

[52] Xia H, Kunieda M, Nishiwaki N. Research on Removal Amount Difference between Anode and Cathode in EDM Process. J Japan Soc Electr Mach Engrs 1994;28:31–40.

[53] Xia H, Hashimoto H, Kunieda M, Nishiwaki N. Measurement of Energy Distribution in Continuous EDM Process. J Japan Soc Electr Mach Engrs 1996;62:1141–5.

[54] Xia H, Kunieda M, Nishiwaki N. Simulation of Electrode Surface Temperature in Die-Sinking EDM Process. J Japan Soc Electr Mach Eng 1996;30:22–8.

[55] Okada a, Uno Y, Okajima I. Energy Distrihution in Electrical Discharge Machining with Graphite Electrode. Mem Fac Eng Okaya Univ 2000;34:19–26.

[56] Zahiruddin M, Kunieda M. Energy Distribution Ratio into Micro EDM Electrodes. J Adv Mech Des Syst Manuf 2010;4:1095–106. doi:10.1299/jamdsm.4.1095.

[57] Zahiruddin M, Kunieda M. Energy Distribution into Micro EDM Electrodes n.d. doi:10.1299/jamdsm.4.1095.

[58] Revaz B, Witz G, Flükiger R. Properties of the plasma channel in liquid discharges inferred from cathode local temperature measurements. J Appl Phys 2005;98:1–7. doi:10.1063/1.2137460.

[59] DiBitonto DD, Eubank PT, Patel MR, Barrufet M a. Theoretical models of the electrical discharge machining process. I. A simple cathode erosion model. J Appl Phys 1989;66:4095–103. doi:10.1063/1.343994.

[60] Oßwald K, Schneider S, Hensgen L, Klink a., Klocke F. Experimental investigation of energy distribution in continuous sinking EDM. CIRP J Manuf Sci Technol 2017:4–11. doi:10.1016/j.cirpj.2017.04.006.

[61] Klocke F, Schneider S, Mohammadnejad M, Hensgen L, Klink A. Inverse Simulation of Heat Source in Electrical Discharge Machining (EDM). Procedia CIRP MConference Model Mach Oper Model Mach Oper 2017;58:1–6. doi:10.1016/j.procir.2017.03.178.

[62] Klocke F, Schneider S, Harst S, Welling D, Klink A. Energy-based approaches for multi-scale modelling of material loadings during Electric Discharge Machining (EDM). Procedia CIRP 2015;31:191–6. doi:10.1016/j.procir.2015.03.044.

[63] Gatto A, Sofroniou M, Spaletta G, Bassoli E. On the chaotic nature of electro-discharge machining. Int J Adv Manuf Technol 2015;79:985–96. doi:10.1007/s00170-015-6894-8.

[64] Sohani MS, Gaitonde VN, Siddeswarappa B, Deshpande a. S. Investigations into the effect of tool shapes with size factor consideration in sink electrical discharge machining (EDM) process. Int J Adv Manuf Technol 2009;45:1131–45. doi:10.1007/s00170-009-2044-5.

[65] Khan AA, Ali MY, Haque MM. A study of electrode shape configuration on the performance of die sinking EDM. Int J Mech Mater Eng 2009;4:19–23.

[66] Crookall JR, Fereday J. An experimental determination of the degeneration of electrode shape in EDM (part2). Microtecnic 1973;4:197–200.

[67] Crookall JR, Fereday J. An experimental determination of the degeneration of electrode shape in EDM (part1). Microtecnic 1973;4:97–9.

[68] Valentinčič J, Junkar M. A model for detection of the eroding surface based on discharge parameters. Int J Mach Tools Manuf 2004;44:175–81. doi:10.1016/j.ijmachtools.2003.10.013.

[69] Valentinčič J, Junkar M. On-line selection of rough machining parameters. J Mater Process Technol 2004;149:256–62. doi:10.1016/j.jmatprotec.2003.11.059.

[70] Valentinčič J, Kušer D, Smrkolj S, Junkar M. Selection of optimal EDM machining parameters for the given machining surface. Management 2005:217–26.

[71] Maradia U, Knaak R, Busco WD, Boccadoro M, Stirnimann J, Wegener K. Spark location adaptive process control in meso-micro EDM. Int J Adv Manuf Technol 2015;81:1577–89. doi:10.1007/s00170-015-7316-7.

[72] Maradia U. Electric discharge machining method and apparatus. 2013, EP 2 610 027 A1.

[73] Maradia U, Taborelli M, Boos J, Buettner H, Stirnimann J, Boccadoro M, et al. Performance and Limitations of the Conventional Electrode Materials for Erosion of High Aspect Ratio Microcavities. Procedia CIRP 2016;42:606–11. doi:10.1016/j.procir.2016.02.220.

[74] Kunieda M, Kobayashi T. Clarifying mechanism of determining tool electrode wear ratio in EDM using spectroscopic measurement of vapor density. J Mater Process Technol 2004;149:284–8. doi:10.1016/j.jmatprotec.2004.02.022.

[75] Marafona J, Wykes C. New method of optimising material removal rate using EDM with copper-tungsten electrodes. Int J Mach Tools Manuf 2000;40:153–64. doi:10.1016/S0890-6955(99)00062-0.

[76] Marafona J. Black layer characterisation and electrode wear ratio in electrical discharge machining (EDM). J Mater Process Technol 2007;184:27–31. doi:10.1016/j.jmatprotec.2006.10.045.

[77] Uhlmann E, Roehner M. Investigations on reduction of tool electrode wear in micro-EDM using novel electrode materials. CIRP J Manuf Sci Technol 2008;1:92–6. doi:10.1016/j.cirpj.2008.09.011.

[78] Khanra a K, Pathak LC, Godkhindi MM. Application of new tool material for electrical discharge machining 2009;32:401–5.

[79] Prihandana GS, Mahardika M, Hamdi M, Mitsui K. Effect of low-frequency vibration on workpiece in EDM processes. J Mech Sci Technol 2011;25:1231–4. doi:10.1007/s12206-011-0307-1.

[80] Bleys P, Kruth J-P, Lauwers B, Zryd a., Delpretti R, Tricarico C. Real-time Tool Wear Compensation in Milling EDM. CIRP Ann - Manuf Technol 2002;51:157–60. doi:10.1016/S0007-8506(07)61489-9.

[81] Yu ZY, Fujino M. Micro-EDM for Three-Dimensional Cavities - Development of Uniform Wear Method - 1998;47:169–72.

[82] Marashi H, Jafarlou DM, Sarhan AAD, Hamdi M. State of the art in powder mixed dielectric for EDM applications. Precis Eng 2016;46:11–33. doi:10.1016/j.precisioneng.2016.05.010.

[83] Shabgard M, Khosrozadeh B. Investigation of carbon nanotube added dielectric on the surface characteristics and machining performance of Ti–6Al–4V alloy in EDM process. J Manuf Process 2017;25:212–9. doi:10.1016/j.jmapro.2016.11.016.

[84] Hinduja S, Kunieda M. Modelling of ECM and EDM processes. CIRP Ann - Manuf Technol 2013;62:775–97. doi:10.1016/j.cirp.2013.05.011.

[85] Tricarico MDU, Delpretti R, Dauw IMS. Geometrical Simulation of the EDM Die-Sinking Process. CIRP Ann - Manuf Technol 1988;37:191–6. doi:10.1016/S0007-8506(07)61616-3.

[86] Chen J, Sun ZM, Lu GD. Simulation for electrode wear predication in die-sinking EDM based on geometry model. Proc - 2013 5th Conf Meas Technol Mechatronics Autom ICMTMA 2013 2013;1000:1000–4. doi:10.1109/ICMTMA.2013.248.

[87] Kunieda M, Kowaguchi W, Takita T. Simulation of Die-Sinking. CIRP Ann - Manuf Technol Ann - Manuf Technol 1999;48:115–8.

[88] Morimoto K, Kunieda M. Sinking EDM simulation by determining discharge locations based on discharge delay time. CIRP Ann - Manuf Technol 2009;58:221–4. doi:10.1016/j.cirp.2009.03.069.

[89] Yeo SH, Kurnia W, Tan PC. Critical assessment and numerical comparison of electro-thermal models in EDM. J Mater Process Technol 2008;203:241–51. doi:10.1016/j.jmatprotec.2007.10.026.

[90] Marafona J, Chousal J a G. A finite element model of EDM based on the Joule effect. Int J Mach Tools Manuf 2006;46:595–602. doi:10.1016/j.ijmachtools.2005.07.017.

[91] Izquierdo B, Sánchez J a., Plaza S, Pombo I, Ortega N. A numerical model of the EDM process considering the effect of multiple discharges. Int J Mach Tools Manuf 2009;49:220–9. doi:10.1016/j.ijmachtools.2008.11.003.

[92] Xie B, Zhang Y, Zhang Y, Dai Y, Liu X. Effect of discharge location on temperature distribution during electrical discharge machining. Int J Smart Home 2015;9:75–80. doi:10.14257/ijsh.2015.9.12.08.

[93] www.rohm.com (Last access 05/2017).

[94] Zhao Y, Kunieda M, Abe K. EDM mechanism of single crystal SiC with respect to thermal, mechanical and chemical aspects. J Mater Process Technol 2016;236:138–47. doi:10.1016/j.jmatprotec.2016.05.010.

[95] www.keyence.com (Last access 12/2017).

[96] www.system3r.ch (Last access 12/2017).

[97] Flaño O, Zhao Y, Kunieda M, Abe K. Approaches for improvement of EDM cutting performance of SiC with foil electrode. Precis Eng 2017. doi:10.1016/j.precisioneng.2017.01.007.

[98] Electrode CW, Wedm H. Development of Coated Wire Electrode for High-Performance WEDM (4th Report) - Effects of high-resistance layer on wire electrode on WEDM characteristics - 2008.

[99] K. Morimoto MK. Fundamental study on Quantitative Estimation of Discharge Delay Time in EDM (2009). Int J Electr Mach 2009;14:43–50.

[100] Bommeli B, Frei C, Ratajski A. On the influence of mechanical perturbation on the breakdown of a liquid dielectric. J Electrostat 1979;7:123–44. doi:10.1016/0304-3886(79)90067-6.

[101] I Araie, S Sano MK. Effect of Electrode Surface Profile on Discharge Delay time in Electrical Discharge Machining. J Jpn Soc Mach Eng 2007;41:61–8.

[102] www.tek.com (Last access 12/2017).

[103] www.pemuk.com (Last access 12/2017).

[105] www.leica-microsystems.com (Last access 06/2017).

[106] Poco Graphite, Inc., 1993. “Manual técnico de EDM”, Poco Graphite Inc.

[107] www.plm.automation.siemens.com (Last access 12/2017).

[108] www.poco.com (Last access 07/2017).

[109] Klink A, Holsten M, Hensgen L. CIRP Annals - Manufacturing Technology Crater morphology evaluation of contemporary advanced EDM generator technology. CIRP Ann - Manuf Technol 2017:7–10. doi:10.1016/j.cirp.2017.04.137.

[110] Gadeschi GB, Schneider S, Mohammadnejad M, Meinke M, Klink a., Schröder W, et al. Numerical Analysis of Flushing-Induced Thermal Cooling Including Debris Transport in Electrical Discharge Machining (EDM). Procedia CIRP 2017;58:116–21. doi:10.1016/j.procir.2017.03.325.

[111] www.ansys.com (Last access 10/2017).

[112] www.edmparts.com (Last access 04/2016).

[113] Poco Graphite, Inc., Properties and Characteristics of Graphite for the EDM industry (1987).

[114] www.ni.com (Last access 12/2017).

[115] www.tcdirect.com (Last access 12/2017).

[116] Singh H. Experimental study of distribution of energy during EDM process for utilization in thermal models. Int J Heat Mass Transf 2012;55:5053–64. doi:10.1016/j.ijheatmasstransfer.2012.05.004.

[117] Zhao Y, Kunieda M, Abe K. A novel technique for slicing SiC ingots by EDM utilizing a running ultra-thin foil tool electrode. Precis Eng 2017:1–10. doi:10.1016/j.precisioneng.2017.11.012.

[118] Xia H, Kunieda M, Nishiwaki N LN. Measurement of Energ Distribution into Electrodes in EDM Processes. Adv Intell Prod 1994:601–6.

[119] König W, Wertheim R, Toren M ZY. Material Removal and Energy Distribution in Electrical Discharge Machining. CIRP Ann - Manuf Technol 1975;45:95–100.

[120] Motoki M HK. Energy Distribution at the Gap in Electric Discharge Machining. CIRP Ann - MT 1967;14:485–9.

[121] Shankar P, Jain V ST. Analysis of Spark Profiles during EDM Process. Mach Sci Technol 1997;1:195–217.

[122] Xia H, Kunieda M NN. Removal Amount Difference between Anode and Cathode in EDM Process. Int J Electr Mach 1996;1:45–52.